FINITE ELEMENT ANALYSIS OF COMPLETE MODEL OF CERVICAL SPINE

BY

MUHAMMAD ARDALANI-FARSA
Mechanical Engineering Department, University of Tehran, 2001

A THESIS
PRESENTED TO RYERSON UNIVERSITY

in partial fulfillment of the
requirements for the degree of
Master of Applied Science
in Program of
Mechanical Engineering

Toronto, Ontario, Canada, 2006

AUTHOR'S DECLARATION

I hereby declare that I am the sole author of this thesis

I authorize Ryerson University to lend this thesis to other institutions or individuals for the purpose of scholarly research.

I further authorize Ryerson University to reproduce this thesis by photocopying or by other means, in total or in part, at the request of other institutions or individuals for the purpose of scholarly research.

BORROWER'S PAGE

Ryerson University requires the signatures of all persons using or photocopying this thesis.

Please sign below and give the address and date.

NIKOLAS TRUTIAK - RYERSON UNIVERSITY 2008

ABSTRACT

Finite Element Analysis of Complete Model of Cervical Spine

Master of Applied Science, Mechanical Engineering, 2006, Muhammad Ardalani-Farsa

School of Graduate Studies, Ryerson University

The finite element method has been applied in the area of the cervical spine since the 1970's. In the present research work, the finite element method was employed to model, validate and analyze a complete model of the human cervical spine from C1 to T1, including interconnecting intervertebral discs, ligaments and joints.

The developed model of the cervical spine was validated by the experimental results presented in the literature. As the values obtained from the finite element analysis were mainly in the range of motion observed in the experiment; it was concluded that the finite element results were consistent with the reported data in the literature. Next, the validated model of the cervical spine was examined under physiological loading modes to locate the areas bearing maximum stress in the cervical spine. Finally, to study the effect of variations in the material properties on the output of the finite element analysis, a material property sensitivity study was conducted to the C3-T1 model of cervical spine. Changes in the material properties of the soft tissues affected the external and internal responses of both the hard and soft tissue components, while changes in those of the hard tissues only affected the internal response of hard tissues.

Dedicated to:

MY MOM AND DAD
AND
MY DEAR SUPERVISOR, DR. KAMRAN BEHDINAN
WHO ALWAYS ENCOURAGED ME TO DO *THE BEST JOB.*

TABLE OF CONTENTS

LIST OF FIGURES

LIST OF TABLES

CHAPTER 1

INTRODUCTION

The cervical spine is one of the most complicated structures in the human body. Its exclusive anatomy makes this structure extremely flexible. The cervical spine is also responsible for providing appropriate support for the skull and protecting the spinal cord from injury. Although the cervical spine is very flexible, it is highly at risk of injury from strong, sudden movements, such as whiplash-type and high gravitational (G) force impact injuries.

Researchers have chosen different approaches to investigate the area of cervical spine injuries. Statistical survey is the basic approach to determining populations at risk of cervical spine injury and the external causes of injury. Clinical studies of cervical spine injuries can assist researchers to define the mechanism and severity of a neck injury. Investigating cervical spine injuries experimentally is the ideal method of simulating the mechanism of injury and its initialization, as controlled loads can be applied to the neck while performing the experiments. Numerical analysis is another method of simulating real life accidents and is more efficient than the experimental approach. This method

enables researchers to develop highly detailed models in which the distribution of stresses and strains can be studied for all of the different components of the cervical spine. All of these approaches are extremely important and considering them together will offer a great opportunity to increase the knowledge of neck injury mechanisms.

The numerous advantages of the finite element method have motivated researchers to investigate the causes of injury in the cervical spine using this approach. The ability to analyze complicated structures, material properties and boundary conditions, whether linear or nonlinear, makes this method a more attractive tool in the investigation of cervical injuries in real life. Taking advantage of fast processor computers, the finite element approach is faster and cheaper than experimental techniques.

The first step in investigating the causes of neck injury using the finite element method is to develop a CAD model of the cervical spine and validate the model via finite element analysis. Stress analyses can be performed on the validated model to obtain the distribution of stress and strain throughout the model. Experts in the area of neck injury can study the finite element results and locate the regions at risk of injury. Also, the output from finite element analyses can be used by engineers to design appropriate neck instrumentations.

It is essential to review available biomechanical models of the cervical spine in order to be familiar with the advantages and disadvantages of each model. This review will also contribute to determining which published paper is most reliable and appropriate to follow when selecting the required geometric parameters and material properties of various components of the cervical spine. The following sections discuss in detail the four major categories of biomechanical models.

1.1 Biomechanical Models of the Cervical Spine

Biomechanical models can assist researchers to define the fundamental mechanisms of injury in the cervical spine, leading to reduced risk of injuries, distinguished causes of neck pains and treatment of clinical problems. There are four main categories of biomechanical models as elaborated in Table 1 [1].

Table 1: Categories of Biomechanical Models [1].

			Advantages	Disadvantages
Physical model		Implant and component testing	Simple, less variable, less expensive, evaluates implant alone	Non-anatomic, unphysiologic implant loading
***in vitro* model**	**Animal**	Implant testing	Less expensive, less variable	Different anatomy and biomechanics, does not represent human variability
	Human	Spinal function and dysfunction studies, and implant testing	Actual human anatomy, physical properties, and population variability	Difficult to obtain, expensive, more variable than animal
***In vivo* model**	**Animal**	Studying phenomena that occur *in vivo* e.g. fusion and adaptation	Essential for studying fusion, adaptation, and effect of drugs	Different anatomy, biomechanics, and biology, has greater variability than in vitro animal model.
	Human	Studying living phenomena in humans, e.g. muscle recruitment	Actual human responses to external stimulus, e.g. head kinematics and muscles recruitment in whiplash simulations	Subjects can not be loaded to cause any injury
Mathematical model		Simulating situations not modeled by other biomechanical models	Capable of simulating real phenomena- effect of muscles, bone healing, tissue adaptation, determining internal loads, strains and stresses	Difficult to validate, tendency to use the model beyond its validation boundaries

1.1.1 Physiological Models

Physical models are those made of man-made materials. These models are mainly used when the bony structure and material properties of the soft tissue are less important than spinal instruments. The popular physical model of the cervical spine that has been widely used by researchers at academic institutes and engineering companies in the industry is

the missing-vertebra model to test the spinal instrumentations. The missing-vertebra model consists of two blocks of high-density polyethylene to which spinal devices are attached. The adjacent models of vertebrae are distanced appropriately to provide a one-level corpectomy (missing-vertebra model). The main purpose of using this model is to test the strength and fatigue of various spinal instruments, such as plating devices and screws.

1.1.2 *In Vitro* Biomechanical Models

In vitro biomechanical models of the cervical spine are the cadaveric specimens of humans or animals. These models are used whenever anatomy is important to investigate the causes of injury in the neck. These models are mainly used to test the strength, fatigue, and stability of the cervical spine specimen or specimen plus the instrumentation. The *in vitro* biomechanical models are generally divided into three categories based on the purpose of the research study. The basic purpose of using *in vitro* biomechanical models of the cervical spine is to assist researchers to record its basic movements in response to applied loads or displacements. The cervical spine's behavior can be investigated in single or multiple directions, under simple or complex loading conditions, and in neutral or other postures. The second purpose is to simulate spinal injuries, diseases, or surgical decompression procedures.

The last objective of using the *in vitro* model of the cervical spine is to evaluate spinal instrumentations or devices. For this purpose, the biomechanical model is first studied intact, then as a clinically injured model simulating the relevant injury, and at last as an instrumented model of the cervical spine. Comparing the model of the cervical spine after injury and installing instrumentation with the intact model assists researchers to evaluate the stability of the installed instrumentation.

Lysell [2] was probably the first researcher to perform an extensive *in vitro* study of the cervical spine motions. He has since presented a thorough review of the literature and research works. Lysell [2] tested complete fresh cadaveric cervical spine specimens (C2-T1). He used four 0.8 mm-steel-balls inserted into each vertebra and quantitative stereo radiography. He measured the three dimensional relative motions between vertebrae and then investigated a total of 28 specimens (age: 11 - 67 years) and found no effect of degeneration on the motions.

Panjabi et al. [3] studied the load-displacement behavior of 4 cervical spine specimens (age: 42 - 70 years). The 6 forces of anterior-posterior shear, medial-lateral shear, and compression-tension were applied to the specimens. The maximum force used was 50 N. Then, they measured three-dimensional motions of each motion segment of the cervical spine specimens were measured. This data could be used for the development and validation of numerical models of the cervical spine.

In another *in vitro* study, Panjabi et al. [4] measured motions of the upper cervical spine in three dimensions. They used 10 cadaveric spine specimens (age: 29 - 59 years) subjected to a maximum moment of 1.5 Nm at the occiput. Next, the three-dimensional motions of occiput-C1 and C1-C2 were measured. In addition to the ranges of motion, the authors also measured the elastic and neutral zones, which are helpful to validate the numerical models of the cervical spine, especially in the presence of its nonlinear behavior.

Moroney et al. [5] tested 35 fresh adult cervical spine motion segments. The load-displacement curves were obtained by applying forces of compression and shear and moments of flexion, extension, lateral bending and axial torsion. The maximum shear forces applied were approximately 20 N, the compression force was about 75 N and all

moments applied were 1.8 Nm. Additionally, they measured the kinematic behavior of the disc alone, after cutting the posterior elements. In this study, the stiffness values of the spinal segments as well as the failure loads were also presented. As mentioned above, this data could be used to develop and validate the mathematical models of the cervical spine.

Goel et al. [6] studied the C0-C1-C2 complex under the application of axial moment until failure. The authors investigated 12 fresh cadaveric specimens (age: 50 -91 years) and measured the moment-rotation relationship of the cervical spine. The average motion measured at 2.0 Nm, was 29.9 degrees with a standard deviation of 11.3 degrees. The failure load was 13.6 Nm with a standard deviation of 4.5 Nm.

1.1.3 *In Vivo* Biomechanical Models

The majority of *In vivo* biomechanical models are animal models, although some experiments in human volunteers may also be conducted. These models are necessary if the biomechanics of a living structure are to be investigated. There are many phenomena that cannot be studied using *in vitro* models. Animal models are used to study phenomena such as fusion or osteopenia (a condition of the bone in which decreased calcification, decreased density, or reduced mass occurs), in response to spinal instrumentation, degenerative processes adjacent to the fusion area, scar tissue formation, and response to an injury to disc and facets. Exercising *in vitro* biomechanical models can lead us to obtain the flexibility-stiffness and strength of the specimen.

Penning [7] tested 20 sound young adults by taking lateral x-rays of their cervical spines in flexion and extension postures. He proposed a technique of super-imposing the two films

and calculating the ranges of motion from occiput-C1 to C6-C7. Although he also graphed the centers of rotations, he reported no numerical values.

Dvorak et al. [8] examined 9 healthy adults (age: 17 - 49 years) and 43 patients with cervical spine injury using CT scans. In this study, the ranges of axial rotation at the levels of occiput-C1, C1-C2, and C2-T1 were measured.

Penning et al. [9] measured axial rotation at each vertebral level in a group of 26 healthy young volunteers (age: 20 -26 years). CT scans were taken throughout the length of the cervical spine with the head turned maximally to the right, and then to the left (simulating axial rotations). This is probably the first and only *in vivo* study in which axial rotations of the cervical spine have been measured.

Dvorak et al. [10] suggested the idea of *in vivo* passive motion measurements in contrast to the *in vivo* active motion measurements. The cervical spines of 59 adults were investigated by means of radiographs. They examined 28 healthy adults and 31 patients who had experienced soft tissue injury to the cervical spine. By laying the flexion x-ray on top of the extension x-ray and using simple graphical construction, they measured the rotational ranges of motion in flexion-extension.

Dvorak et al. [11], in another study, measured motions of the cervical spine in 44 adults (22 women and 22 men) in a younger age group (23 - 49 years). These were normal subjects who underwent passive flexion-extension motion and were examined by lateral x-rays at the ends of the range of motion. The authors implemented a computer program to determine ranges of rotatory and translatory motions as well as centers of rotations.

1.1.4 Numerical Models

A numerical model is a set of mathematical equations that incorporate the geometry and material properties of a specific structure. These models are ideally suitable to investigate the phenomena that cannot be thoroughly studied in other models.

The most common mathematical model of the cervical spine is a finite elment model. The finite element models incorporate realistic geometry of the vertebrae and material properties of the soft tissue connecting the vertebrae. Studies of kinematics (intervertebral motions), kinetics (motions in response to applied loads), and internal strains and stresses are possible outputs for using this model. Although kinematics and kinetics can be studied by *in vivo* and *in vitro* experiments, determining the internal stresses and strains cannot be measured experimentally. Knowing the stresses and strains in the vertebrae or interconnecting soft tissues in response to the loads applied to the specimen, it is possible to locate the regions at risk of misplacement, fracture or rupture.

Like all other biomechanical models, mathematical or computer models are not universal; they are reliable only for the specific purpose for which they are developed. For instance, if a numerical model is developed to study the dynamics of a spine, in a whiplash simulation in which the goal is to measure the intervertebral motions in response to a horizontal acceleration, then a model may consist of a series of vertebral bodies (modeled as rigid bodies) connected by ligaments and discs (modeled as springs). On the contrary, if the model is designed to study internal stresses and strains in the disc, the vertebrae and discs may be modeled more realistically as consisting of thousands of solid elements connected by flexible spring-like links.

The first numerical spinal models were developed in the late 1950's to understand the biomechanics behind spinal injury due to pilot ejection [12]. Since then, research with numerical techniques, such as the finite element method, has progressed toward a better understanding of spinal behavior and injury mechanisms. Lumped parameter models can also be used to study kinematics, but do not give the possibility to evaluate tissue stresses and strains, since they are built up of rigid bodies. Knowing the stresses and strains in response to a given load, it is possible to predict the result important for injury prevention. The anatomical details give a more reliable kinematical response than spherical representations of vertebrae and joints used in the lumped parameter models.

Also, the lumped parameter models of the cervical spine have been developed by many researchers such as Merill et al. [13], Li et al. [14], De Jager et al. [15,16].

The following sections outline the history of finite element models presented in literature to characterize the motion of the cervical spine and demonstrate the mechanisms of neck injuries.

1.1.4.1 Model of Single Vertebra of Cervical Spine

The finite element model of a single vertebra of the cervical spine has been developed mainly from CT-images and used to analyze stress patterns in the vertebral bone during loading to predict fracture mechanisms. Teo et al. [17] modeled C2 with anatomical detail but assumed the vertebra to be entirely made of cortical bone, while Graham et al. [18] included both cortical and cancellous material properties in the analysis of odontoid fractures. Teo et al. [19] investigated fracture mechanisms in two separate anatomically detailed models of C1, but considered only cortical material property for the vertebra. In a model of C4 developed by Bozic et al. [20], separate material property was set for each

region, although the accuracy of the anatomy was compromised as it was meshed with brick elements.

1.1.4.2 Model of Cervical Motion Segment

Finite element models of cervical motion segments have been developed mainly to study the force-displacement of single- or multi-motion segments of the cervical spine. Maurel et al. [21], Yoganandan et al. [22], Ng et al. [23], Teo et al. [24], and Wilcox et al. [320] considered linear elastic material properties for their models to measure load-displacement and stress and strain distributions within the models.

Maurel et al. [21] developed a three-dimensional geometrical and mechanical FE model of the complete lower cervical spine. The geometry of the vertebrae was a parameterized, which allowed the model to fit different morphologies of vertebrae. The results obtained with a single motion segment model and with the complete model were validated with those from experimental studies. Since the authors used parameterized model, they could study the influence of geometric parameters on the mechanical behavior of the cervical spine.

The research work conducted by Yoganandan [25] investigated a detailed three-dimensional finite element model of a three-vertebra segment, C4-C6, of human cervical spine using computed tomography scans and validated against experimental data. As they included three levels in the spinal structure, they could determine the mechanical behavior of the various components at each level. Their results indicated that the stresses in the anterior column were higher compared to the posterior column at the inferior level, while the opposite true at the superior level. The superior and inferior endplate stresses were higher compared to posterior column at the inferior level, while the opposite was

found to be true at the superior level. The superior and inferior endplate stresses were higher in the middle vertebral body compare to the adjacent vertebrae. In addition, the stresses in the cancellous core of the middle, unconstrained vertebral body were higher.

Kumaresan et al. [26] developed an anatomically detailed model of C4-C6 motion segment of the human cervical spine. The vertebrae were represented with shell elements for the cortical bone and solid elements for the cancellous bone. The intervertebral discs were modeled with annulus fibers including a ground substance resembling annulus fibrosus in combination with linear elastic solid elements for the nucleus pulposus. This model of the intervertebral disc is the first model considering anisotropic behavior. Also, non-linear spring elements were used to model the ligaments. The authors validated their model for compression, flexion, and torsion.

Wheeldon et al. [27] added C2, C3, C7 and T1 to the C4-C6 model of Kumaresan [28], to have a model of the complete C2-T1 segment. Validation of this model has not yet been published.

Goel et al. [29] considered non-linear material properties for the ligaments in a finite element model of the C5-C6 motion segment. The model was validated for compression, flexion, extension, axial rotation, and lateral bending.

1.1.4.3 Model of Upper Cervical Spine

To consider the coupling between the head and the neck, it is essential to include a model of the skull in the finite element model of the cervical spine. Except for the models by Yang et al. [30] and Jost et al. [31], other researchers have simplified the joints and the anatomy of the upper cervical spine.

The model by Jost et al. [31] developed an anatomically accurate upper cervical spine. In his model, the occipitoatlantal and atlantoaxial joints were modeled with facet surfaces, where the gap between the surfaces was filled with linear elastic solid elements and a system of springs and dampers.

Lee et al. [32] developed a three-dimensional finite element model of the upper cervical spine including nonlinear ligaments and sliding-contact for contact surfaces. The authors quantified the biomechanical behavior of the model under various load conditions. For the first time, in this model alar and transverse ligaments of the neck were modeled by 8 node brick elements.

A recent finite element model of the upper cervical spine was developed by Brolin [33]. The detailed anatomy of occiput to C3 was obtained by computed tomographic images. In her model, ligaments were modeled as nonlinear spring elements. The model was validated for axial rotation, flexion, extension, and lateral bending. The model realistically simulated the complex kinematics of the craniocervical region. It was highlighted that the injuries changing the material characteristics of any spinal ligament will influence the structural behavior of the upper cervical spine [33].

1.1.4.4 Complete Model of the Cervical Spine

The first complete model of the cervical spine was developed by Kleinberger [34]. He included a rigid head in a model of the cervical spine and used it for dynamic simulations. The vertebrae were modeled as rigid bodies. Homogenous material property was selected for intervertebral discs and the ligaments were modeled with brick elements. Material property for all soft tissues was set as linear, homogenous and isotropic. The occipitoatlantal joint was simplified as a pin joint, allowing for a rotation of about one

axis to simulate flexion and extension motion and maintain skull-atlas contact in tension. The model was validated for axial compression and frontal impacts.

Later, Stemper et al. [35] changed the material properties in Kleinberger's model and used the same model to investigate the mechanical behavior of the cervical spine. They concluded that the rotation of the center of gravity for the head increased when the elastic moduli of the vertebrae and discs were increased, while the Poisson's ratio did not affect the head motion.

Another head and neck model was developed by Yang et al. [30]. The material property for the cortical and cancellous bone was simplified and assumed to have the same stiffness. They divided intervertebral discs into a linear viscoelastic model of the nucleus pulposus and linear elastic elements for the annulus fibrosus. The ligaments were modeled with nonlinear tension-only membrane and bar elements. The difference in material properties of ligaments at different spinal levels was neglected. Data for the lumbar spine ligaments was used and scaled to represent the ligaments in the cervical spine region. The model by Yang et al. [30] was validated by experimental head-neck drop tests and rear impact sled tests.

Jost et al. [31] developed another complete model of the cervical spine with a rigid head, as a part of a finite element model of the whole body. The lower and upper cervical spine was modeled with anatomical detail. The vertebrae were modeled with shell elements to represent the cortical bone. The cancellous bone in the vertebrae was ignored. Ligaments were modeled with tension-only membrane elements with linear elastic material properties, in combination with spring-damper elements to simulate the viscoelastic

material behavior. The model was validated at low and high G-level lateral accelerations and only the head motion was measured.

Although research works are published in the modeling of the cervical spine, there is still much work to be done before a complete validated finite element model of the cervical spine can be used for all purposes. More accurate material models need to be developed to resemble biological materials, and there is also a need for more accurate geometrical models.

1.1.4.5 Models of Cervical Injury

Several researchers developed finite element models of the cervical spine to simulate fracture mechanisms in the bony structure of the vertebrae [36,37,38,39,40,41]

Teo et al. [24] conducted a parametric study on the roles of ligaments, facets, and disc nucleus of the lower human cervical spine (C4–C6) using the finite element method. In this research, a three-dimensional finite element model of the lower human cervical spine was developed and validated against the published data under three load conditions: axial compression, flexion and extension. The finite element model was further modified accordingly to investigate the role of discs, facets and ligaments in preserving cervical spine motion segment stability in these load configurations. The model predicted the nonlinear force-displacement response of the human cervical spine, with increasing stiffness at higher loads. It also predicted that the role of ligaments, facets or disc nucleus is substantial to maintain the cervical spine stability, in terms of sagittal rotational movement or distribution of load.

In another study, Tan et al. [42] generated the three-dimensional, nonlinear finite element model of the C2–C3 motion segment from human cadaveric data and examined it under

varying load conditions to investigate stress patterns on the odontoid process. The model consists of C2 and C3 vertebrae, the single intervertebral disc and all biomechanically important ligaments. To evaluate the stress distributions in the odontoid process, pressure loads were applied on the dens at the point where it is about to come into contact with the surrounding neck construct. Such contacts may take place when the dens comes in contact with the anterior arch of the atlas, transverse ligament or the lateral masses of the atlas. Therefore, pressure loads on the surface of the dens were changed from the posterior to anterior directions at 45° substeps in five load cases to define stress patterns. They concluded that the direction of the load vector is an important factor for the dens fracture.

A simplified model of the cervical spine was developed by Sadegh et al. [43] to examine stress distributions in the bony structure of vertebrae. The loads and the moments applied to the model were collected from the biodynamic responses of human volunteers during high gravitational acceleration. Beam elements with various material properties were used to simulate the ligaments, articular facets and muscles. The complete model of the cervical spine was subjected to 11 cases of loading, ranging from 8 G to 20 G. They concluded that the maximum stress in all loading cases increased as the magnitude of the acceleration increased. The stresses in the 10 G to 12 G were comfortably below the injury level and the majority of the maximum stresses occurred in C6 and C4 regions.

1.1.4.6 Material Property Sensitivity Model

The result of finite element analysis is highly dependant on the selection of material properties for various components of the model. The effect of material property variations of spinal components on the human lumbar spine biomechanics is fully

investigated. With regards to the cervical spine, Ng et al. [44] and Kumaresan et al. [28] have presented some research.

Kumaresan et al. [28] developed a three-dimensional anatomically accurate finite element model of the C4-C6 unit including the three vertebrae, two interconnecting intervertebral discs, and the anterior and posterior ligament complex to determine the effect of variations in the material properties of the cervical spinal components on the results of the finite element analysis under physiological loads. The authors conducted a parametric study on the variations in the material properties of all of the cervical spine components including the cortical shell, cancellous core, endplates, intervertebral disc, posterior elements and ligaments under flexion, extension, lateral bending and axial torsion loading conditions. Low, basic and high material property cases for each of the six components under all four physiologic loading conditions were considered in the finite element analysis. The results were evaluated to analyze the external angular rotation and the internal stresses in the middle vertebral body, the superior and inferior endplates and the two intervertebral discs. It was concluded that variations in the material properties of the different cervical spinal components produced dissimilar changes in the external and internal responses. Variations in the material properties of the cancellous core, cortical shell, endplates and posterior element structures representing the bony structure of vertebrae did not affect the external angular motion and the internal stresses of the inferior and superior intervertebral discs. In contrast, variations in the material properties of the intervertebral disc and ligament structures significantly affected the angular motion and the stresses in the inferior and superior intervertebral discs of the cervical spine.

A systematic approach using factorial analysis was conducted by Ng et al. [44] on the finite element model of C4–C6 unit to analyze the influence of variations in the material properties of the cortical shell, cancellous core, posterior elements, endplate, disc annulus and disc nucleus, on the internal stresses and external biomechanical responses under compression, anterior and posterior shear. Results demonstrated that material property variation of the disc annulus has a significant influence on both the external biomechanical response and internal stress of the disc annulus and its adjacent hard bones. They found that variation in the cortical shell modulus has significant influence on the cancellous bone under compression and anterior-posterior shear.

1.2 Objective and Method of Approach

The main objective of the present study is to develop a finite element model of the cervical spine from C1 to T1 and validate it against experimental results reported in literature. The validated model will then be used to conduct stress analyses and investigate the material sensitivity in the cervical spine.

In the previous sections, the four main categories of biomechanical models were outlined: the physiological models, *in vitro* biomechanical models, *in vivo* biomechanical models, and numerical models. These models have assisted researchers to understand the mechanisms of cervical injury and, therefore, to improve the prevention, diagnosis, and treatment of clinical problems. The background and history of each biomechanical model was also discussed.

In the next chapter, the anatomy of the cervical spine is outlined. The various components forming the structure of the cervical spine, such as vertebrae, intervertebral discs, ligaments, muscles and joints are presented in detail. It is essential to have knowledge of

the anatomy of the cervical spine in order to develop an anatomically accurate model of the human cervical spine.

Chapter 3 presents the main injuries of the cervical spine. Numerous studies have been conducted in this area. In this chapter, the injuries causing instability in the cervical spine are fully explained.

One of the challenging subjects in the finite element modeling of the cervical spine is defining the material properties of soft tissues. This important issue is discussed in chapter 4. As soft tissues, especially ligaments, play a prominent role in the finite element model of the cervical spine, the structure, function, mechanical testing, and material models of ligaments and muscles are carefully reviewed in this chapter.

In chapter 5, a three-dimensional CAD model of the cervical spine is constructed using average parameters reported in the literature for various components of the human neck. Based on the developed CAD model and the most common material properties presented in literature for the bony and soft tissues of the cervical spine, the finite element model of cervical spine is developed. The developed finite element model consists of vertebrae, interconnecting intervertebral discs, ligaments and joints.

Finally, in chapter 6, the three-dimensional finite element model of the cervical spine developed in chapter 5 is validated using the experimental results published by other researchers. This validation is performed in three steps; the single motion segment of C5-C6, the model of C3-T1 unit, and finally, the complete model of the cervical spine. To locate the maximum stress areas in cervical spine under various physiologic loading modes, stress analysis is performed for complete model of cervical spine. Finally, to study the effect of variations in the material properties of the cervical spinal components

on the output of the finite element analysis, a material property sensitivity study is conducted to the model of the C3-T1 unit.

CHAPTER 2

ANATOMY OF CERVICAL SPINE

The cervical spine is made up of the first seven vertebrae in the spine. It begins just below the skull and finishes just above the thoracic spine. The cervical spine has a lordotic curve (a backward "C"-shape), just like the lumbar spine. The cervical spine is much more flexible than both the thoracic spine and lumbar spine. It is therefore possible to rotate the cervical spine in different directions and angles. There are special holes in each vertebra of the cervical spine for the arteries (blood vessels that carry blood away from the heart). These openings can only be observed in the cervical area. The skull and vertebrae are joined by the ligaments and intervertebral discs to make the neck a stable yet flexible structure [45].

2.1 Vertebra

The first two vertebrae in the cervical spine, the atlas and the axis, are different from the other vertebrae because they are developed specifically for axial rotation (Figure 1). These two vertebrae allow the neck to rotate in different directions [46].

Atlas is the first cervical vertebra. It is located between the skull (occiput) and the rest of spine. It does not have a vertebral body, but has a thick arch anteriorly and a thin arch posteriorly, with two facet masses.

Atlas sits on top of the second cervical vertebra, Axis. Axis has a bony projection called the odontoid process that runs through the hole in the atlas. This special arrangement enables the head to turn from side to side as far as it can.

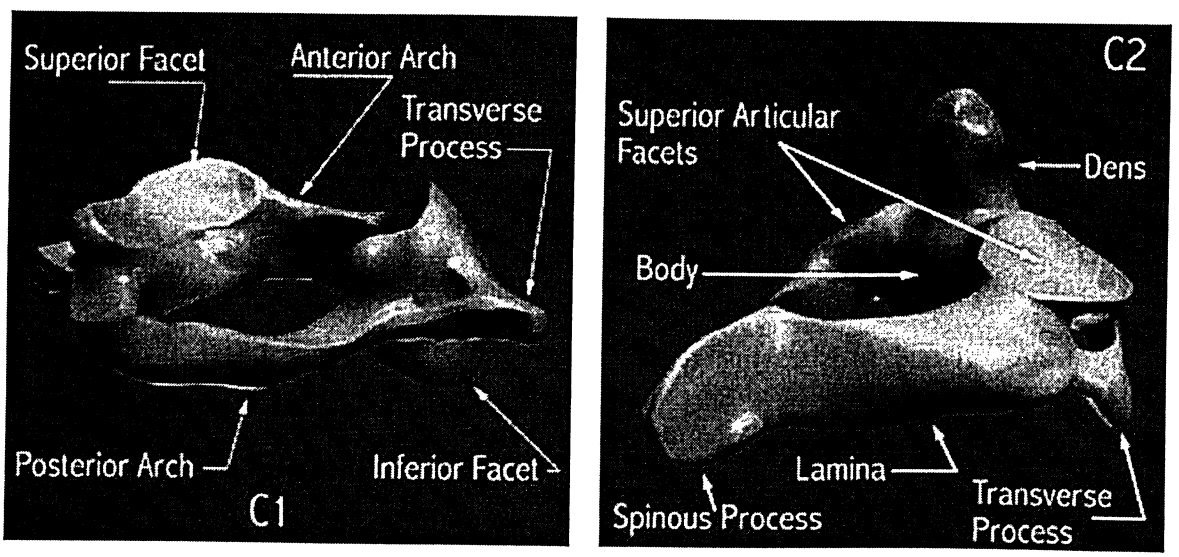

Figure 1: Left, the first vertebra of cervical spine, Atlas. Right, the second vertebra of cervical spine, Axis [47].

Cervical vertebrae C3 through C7 are considered to be typical (Figure 2). They each have a vertebral body, pedicles, a transverse process, facets, lamina, a posterior process, a spinous process and are linked through intervertebral discs that distribute and absorb

loading forces. The superior surface of the vertebral body is convex anteriorly and concave from side to side. The inferior surface of the vertebral body is concave anteriorly and convex from side to side. The anterior region of the vertebral disc is thicker than the posterior region [48].

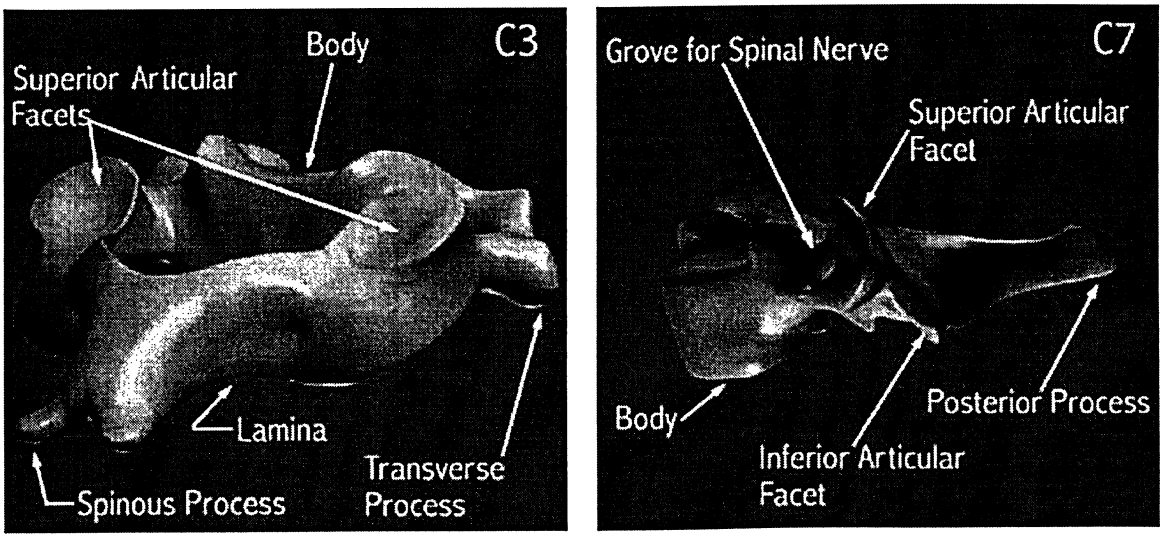

Figure 2: The typical vertebra of cervical spine, C3 to C7 [47].

2.2 Intervertebral Disc

The intervertebral disc fills the gap between the vertebral bodies (Figure 3). It is the largest avascular structure in the human body. It can be considered as a joint since movements of vertebrae against one another are only possible through the discs and the zygapophyseal joints (two paired processes of the neural arch of a vertebra that articulates with corresponding parts of adjacent vertebrae). Moreover, it contributes to the elasticity of the spine and acts as a shock absorber [46].

Each intervertebral disc has four components: nucleus pulposus at the interior of the disc, two cartilaginous end-plates on the facing vertebral surface, and annulus fibrosus [45]. The annulus fibrosus surrounds the area of the nucleus pulposus and consists of irregularly arranged lamellae encircling the area of the nucleus. The thickness of the

individual layers changes from 200 μm in the inner zones to 400 μm in the outer zones. The fibers of the individual layers make an angle of +30° and -30° with the horizon. The fibers contain 16% of the annulus volume [48]. The cartilaginous plates of the vertebral bodies form the anatomical border of the intervertebral disc [46].

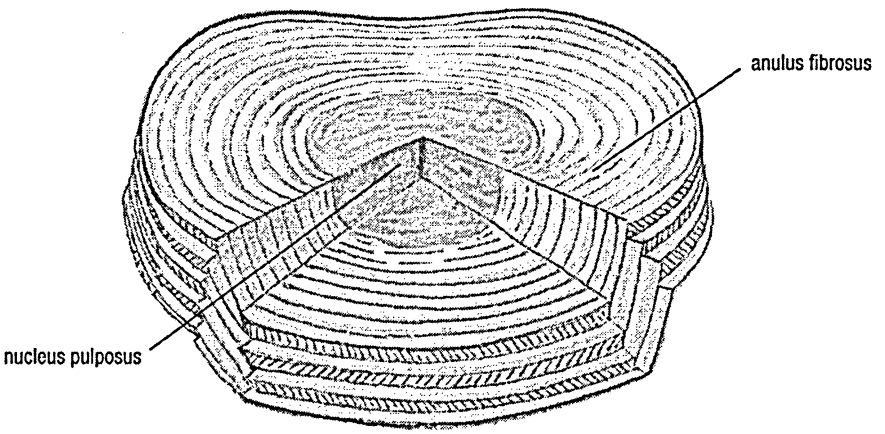

Figure 3: Anatomy of intervertebral disc [49].

2.3 Ligaments

Ligaments make the joints stable in the spine and restrict their motion. Figure 4 and Figure 5 demonstrate ligaments in the upper and lower regions of cervical spine. The lower cervical spinal ligaments are the anterior longitudinal ligament (ALL), the posterior longitudinal ligament (PLL), the capsular ligaments (CL), the ligamentum flavum (LF), the inter spinous ligaments (ISL), and the super spinous ligaments (SSL). The upper portions of these ligaments also belong to the upper cervical spine. Ligaments that belong specifically to the upper cervical spine (occiput, atlas and axis) are the apical ligament, the alar ligament, the transverse ligament (TL), the tectorial membrane (TM), the anterior atlanto-occipital membrane (AAOM), and the posterior atlanto-occipital membrane (PAOM). The PLL changes to TM from C2 to the occiput

and the ALL to the AAOM from C1 to the occiput [50]. Table 2 shows the list of the lower and upper cervical spinal ligaments.

Table 2: List of the lower and upper cervical spinal ligaments.

	Ligament	Mnemonic
The Lower Cervical Spinal Ligaments	Posterior Longitudinal Ligament	**PLL**
	Anterior Longitudinal Ligament	**ALL**
	Capsular Ligaments	**CL**
	Ligamentum Flavum	**LF**
	Interspinous Ligaments	**ISL**
	Superspinous Ligaments	**SSL**
The Upper Cervical Spinal Ligaments	Alar Ligament	**AL**
	Transverse Ligament	**TL**
	Tectorial Membrane	**TM**
	Anterior Atlanto-Occipital Membrane	**AAOM**
	Posterior Atlanto-Occipital Membrane	**PAOM**

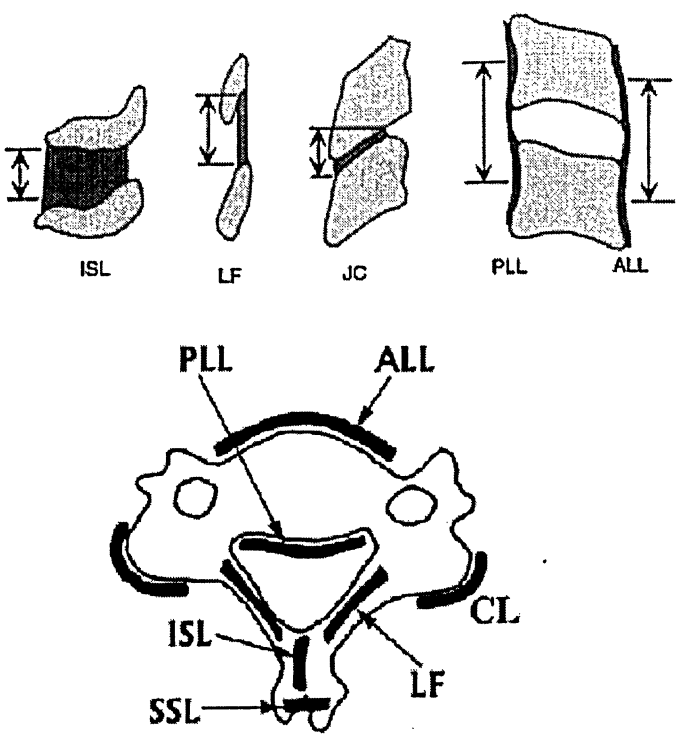

Figure 4: The lower cervical spine ligaments: Inter spinous ligaments (ISL), Ligamentum flavum (LF), Capsular ligaments (JC or CL), Anterior longitudinal ligament (ALL), Posterior longitudinal ligament (PLL), Superspinous Ligaments (SSL) [51].

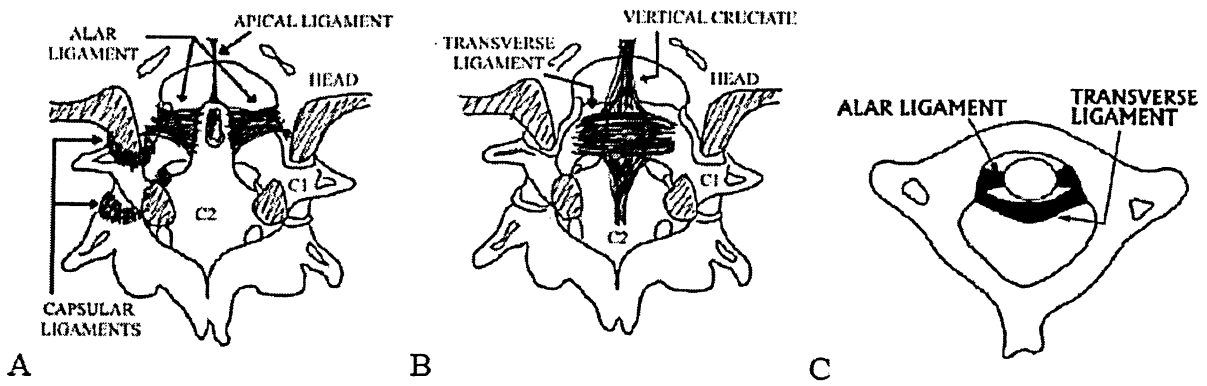

Figure 5: The upper cervical spine ligaments: Apical Ligament, Alar Ligament, Transverse Ligament (TL), Vertical Cruciate Ligament [51].

2.3.1 The Apical Ligament

The apical ligament locates posteriorly at the superior surface of the dens and on the occipital foramen. It is thin and V-shaped, with the fibers concentrated mainly in the middle. The purpose of apical ligament is to restrain motion of the cervical spine in flexion.

2.3.2 The Alar Ligament

The alar ligament constrains the axial rotation of the occipito-atlantal joint. Its origin is on the upper portion of the dens and the insertion is on the occiput [52]. The main fiber forming the alar ligament is collagen, thus it is an inelastic ligament with a large stiffness.

2.3.3 The Transverse Ligament

The transverse ligament's origin is on one side of the lateral masses of the atlas and the insertion is on the other, passing on the posterior side of the dens. It works as a constraining band on the dens, holding it against the anterior ring of the atlas, therefore preventing movement of the dens toward the spinal cord. The transverse ligament has two vertical extensions: an upward projection to the occiput and a downward prolongation to the vertebral body of the axis. These vertical fibers are named the vertical cruciate and control

the flexion of the head (Figure 5). The transverse ligament fibers are mainly made of collagen, as the alar ligaments [53].

2.3.4 The Anterior Longitudinal Ligament and the Anterior Atlanto-occipital Membrane

The ALL tightly attaches to the anterior surface of the vertebral bodies and the discs between them. It is a broad ligament whose thickness reduces at the C1-C2 level. The ALL changes its name to the anterior atlanto-occipital membrane at the C0-C1 level [50].

2.3.5 The Posterior Longitudinal Ligament and the Tectorial Membrane

The PLL extends on the posterior surface of the vertebral bodies. The PLL runs along the spine up to the C2 vertebra. The TM prolongs between C2 and the occiput, as a continuation of the PLL.

2.3.6 The Ligamentum Flavum

The ligamentum flavum links adjacent lamina and is placed within the spinal canal, on the posterior surface. Unlike most ligaments, it contains a high concentration of elastin fibers, thus, it is a tough ligament.

2.3.7 The Supraspinous and Interspinous Ligament

The SSL and ISL join the spinous processes of adjacent vertebrae. They constrain extension of the spine. The SSL does not appear in the upper cervical spine, while the ISL exists at the top level (C1-C2).

2.3.8 The Capsular Ligament

The CL links two adjacent facet joint surfaces. One of their main functions is to keep the synovial fluid inside the joint. The CL is a thin and loose ligament, especially in the occipito-atlantal (C0-C1) and atlantoaxial (C1-C2) joints.

2.4 Muscles

Muscles perform three tasks in the human neck. Firstly, muscles provide stability to the neck and head in a certain posture. Secondly, they enable movement of the head during physiological activity. The third task is to assist in the protection of the cervical spine [54,55,56].

Despite the importance of including muscles in the cervical spine area to develop the finite element model of the head and neck, not many researchers have considered them in their finite element models. Therefore, finding the geometrical properties of the muscles in this area is not clearly reported in the literature, and the material properties of the muscles are rarely mentioned. The functions as well as origins and targets of the main muscles in the area are briefly discussed below.

2.4.1 Rectus Capitis, Obliquus Capitis, Sternocleidomastoid

Examples of muscles that can be represented by straight lines connecting points of origin to points of insertion are the suboccipital muscles, rectus capitis posterior major and minor and obliquus capitis superior, which arise on the first or the second cervical vertebra and insert into the skull, and the obliquus capitis inferior, which arises on the second cervical vertebra and inserts into the first (Figure 6). Likewise, the anterior vertebral muscles rectus capitis anterior and rectus capitis lateralis, which originate on the atlas and insert into the skull, can be represented by straight lines. The sternocleidomastoid, which passes obliquely across the side of the neck, arises by two heads-the medial or sternal head from the ventral surface of the manubrum sterni and the lateral, or clavicular head from the superior border and anterior surface of the medial third of the clavicle to the mastoid process of the skull (Figure 7). This

muscle is modeled by two lines – one from the thorax and one from the clavicle, both inserting into the skull.

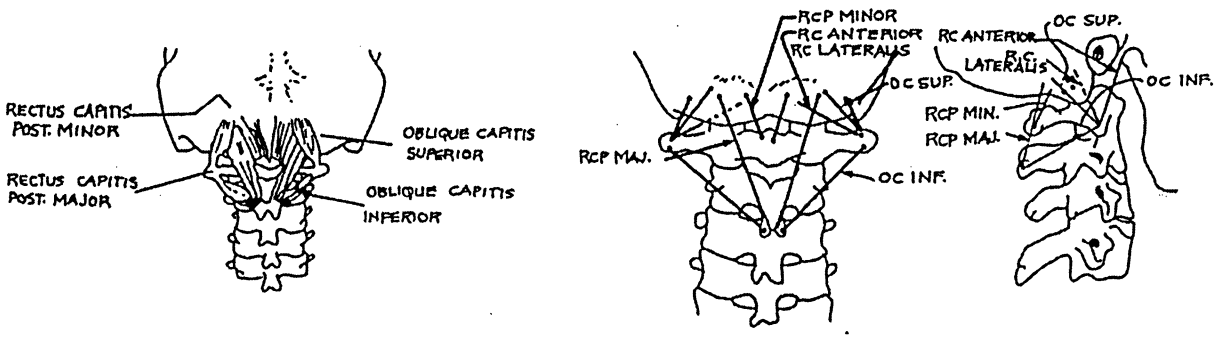

Figure 6: The suboccipital muscles, rectus capitis posterior major and minor and obliquus capitis superior and inferior [56].

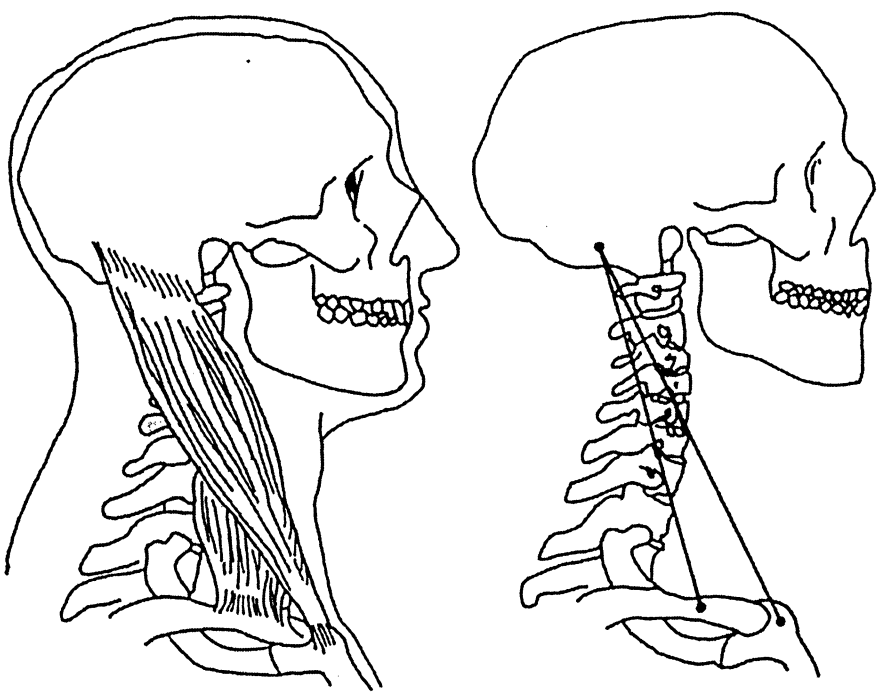

Figure 7: Muscle model for Sternocleidomastoid[56].

2.4.2 Sternothyoidus, Sternothyroideus

The infrahyoid muscles, sternothyoidus and sternothyroideus, spanning the hyoid bone and the thorax may assist the anterior vertebra neck muscles by keeping the hyoid bone fixed. It was decided, therefore, to include these muscles in the model even though they are primarily responsible for the actions of the larynx and hyoid. The sternohyoideus arises from the posterior aspect of the sternal end of the clavicle and from the back of the manubrium sterni and inserts into the lower border of the body of the hoyid bone. It is modeled by two lines-one from the thorax and one from the clavicle both inserting into the hyoid bone, which is assumed to be intergral with the skull. Similarly, the sternothyroideus, which arises from the dorsal surface of the manubrium sterni and the cartilage of the first rib and inserts into the lamina of the thyroid cartilage, is modeled by a line connecting the thorax to the thyroid cartilage, which is also assumed to be integral with the skull.

2.4.3 Longus Colli

The longus colli lies on the anterior surface of the vertebral column between the first cervical vertebra and the third thoracic vertebra and consists of three portions. The superior oblique portion arises from the anterior tubercles of the transverse processes of vertebrae C3 to C5 and inserts on the anterior tubertcle of the atlas (C1) and the body of the axis (C2). Consequently, this part of the muscle is modeled by six lines, a set of three from C3, C4 and C5, respectively, connected to C1, and another set of three from the same three vertebrae connected to C2.

The inferior oblique portion arises from the bodies of vertebrae T1 to T3 and inserts into the anterior tubercles of the transverse processes of the fifth and sixth cervical vertebrae.

This part is modeled by two lines: one line from the thorax between T1 and T3 going to C5 and another line from the same location going to C6.

The vertical portion of the longus colli arises from the anterior surface of the bodies of the upper three thoracic and the last three cervical vertebrae and insets into the anterior surface of the bodies of the first four cervical vertebrae. Consequently, the muscle is represented by sixteen lines: four sets of four each from C5, C6, C7 and the thorax (between T1 and T3), respectively, connected to C1, C2, C3 and C4, respectively. The muscle model for the longus colli is illustrated in Figure 8.

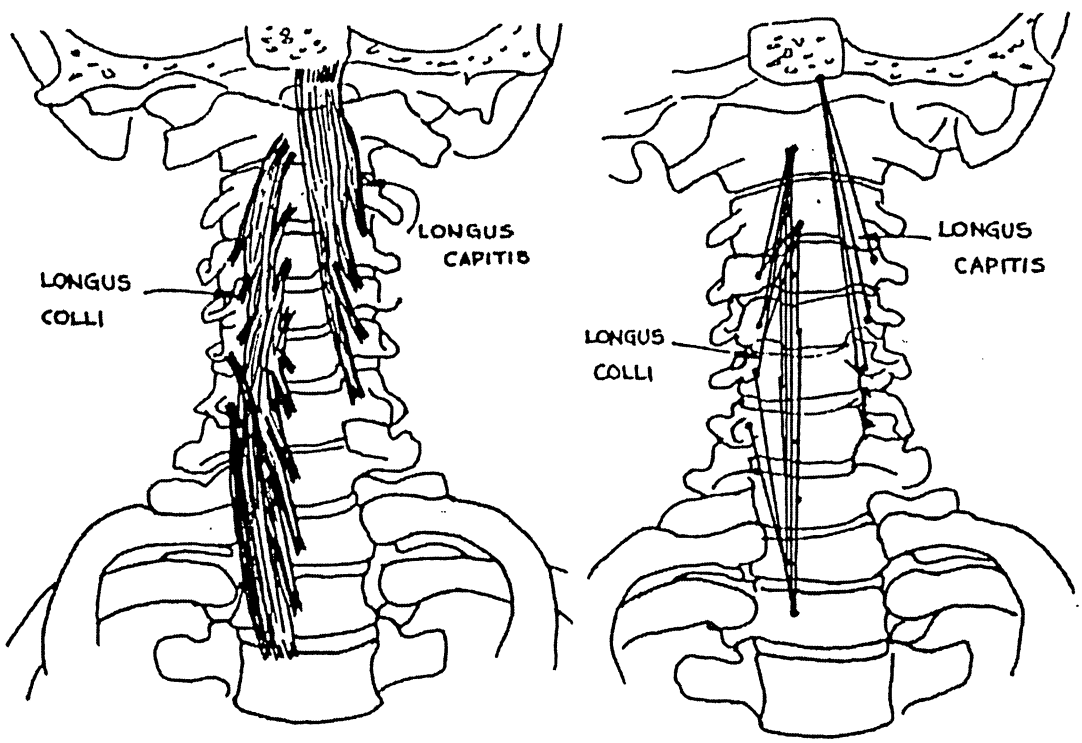

Figure 8: Muscle models for Longus colli and Longus capitis [56].

2.4.4 Longus capitis

The longus capitis arises from the anterior tubercles of the transverse process of the vertebrae C3 to C6 inclusive and inserts into the inferior surface of the basilar part of the occipital bone in the skull (Figure 8). The muscle can be modeled by four lines from C3, C4, C5 and C6 vertebrae respectively, and are connected to the skull.

2.4.5 Scalenus

The scaleni are three lateral vertebral muscles; anterior, medius and posterior. The scalenus anterior originates from the anterior tubercles of the transverse processes of the vertebrae C3 to C6 and insets into the scalene tubercle on the inner border of the first rib. It is represented by four lines from the four cervical vertebrae (C3-C6) joining the thorax. The scalenus medius, which arises from the posterior tubercles of the transverse processes of all the cervical vertebrae and inserts into the first rib, is modeled by seven lines, one each from the seven cervical vertebrae joining the thorax. Finally, the scalenus posterior, which takes its origin from the posterior tubercles of the transverse processes of the last three cervical vertebrae and inserts into the outer surface of the second rib, is conveniently modeled by three lines connecting the three cervical vertebrae (C5-C7) to the thorax (Figure 9).

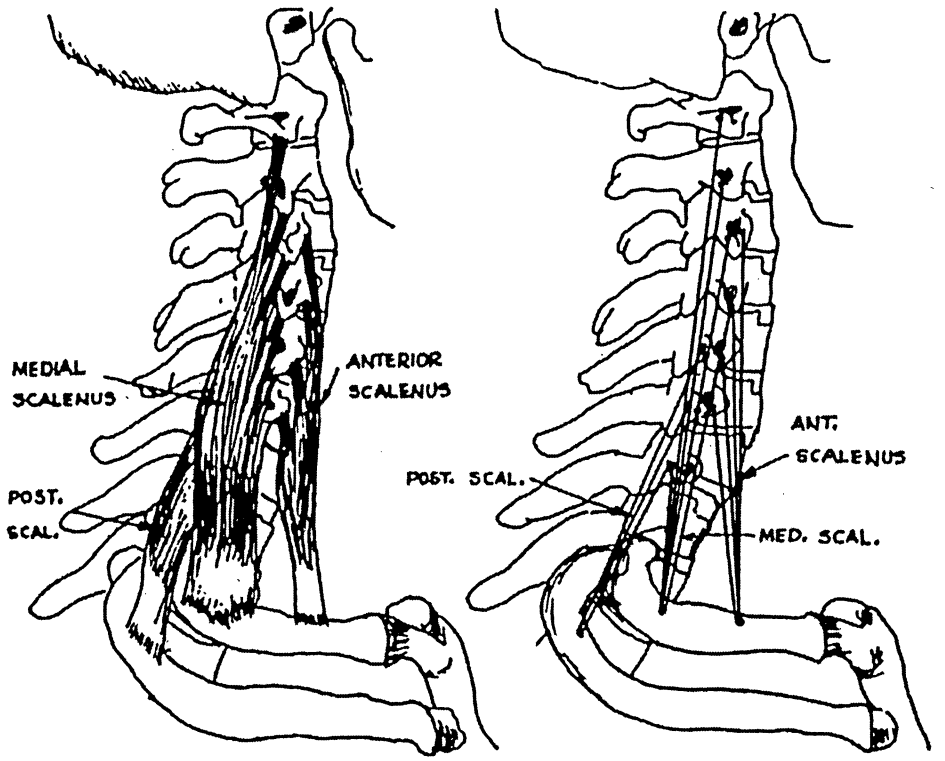

Figure 9: Muscle models for scalenus anterior, medial and posterior [56].

2.4.6 Semispinalis Capitis, Splenius Capitis, Longissimus Capitis

These muscles in general originate on the cervical and thoracic vertebrae and insert into the skull. For example, the semispinalis capitis takes origin from the transverse processes of the upper six thoracic vertebrae and the articular processes of the lower four cervical vertebrae and inserts into the occipital bone of the skull. The part of the muscle with wide thoracic origin is represented by one line connecting the thorax to the skull, best representative of the expansive origin from the upper six thoracic vertebrae. In this manner, inclusion of excessive lines of action (from each of the thoracic vertebrae) is not necessary and the number of lines in the muscle model may be kept to a minimum without mitigating the function of the entire group. This technique will be adopted from the modeling of all the muscles with extensive origin from the thoracic vertebra. The remainder of the

semispinalis capitis arising from the lower four cervical vertebrae is modeled by four lines connecting these bodies to the skull (Figure 10 and Figure 11).

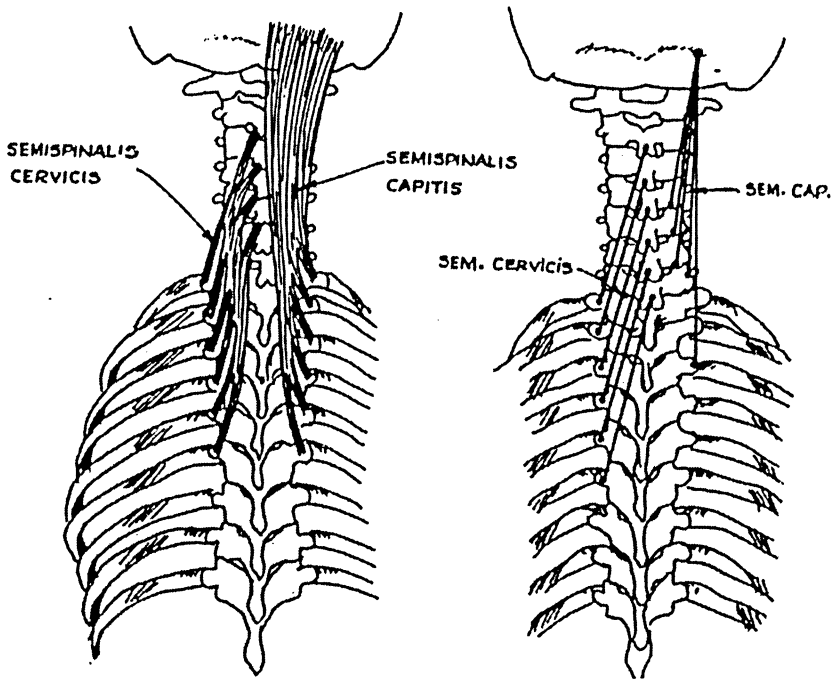

Figure 10: Muscle models for semispinalis capitis and cervicis [56].

The splenius capitis and the longissimus capitis, which arise on the cervical and thoracic vertebrae and insert into different regions of the skull, are also modeled in the same fashion.

2.4.7 Iliocostalis Cervicis, Splenius Cervicis, Semispinalis Cervicis and Longissimus Cervicis

With the exception of the iliocostalis cervicis which arises from the angles of the ribs, all of these muscles arise from different parts of the cervical and thoracic vertebral regions of the spinal column and inset either into the spinous processes or into the posterior tubercles of the transverse processes of the cervical vertebrae. They are all modeled by several lines connecting their origins on the thorax (or on the cervical vertebrae) to their insertions on the cervical vertebrae (Figure 10 and Figure 11).

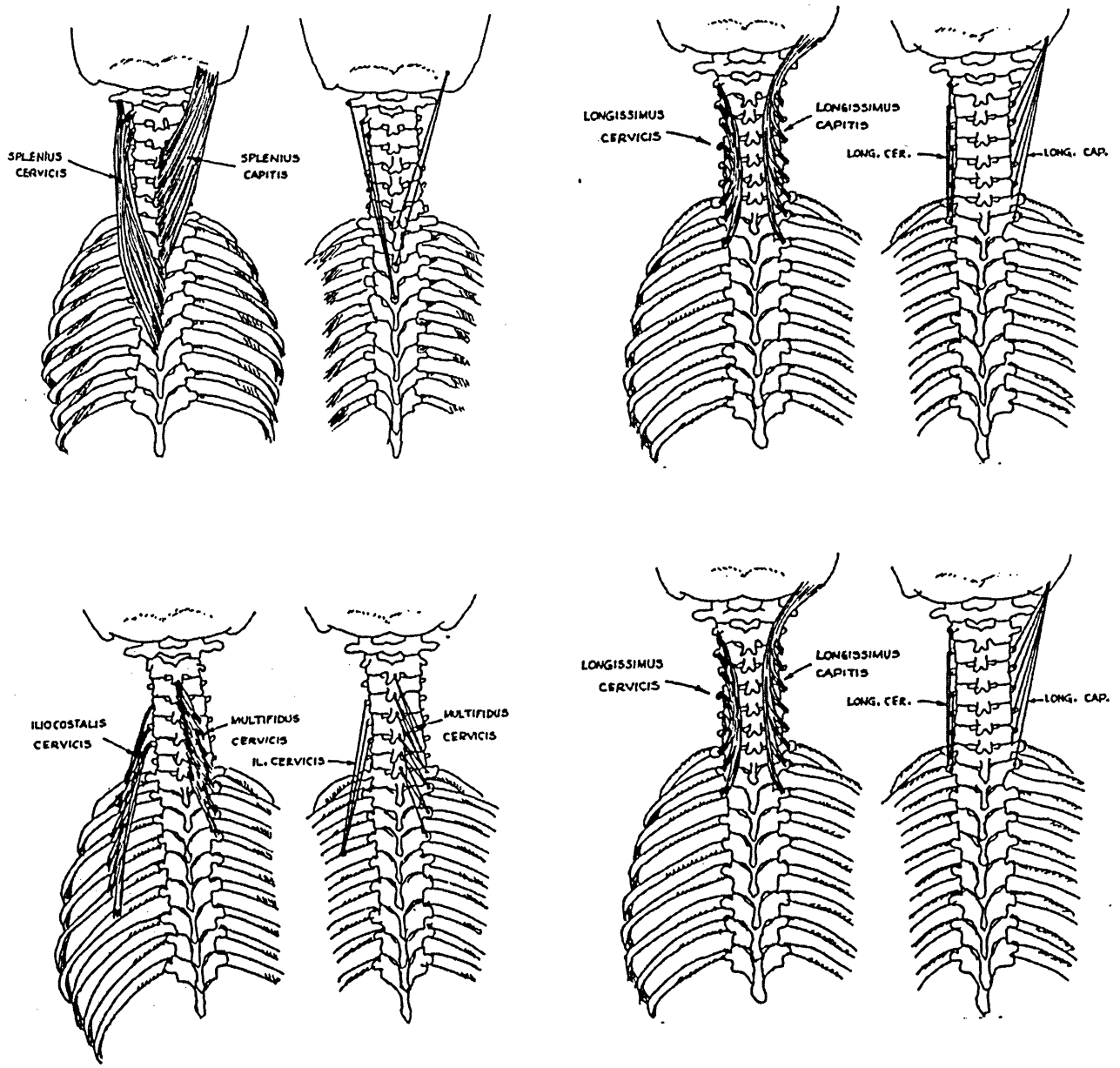

Figure 11: Muscle models for splenius and longissimus capitis and for splenius, longissimus, Iliocostalis and multifidus cervicis [56].

2.4.8 Multifidus and Rotatores

The multifidus cervicis and lumborum, and rotatores cervicis and lumborum are actually prolongations of the multifidus and rotatores muscles. They belong to the transversospinal muscle group with origins in transverse processes and insertions in

spinous processes of the vertebrae. The multifidus extends throughout the length of the vertebral column, its transverse attachments being to transverse processes in the thoracic region to articular processes at cervical levels, and to mammillary processes at lumbar levels. Its lowest fibers originate from the posterior surface of the sacrum and its highest origin is on the fourth cervical vertebra. The fibers of multifidus ascend obliquely to insert two to four segments above their origin into the spinous processes of all vertebrae from the last lumbar to the axis. Accordingly, the cervicis portion of this muscle is modeled by twelve lines, each with two inserting into the spines of each of the six cervical vertebrae C2 through C7 inclusive. Their corresponding origins lie two and three segments below these insertions (Figure 12).

The rotatores muscles are the shortest representative of the transversospinal group. Their general plan of attachment is similar to the multifidus described above their origin (rotatores breves) or the second vertebral spine above their origin (rotatores longis). Consequently, the cervicis portion of the rotatores muscles is modeled by eleven lines. There is a pair of lines from each of the four cervical vertebrae C4 to C7 inclusive, and from the first thoracic vertebrae T1, inserting into the spines of the first and second segment above their origins. The inferior portion of the muscle is represented by a line connecting the second thoracic vertebra T2 to the last cervical vertebrae, C7.

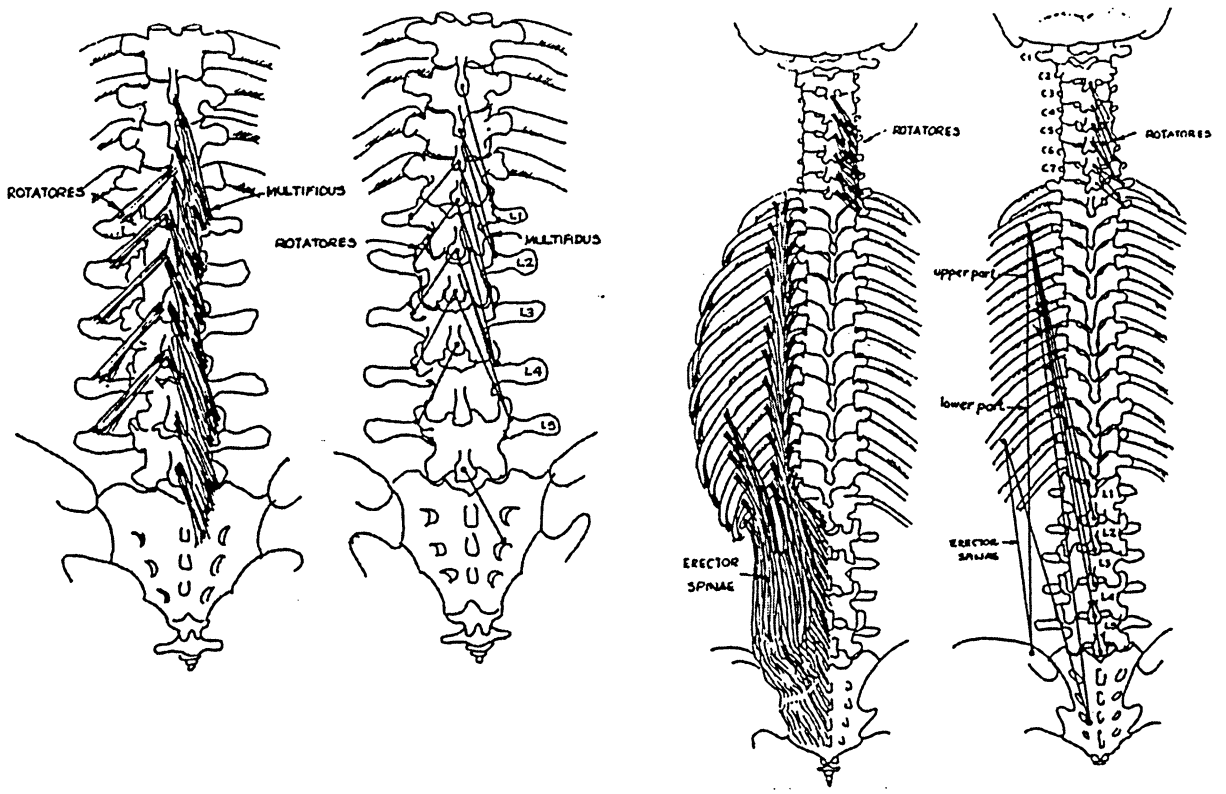

Figure 12: Muscle model for Rotatores cervicis and lumborum [56].

2.4.9 Trapezius

The trapezius is a flat, triangular muscle placed superficially on the upper back and the back of the neck. It takes origin of the skull from the external occipital protuberance and the medial part of the superior nuchal line from the ligamentum nuchae (ligament joining the spines of the cervical vertebrae), from the spine of the seventh cervical vertebra and the spinous processes of all thoracic vertebrae. The fibers converge laterally towards the point of the shoulder for insertion. The occipital and upper cervical fibers are inserted in the posterior margin of the outer third of the clavicle; the lower cervical and the crest of the spine of the scapula, and the lower thoracic fibers converge to insert into the tubercle of the crest of the spine of the scapula, and the lower thoracic fibers converge to insert

into tubercle of the crest of the spine of the scapula. The model for trapezius muscle is shown in Figure 13.

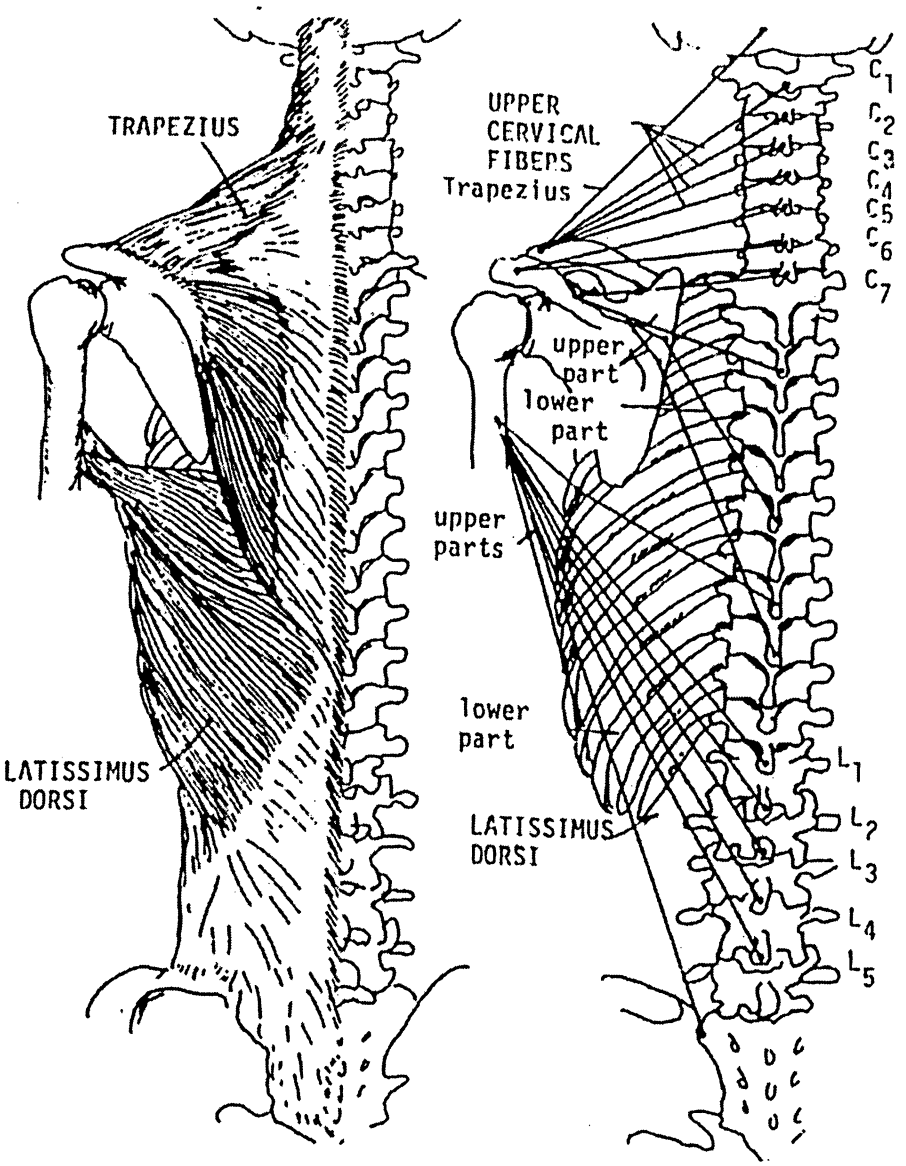

Figure 13: Muscle models for trapezius muscles [56].

The clavicular part of the muscle is shown by lines from the skull and the upper four cervical vertebrae going to the clavicle. The scapular part of the muscle is modeled as:

a) Two lines from the vertebrae C5 and C6 respectively, connected to the acromion of the scapula.

b) A line from C7 representing fibers originating from T1 through T3, both joining the middle of the spine of the scapula.

2.4.10 Rhomboideus

The rhomboideus major and minor arise from the lower part of ligamentum nuchae, the spines of the last cervical and the upper five thoracic vertebra. The fibers pass downward and laterally and insert into the medial border of the scapula below the root of the spine. The muscles are modeled by five lines, two from the spines of the cervical vertebrae C6 and C7 and three from the thoracic spines.

2.4.11 Levator scapulae

The levator scapulae arises from the transverse processes of the atlas and axis and from the posterior tubercles of the transverse processes of the third and fourth cervical vertebrae and inserts into the vertebral border of the scapula from the superior angle to the spine. The muscle is modeled by four lines; a line each from the four cervical vertebrae C1 through C4, joining the scapula (Figure 14).

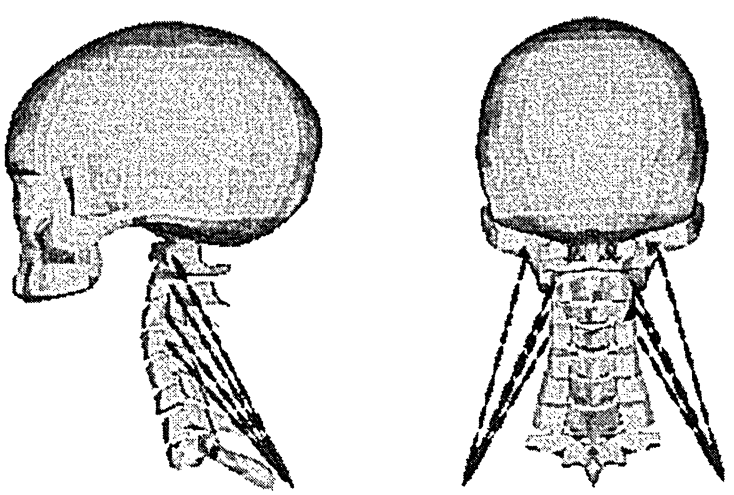

Figure 14: Muscle models for levator scapulae[55].

2.5 Joints

In the upper cervical spine there are two kinds of joints, the occipito-atlantal joint and the atlantoaxial joint. These joints are different from those in the lower cervical spine, since in this level there is no disc between vertebrae. The occipito-atlantal joint is more flexible in flexion-extension motion of the head. The main function of the atlantoaxial joint is to allow axial rotation of the head. Lateral bending is distributed between the spinal joints [57].

2.5.1 The Occipito-atlantal Joint

The occipito-atlantal joint is where the occipital condyles on the skull base sits on the superior facet surfaces of Atlas. The absence of a vertebral body on C1 and the structure of the joint surfaces form considerable mobility in flexion-extension of this joint [57].

2.5.2 The Atlantoaxial Joint

The atlantoaxial joint is made of three synovial joints between Atlas and Axis. The superior facet surfaces of Axis and the inferior facet surfaces of Atlas form two facet joints; the third joint is between the anterior arch of Atlas and the dens. This joint enables the axial rotation of the head, as Atlas rotates around the dens on Axis [57].

2.5.3 The Lower Cervical Spine Joints

The joint between C2 and C3 is the same as the joints in the lower cervical spine (C3-C7). In this area, there are two joints: two posterior facet joints which are called zygapophyseal joints and an intervertebral disc. The intervertebral disc is called a fibro-cartilaginous joint [57].

CHAPTER 3

CERVICAL SPINE INJURY

Many experimental analyses have been conducted on the cervical spine using physiological loading modes such as flexion, extension, axial rotation and lateral bending to find out the causes of cervical spine injury. Roberge et al. [58], Lowery et al. [59] and Holly et al. [60] reported cervical spine injuries from patients attending emergency hospitals. There are a few analyses of neck injuries in traffic accidents, such as research works by Thorson [61], Huelke et al. [62], Krantz [63], Yoganandan et al. [64]. The causes of cervical injuries reported by these researchers will assist in both designing preventive devices and treatment methods. Having knowledge of cervical injury helps physicians to avoid aggravating the injury by applying forces that increase the instability of cervical spine.

The type and degree of cervical spine injury may be influenced by clinical factors that are deduced from a variety of historic and radiologic evidence. The methodology of the clinical studies are different from laboratory investigations, which are controlled and carefully observed, whereas, the clinical situation is uncontrolled and frequently unobserved.

3.1 Background

Cervical spine injuries are more often connected with spinal cord injuries than the lower spinal regions [64]. There is also a strong connection between head and face trauma and neck injuries [60]. Based on the research work published by Yoganandan et al. [64] in the cervical spine, the craniocervical junction (Occiput–C2) and the C5-C6 motion segment are the primary locations of cervical injury. The craniocervical junction is at risk of injury because of the flexibility of the upper cervical spine. The most inferior motion segments are vulnerable because the stiffness changes between the cervical spine and the thoracic spine. Brolin et al. [65] showed that older people are more at risk of upper cervical injuries rather than lower cervical injuries.

Cervical spine injuries can be classified into two major categories: vertebral fractures and soft tissue injuries [66]. Neck injuries are usually addressed by the physiological loading modes, which are the motions of the head relative to the cervical spine. This statement is not always true, as the local loading modes between the two consecutive vertebrae may differ from the global motion. For instance, a compression loading of the head may cause local compression, flexion, and extension loading in different motion segments. Figure 15 illustrates the four global motions of cervical spine and Figure 16 shows the corresponding local loading modes. Another way of classifying cervical injuries is through the Abbreviated Injury Scaling (AIS), where AIS 0 means there is non-injury and AIS 6 means a serious injury.

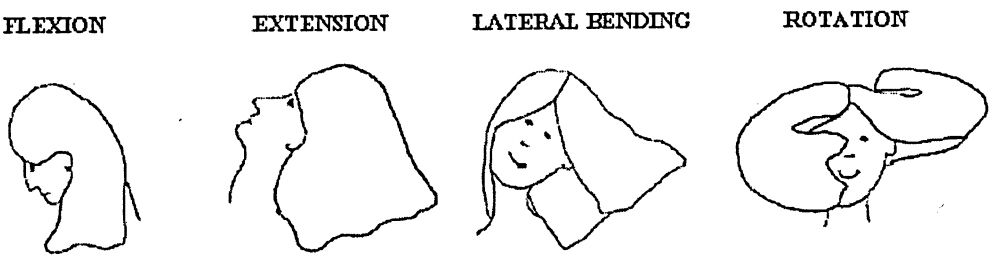

Figure 15: Global motions of the head compared to the torso [51].

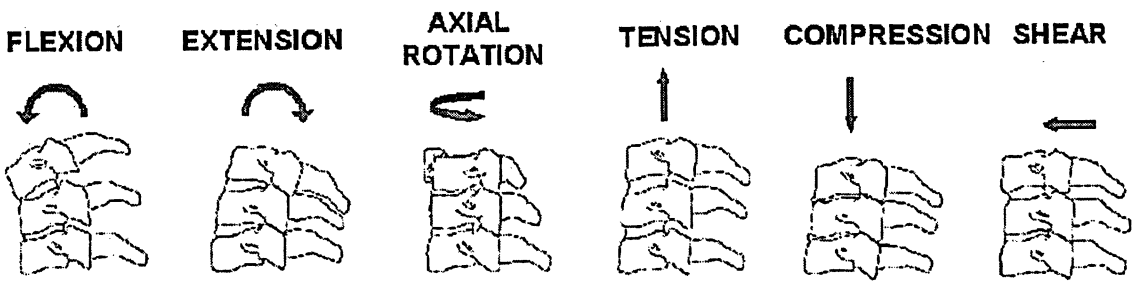

Figure 16: Local motions of lower cervical spine segments, due to different loading modes [51].

Clinically, spinal injury is defined in terms of spinal stability. An unstable cervical spine threatens the spinal cord and medical treatment is required to decrease the risk of spinal cord injury. A stable spine can protect the spinal cord under normal physiological load modes and less medical care is needed. It is important to differentiate between the medical meaning of spinal stability and the mechanical meaning. There are two major types of spinal instability, acute and chronic instability. For injuries with acute instability even small spinal movements can cause spinal cord damage. An injury with chronic instability is considered stable from the beginning but it may lose stability over time; therefore the spinal cord injury may happen many years after the first accident.

The main reason for acute injuries is the drastic change in column stiffness (fracture, dislocation, ligamental compromise, etc.). Instability has been defined in anatomical,

biomechanical, and clinical terms, but because of the variability of clinical presentations instability should be defined in anatomical terms [67,68]. The various components of the cervical spine may result in deformation, either acute or chronic, under physiological loads. Larson [67,68] has demonstrated that a stable spinal column is symmetric in movement and configuration, whether normal or abnormal, and stays the same forever. To consider spinal instability, it is important to review the column theory of vertebral stability [67,68]. The two- or three-column models of Denis [69], Holdsworth [70], Louis [71] and White [72] are commonly used to evaluate the mechanical integrity of the spinal column. Figure 17 presents the two-column model of the cervical region, where the anterior column consists of vertebral bodies, intervertebral discs, and anterior and posterior longitudinal ligaments, whereas the posterior column consists of zygapophysial joints, capsular ligaments, spinous processes, and lamina and interspinous ligaments. The degree of injury in soft tissues (ligaments, discs, etc.) and bony components of a column will assist researchers to determine the risk to the neural structure of the cervical spine from changes in curvature or alignment. Although considering a middle column theoretically is important in thoracic and lumbar injuries, it is not as important in the cervical area and it is reasonable to use the two-column model in the cervical area.

The degree of instability has an important influence on the risk of neurologic injury and, therefore, determination of the degree of component injury and a more accurate measurement of displacement will assist in the evaluation of the threat to neurologic integrity [73].

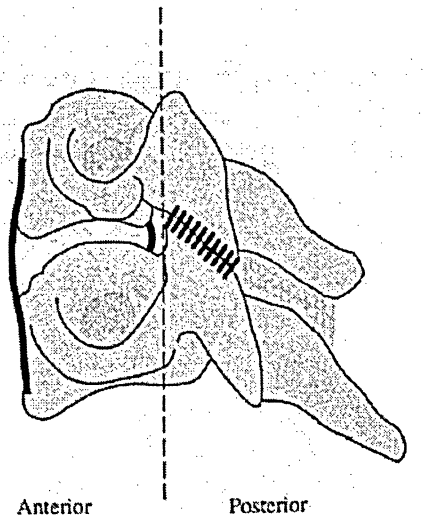

Figure 17: The two-column model of the cervical region [74].

Since it is not possible to cover all neck injury research, this chapter gives a brief overview of some of the most common neck injuries and their injury mechanisms.

3.2 Atlas Fractures

The multi-fracture of the first cervical vertebra is often called Jefferson's fracture, although Jefferson's fracture is known as a four-part fracture [75]. This injury can be serious as the nerve roots leaving the spinal canal at this level are mainly in control of the autonomous systems such as heart functions and breathing. Atlas fractures are generally classified into three categories; Type I fracture is classified as a single arch fractures, where either the posterior or the anterior arch is intact. As it is shown in Figure 18, Type II fracture has both posterior and anterior arch fractures. In Type III fracture, besides posterior and anterior arch fractures, fracture of the lateral masses is included [76]. The Type III fracture is generally classified by the displacement of the lateral masses of Atlas, rather than the number of fractures [76,77].

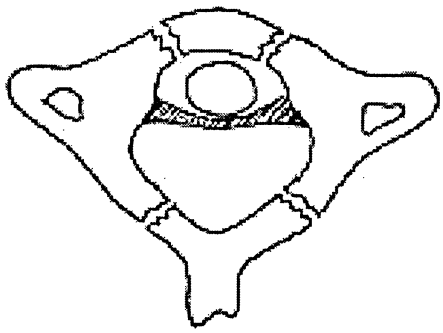

Figure 18: Atlas fracture, type II [51].

The overall situation of the transverse ligament is crucial for the stability of these types of fractures. If the transverse ligament is not damaged the fracture is considered stable, while a combination of fracture and rupture of the transverse ligament is determined as an unstable injury. Lateral mass displacement larger than 5-7 mm can cause a transverse ligament rupture and consequently spinal instability [78,79].

3.3 Axis Fractures

Axis fractures can cause death immediately after occurrence of the accident; and therefore not be considered in statistical studies [80]. Axis fractures can be divided into three major types: dens fracture, hangman's fracture, and vertebral body fractures.

3.3.1 Dens Fracture

The dens fracture or odontoid fracture is a fracture happening to the odontoid process. This type of fracture is divided into three major groups: Type I, II, and III (Figure 19). The local shear loading between C1 and C2 is the main reason of dens fracture. The source of local shear at this level can be global shear or extreme flexion, extension, or axial rotation. According to Graham et al. [18], lateral loading of the dens or the C1, applied either from global lateral bending or axial rotation will cause Type II fractures.

They also demonstrated that global extension is the source of Type III fractures. The Type II odontoid fracture is the most common fracture of Axis and at the same time the most difficult one to treat [80]. According to Green et al. [80], the Type III odontoid fracture is more stable than the Type II fractures.

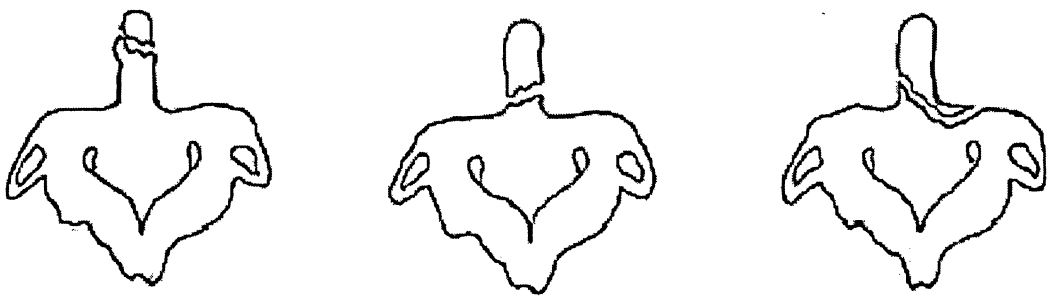

Figure 19: Dens fractures, type I, II and III [51].

3.3.2 Hangman's Fracture

Hangman's fracture is the fracture of the pedicles in the posterior arch of Atlas (Figure 20). This injury mainly occurs as the result of either tension or tension-extension loading. However, it can also be caused by a flexion-compression loading [18,75].

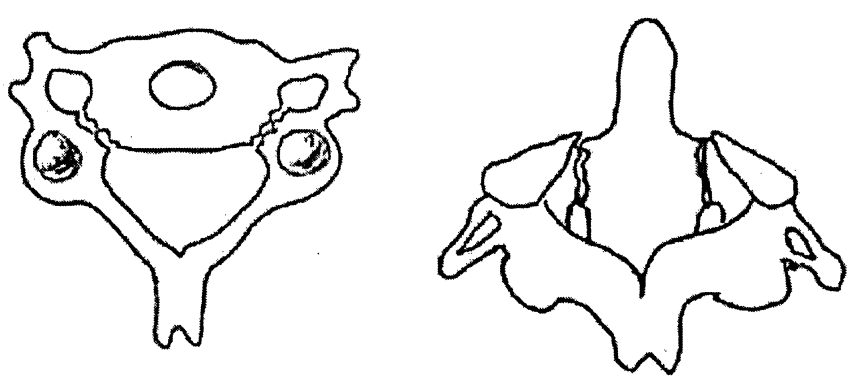

Figure 20: Hangman's fracture, superior and posterior view of C2 with fractured pedicles [51].

3.4 Lower Cervical Spine Fractures

3.4.1 Burst Fracture

The burst fracture is distinguished as fracture of the vertebral body into several smaller pieces (Figure 21A). This injury is usually associated with fractures of the endplates and rupture of the intervertebral disc. Burst fracture often causes neurological injuries, as the broken pieces of bone can penetrate into the spinal cord [75,79,81]. Strong axial compressive forces applied to the vertebral body are assumed to be the source of burst fracture [20].

3.4.2 Teardrop Fracture

The teardrop fracture is recognized by a triangular shaped bone fragment that separates anteriorly from the inferior area of the vertebral body (Figure 21B). The injury is extremely unstable in extension, since the anterior longitudinal ligament is ruptured. It is considered stable in flexion because the posterior ligaments are intact [79,82].

3.4.3 Wedge Fracture

The wedge fracture is characterized as a fracture of the anterior segment of vertebral body (Figure 21C). Strong flexion moment and compression forces on the vertebral motion segment produce this type of injury. According to Carter et al. [83] slow compressive loading can cause wedge fractures, while a sudden quick loading develops burst fractures. If the ligaments are not injured, the wedge fracture is considered stable injury.

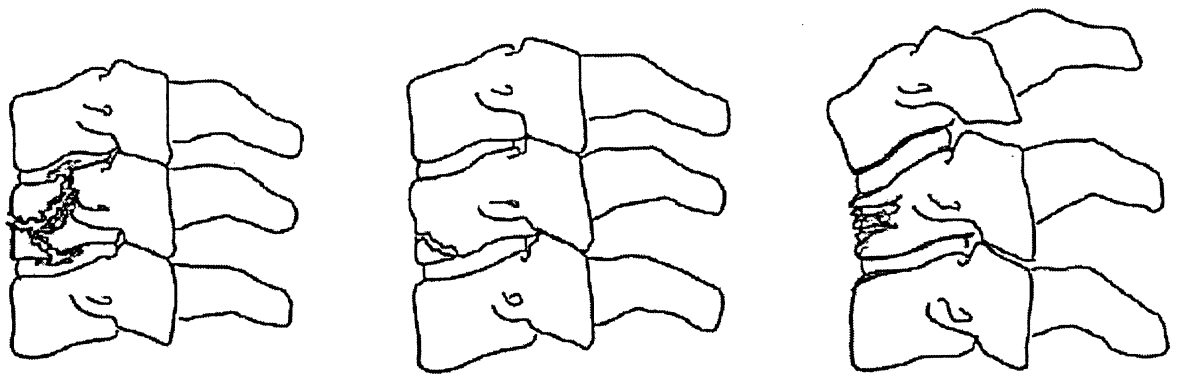

Figure 21: Lower vertebral fractures: A) Burst fracture, B) Teardrop fracture, C) Wedge fracture [51].

3.4.4 Posterior Element Fracture

Fracture of the posterior elements of the cervical spine occur throughout the upper and lower cervical spine. This injury can cause single or multiple fractures (

Figure 22). These fractures can be observed in the laminae, the pedicles, the spinous processes, and the facet joints. If this injury is associated with vertebral body displacement it is highly unstable and requires internal fixation of several motion segments [79]. According to McElhaney et al. [75] posterior element fracture is the result of bony contact between adjacent posterior elements, caused by extreme local extension. The local extension may appear in global extension, flexion, or compression of the neck.

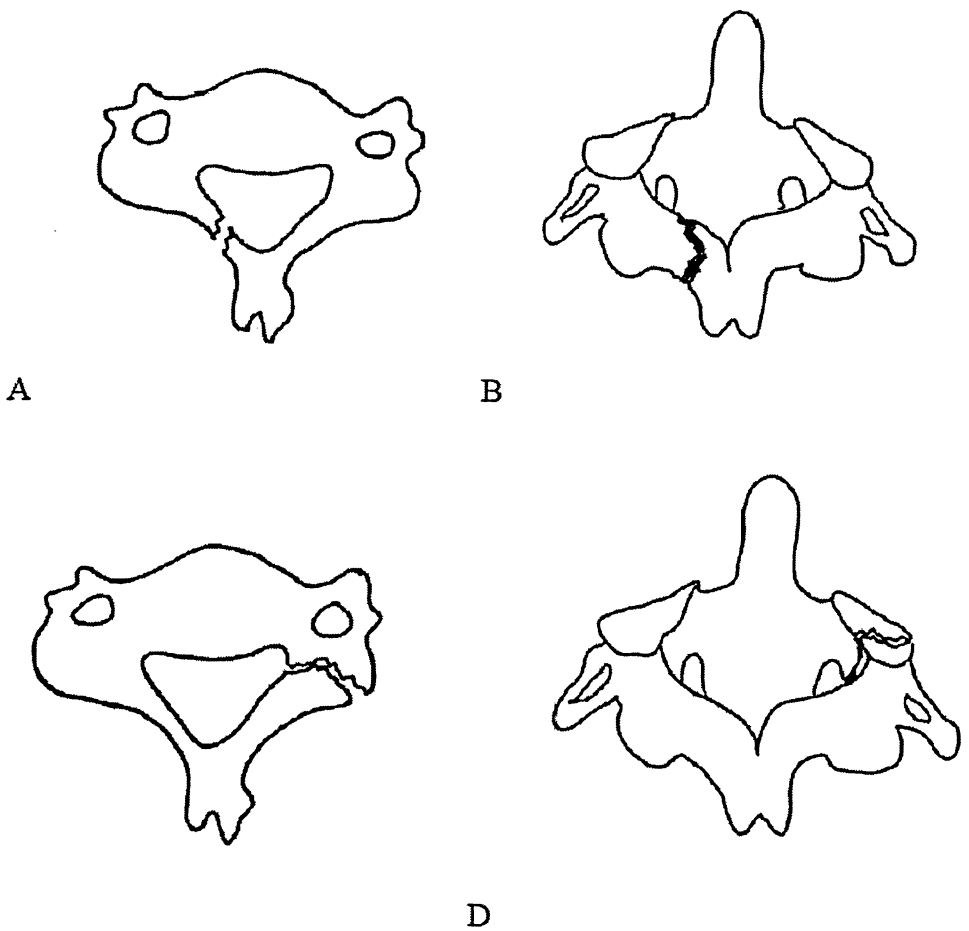

Figure 22: Posterior element fracture. Fracture of spinous process: (A) superior view and (B) posterior view. Fracture of the lamina: (C) superior view and (D) posterior view [51].

3.5 Soft Tissue Injuries

3.5.1 Facet Dislocation

Facet dislocation occurs in the cervical spine when the superior vertebra is dislocated anteriorly compared to the inferior vertebra (Figure 23). In this injury, one or both of the facet joints can be dislocated. If both of the facet joints dislocate, the spinal canal diameter reduces significantly, thus it can be associated with spinal cord injuries. The facet dislocations are frequently combined with facet fractures; therefore, the treatment methods will be complicated. It is suggested by An [6] that local tension-flexion can produce this injury, while McElhaney et al. [75] believe that compression-flexion with tensile strains in the posterior ligaments is the source of facet dislocation.

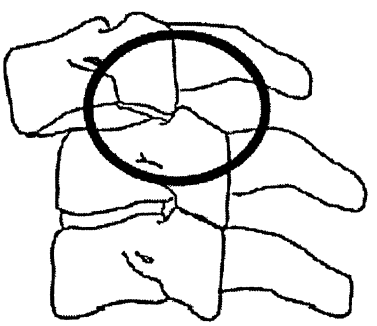

Figure 23: Facet dislocation between two vertebrae in the lower cervical spine [51].

3.5.2 Rupture of Ligaments

Large tensile strains are the main reason for ligament ruptures. The injury begins with failure of some of the collagen fibers and if the tensile loading increases the elastin fibers will start to break, until complete rupture of the ligament occurs. As can be predicated, global extension motions can damage the anterior ligaments, while posterior ligament ruptures occur in global flexion [84]. The load required to cause rupture varies for different

ligaments and factors such as size, proportion of collagen and elastin fibers, fiber organization and ligament position are significantly affected [85].

Alar ligament failure allows more axial rotation in the cervical spine combined with relative motion between the atlas and axis; thus resulting in spinal cord compression. Transverse ligament rupture causes spinal instability, as there would be no restraining ligament keeping the odontoid process in contact with the anterior segment of Atlas. Rupture of other ligaments in the cervical region can cause spinal instability if associated with other injuries.

3.5.3 Subfailure of Ligaments

Subfailure of ligaments occurs when the cervical ligaments undergo extensive stretch. Consequently, some of the collagen fibers may break with no noticeable influence on spinal stiffness. This is associated with injury of some of the neural cells on the ligaments. The damaged cells will send inappropriate signals to the spinal muscles, causing them to react abnormally.

3.5.4 Rupture of the Disc

Rupture of the intervertebral disc or herniation of the disc occurs when the disc contents protrude through an opening in the wall of the disc. If the outer surface of disc cracks or breaks, the nucleus may leak out. Intervertebral disc trauma is frequently followed by vertebral body fractures [84]. Compression in combination with flexion or extension may cause this type of injury.

Figure 24 illustrates four variations of disc disorder. The first case indicates a crack in the annular wall. In the second case a bulging disc is shown. It is essential to notice that the annular wall has been deformed but not broken yet. A bulging disc may be followed by a

herniation. When a disc herniates, the nucleus leaks into the spinal canal, leading to the compression of sensitive nerve roots. In addition, the nucleus releases a chemical substance that temporarily irritates surrounding nerve structures causing inflammation and pain.

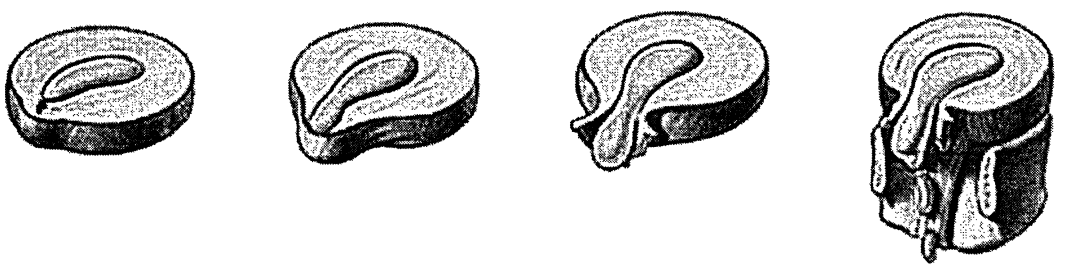

Figure 24: Four variations of disc disorder [86].

CHAPTER 4

SOFT TISSUE MODELING

Soft tissues are different from other body tissues like bones because of their flexibility and soft mechanical properties. Generally speaking, soft tissues are described as quasi-incompressible, non-homogeneous, anisotropic, non-linear viscoelastic materials in large deformation [87]. The general method to describe the model of soft tissues is a combination of continuum associated with stress-strain constitutive relationships. Applying finite element methods is essential in this area of study due to the geometric and physical nonlinearities involved in the mathematical modeling of soft tissues. Therefore, analytical solutions are often impossible to obtain. To formulate the governing constitutive equations of soft tissues, it is necessary to observe their mechanical properties carefully to choose the most realistic model appropriate for the type of analysis to be conducted.

4.1 Mechanical Properties of Soft Tissues

Fung et al. [88] suggested that in general, all soft tissues in the body are composed of collagen, elastin, reticulin and ground substance (a hydrophilic gel). However, soft tissues are different in their mechanical properties. This difference is mainly due to their structure rather than to the relative amount of constituents. Ligament and tendon fascicles are composed of parallel hierarchical bundles of fibers arranged in the direction, they are supposed to be more active.

Non-linear elasticity is an important property of all soft tissues. Paraspinal muscles, ligaments and annulus fibrosus which are considered as parallel-fibered collagenous tissues exhibit a non-linear stress-strain relationship when they are stressed uniaxially. This stress relationship is described by Woo et al. [89] as an initial low modulus region, caused by the unfolding of the fibrils followed by an intermediate region of gradually increasing modulus because of the stress directly causing strain on the fibrils. As the stress increases gradually, fibrils become taught. Next, the modulus reaches a peak and the tensile stress starts to increase linearly with increasing strain. Finally, the fibrils reach their ultimate tensile stress and as a result of rupture in the tissues the modulus decreases (Figure 25). The first part of the curve is more useful since it represents the physiological range in which the soft tissues normally function.

Although this procedure might be observed in the slow, unidirectional loading, Fung et al. [88] suggest that this may not be true for the dynamic situation, therefore they introduced a quasi-linear viscoelastic model. When the equilibrium is not obtained, a time-dependent component appears in the mechanical behavior of soft tissues [88]. Therefore, for the same value of strain, the stress values appear higher than those at equilibrium (Figure 26).

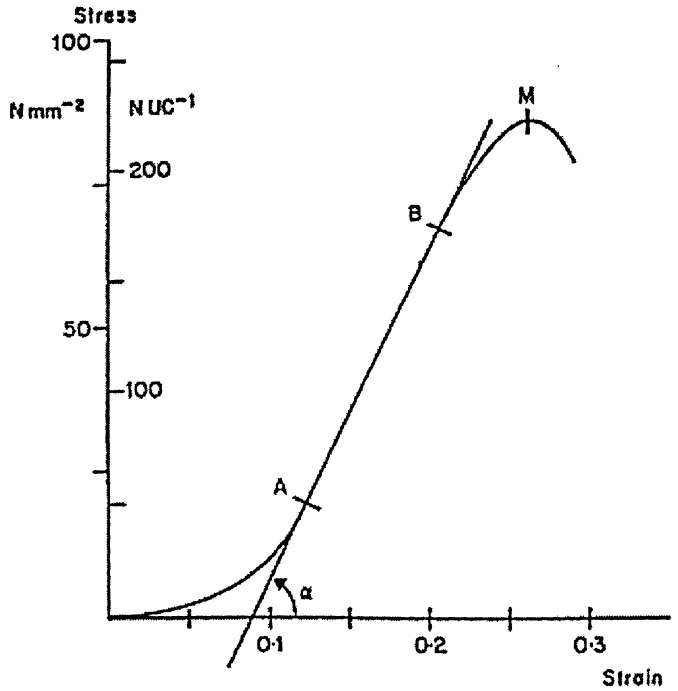

Figure 25: State of stress strain for soft tissue [87].

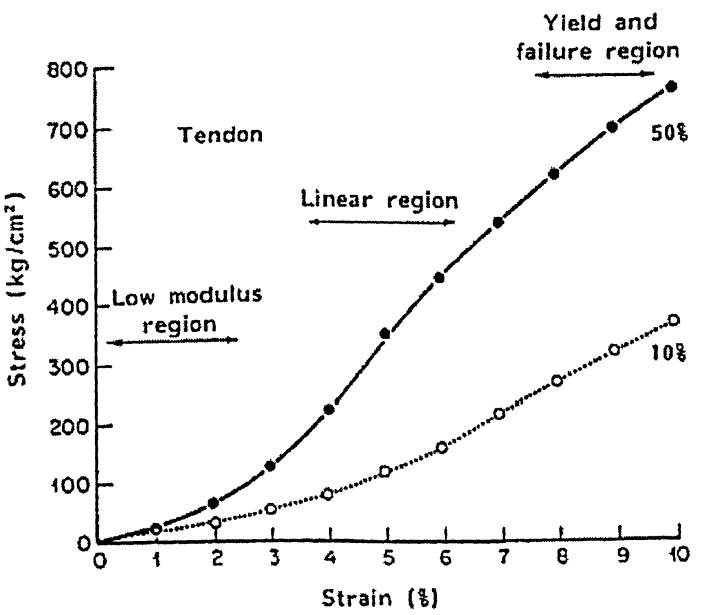

Figure 26: Influence of the dynamic loading [89].

When soft tissues are suddenly stretched and kept at new length, the stress slowly decreases against time. This phenomenon is called stress relaxation (Figure 27A). When a constant load is applied to a soft tissue, its lengthening velocity decreases in time until it reaches the equilibrium. This phenomenon is called creep (Figure 27B). Under cyclic loading, the stress-strain curve exhibits two distinct paths responding to the loading and unloading. This phenomenon is called hysteresis (Figure 27). These mechanical properties, observed for all soft tissues, describe a common physical phenomenon called viscoelasticity [88].

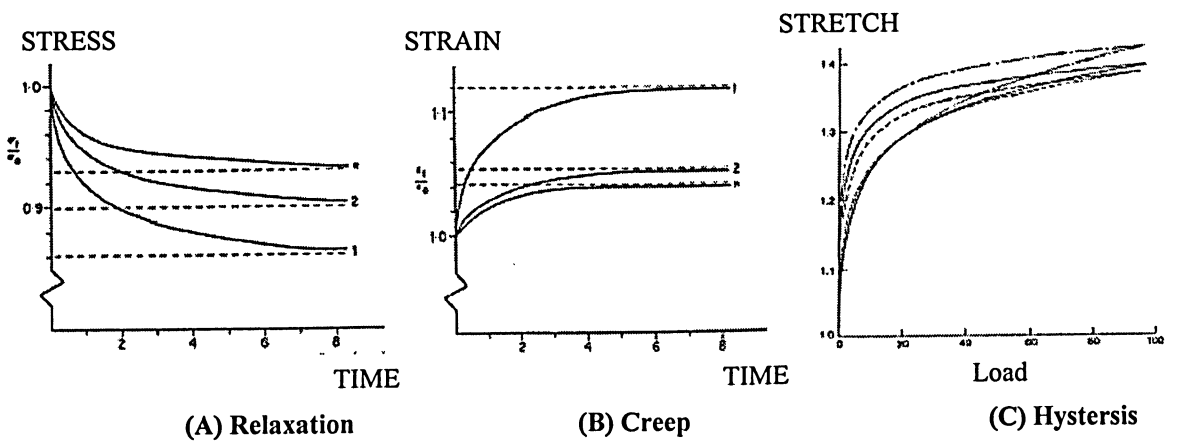

(A) Relaxation **(B) Creep** **(C) Hystersis**

Figure 27: Viscoelastic behaviors [88].

Soft tissues are frequently assumed to be incompressible materials. Besides, during loading-unloading, the stress-strain curve is gradually shifted to the right. After several loading-unloading cycles, the mechanical response of the soft tissue becomes steady. This phenomenon occurs because the internal structure of the soft tissue changes, until a steady state of cycling is reached. This is a common behavior of soft tissues which is usually used as preconditioning of the tissues prior to experimentation.

Another important property of soft tissues is the ability to undergo large deformations. Small strain is valid only for strains smaller than 2% of the initial length. However, soft tissues

usually exceed this limit in their physiological range of functioning. For instance, a normal strain for tendons is around 4% but they may extend up to 10% of their original length.

The objective of the following sections is to provide a summary of the structure, function and historical review of the efforts made to model ligament and muscle mechanics.

4.2 Ligaments

The ligaments are short connective fibrous tissues that keep bones together across the joints. The main responsibility of ligaments is to support joint motion and restrain the movement of joints. Under abnormal joint motion, ligaments can be overloaded and therefore, be damaged or completely disrupted.

Experimental studies of ligament mechanics are difficult, expensive, and prone to error. However, achievements in the area of constitutive modeling, computational methods and computer science have resulted in the extensive application of numerical methods to analyze mechanical systems.

To apply finite element method to study the properties of ligaments, a detailed mathematical description of the material behavior of the ligaments are required. It is necessary to conduct detailed experimental measurements of the material structure and mechanical behavior to develop a constitutive model for ligaments.

In the last 20 years, numerous research works have reported the material behavior of soft and hard musculoskeletal tissues, as well as changes associated with injury, repair, immobilization, exercise, and so on. Therefore, it is possible to consider these effects in the constitutive models of the ligaments to model changes in their material properties due to changes in the mechanical or biological environment.

This section reviews the structure, function, mechanical testing, and material models of ligaments. An understanding of each of these topics is necessary for the critical evaluation of constitutive models for ligaments and tendons.

4.2.1 Structure of Ligaments

Joint stability is mainly provided by a combination of bony geometry and ligament and other existing soft tissue in the area. As was mentioned before, ligaments support the motion of joints and at the same time restrain their abnormal movement.

Ligaments are well equipped to perform their physiological functions perfectly. Ligaments are a biological composite consisting of a ground substance matrix reinforced by collagen and elastin. The ground substance matrix is composed of proteoglycans, glycolipids, and fibroblasts, and holds large amounts of water [90] (Figure 28). Almost two-thirds of the weight of a ligament is made up by water. Fibrillar protein collagen makes up about 70 to 80% of the remaining weight [91]. Collagen is the primary component in ligaments that resists tensile stress.

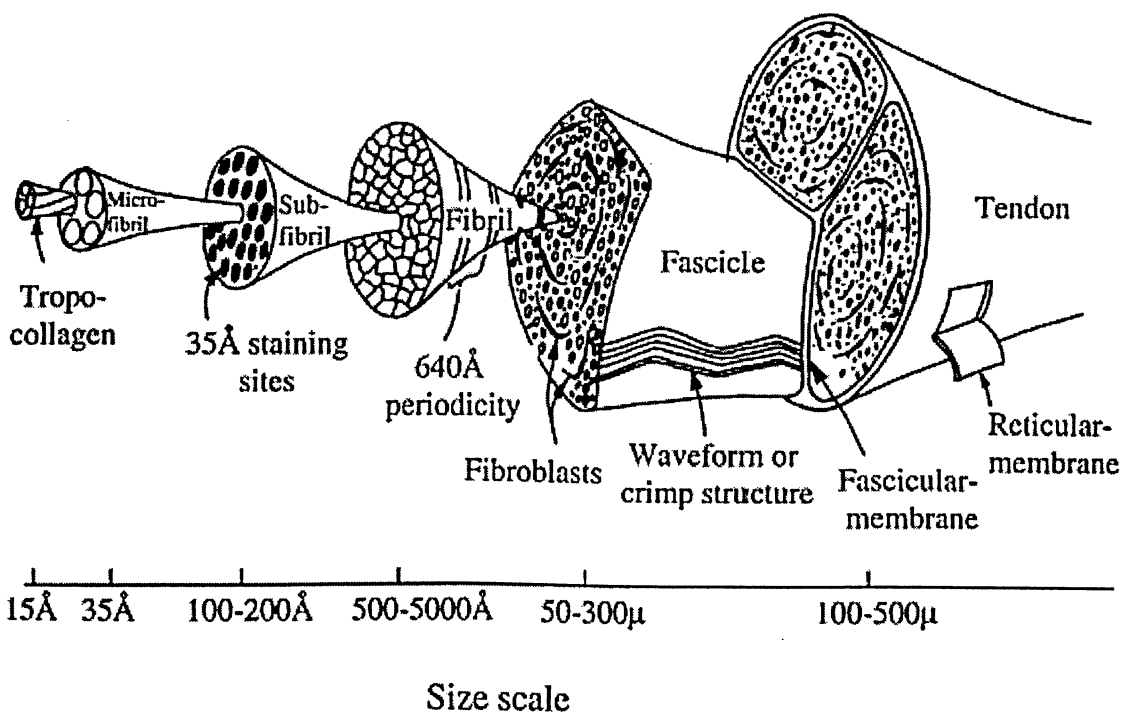

Figure 28: The structural hierarchy of ligament and tendon [92].

4.2.2 Material Testing of Ligaments

To properly study the material properties of ligaments, it is essential to understand the experimental testing methods and tools that have been used to measure these properties. In experimental studies of ligaments, it is important to distinguish between structural properties and material properties. Structural properties are obtained from tests of entire bone-ligament-bone structures, while material properties are derived from tests of isolated ligament tissue [93].

Material properties must be derived from experiments that test an area in the center of the ligamentous tissue under a state of homogenous uniaxial strain. Structural properties are often exhibited by a load-elongation curve (Figure 29A). This curve represents properties such as ultimate load, ultimate elongation, stiffness, and energy absorbed at failure. The ultimate load and elongation are determined at the point of failure of the bone-ligament-bone complex and the stiffness is the slope of the linear portion of the curve. The energy absorbed to failure is equal to the area under the load-elongation curve up to failure. Structural properties directly depend on both the material properties of the ligaments and the geometry of the bone-ligament-bone structure. The stress-strain relationship for ligamentous tissue can be obtained by combining the load-elongation data with the initial cross-sectional area of the ligament and strain measurements. Material properties such as tensile strength, ultimate strain, and tangent modulus can be obtained from the stress-strain curve (Figure 29B).

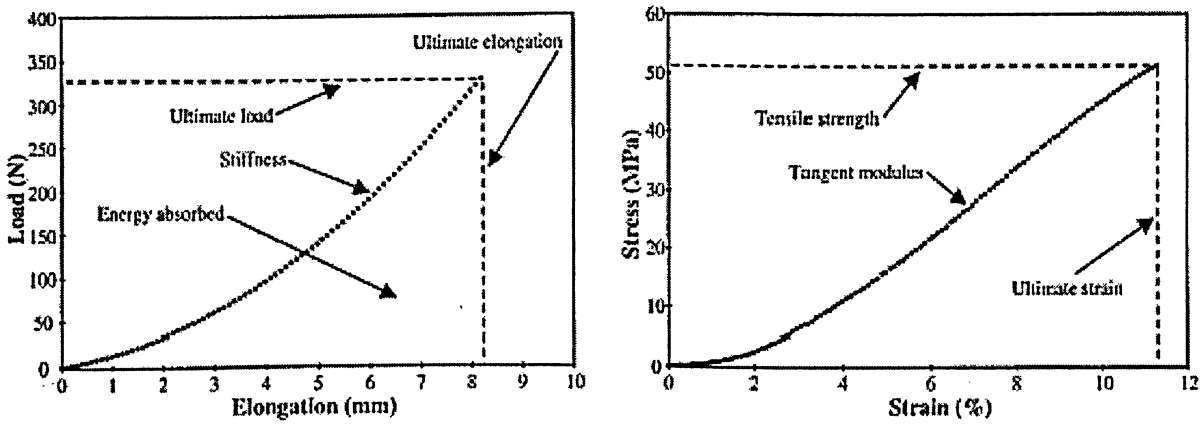

Figure 29: Load-elongation and stress-strain curves for a bone-ligament-bone complex under uniaxial tension. (A) Structural properties represented in a load-elongation curve, (B) Material properties represented in a stress-strain curve [94].

Testing considerations can extremely influence the material properties of ligaments. Depending on the required information, it is important to figure out what test would yield that information. A variety of tests such as uniaxial tension [93], strip biaxial tension [95], and shear [96,97] may be performed according to the goal of the experiment. These tests can be used to conduct experiments at a fixed strain rate, to obtain the effects of cyclic loading [98] or to study viscoelastic behavior under creep or stress relaxation conditions [99,100]. Uniaxial tensile tests are often used to investigate the ligament behavior and are conducted on samples with high length-to-width ratios. Uniaxial tensile tests provide information on the one-dimensional, tensile behavior of ligaments. Strip biaxial tests are conducted on specimens with low length-to-width ratios to reduce the tissue's lateral stretch. As is expected, this test provides two-dimensional data on the material behavior of ligaments. The strip biaxial test is similar to a biaxial test configuration, but the goal of the former is to maintain the stretch ratio in the lateral direction at a value of 1.0. Also, shear tests are often useful to study the multiaxial behavior of ligaments [97].

Compressibility is another important feature in the formulation of a constitutive model [101]. Creep, stress relaxation and cyclic tests are often performed to determine the viscoelastic behavior of ligaments. By noting the changes in peak stress (creep testing) or peak strain (stress relaxation) with each cycle, viscoelastic material coefficients may be estimated.

Tensile testing of ligaments is associated with several experimental difficulties. Most of these difficulties are due to the poor interface between the ligament and the rigid clamps of a material testing machine. Slipping from these clamps during testing or failure at the stress concentration area induced as soft tissue is compressed between the rigid clamps are the most common problems in the tensile testing of ligaments. Some researchers have resolved these problems by using liquid nitrogen or dry ice to freeze the tissue grasped by the clamps [102,103,104]. This local hardening of the tissue at the clamped area of the specimen prevent the ligament from slipping or failing. Also, the specimens often have poor aspect ratios and irregular geometries, which induce nonuniformities in the stresses and strains during the experiments. To maintain uniform loading conditions, specimens with appropriate length-to-width ratios are often cut from intact ligaments [93,105].

It is highly important to select an appropriate measurement technique to test a ligamentous tissue. To calculate stress in ligaments under uniaxial tension, the tissue cross-sectional area and the applied load must be measured accurately. The measurement of load can be made easily by using a load cell positioned in series with the clamping system. On the contrary, measurement of the cross-sectional area is often a tedious task since the ligament cross-section is rarely uniform and varies remarkably along the length of the ligament [106]. Calipers are usually used but yet requires the assumption of a regular

cross-sectional shape. Additionally, calipers may increase error by deforming the tissue [106]. Despite the disadvantages, calipers are used extensively, since they are easy to work with and provide a sufficient level of accuracy for many applications.

The cross-sectional area of ligaments can also be measured by area micrometers. They compress the sample into a defined cross-sectional geometry through a prescribed transverse pressure. The actual cross-sectional area of a specimen will be underestimated since the ligament deforms as pressure is applied by the micrometer [107]. However, it is a reliable method to approximately measure the cross-sectional area of specimens.

Non-contact methods, such as laser micrometers, have been introduced in recent years to measure the cross-sectional area of ligaments [106,108]. One of the disadvantages of these techniques is the time required to perform such measurements.

Numerous techniques have been used to measure strain in soft tissues, such as spinal ligaments. Computed tomography (CT) and magnetic resonance imaging (MRI) are other tools to measure length and cross-sectional areas of ligaments.

Some researchers have attempted to measure the geometry of anterior and posterior longitudinal ligaments of the mid-lower cervical spine by the use of electromagnetic digitizer, laser micrometers [109], and micro dissection approach [110].

Cryomicrotomy techniques have also been used to define the geometry of ligaments [111,112,113]. Although this technique is destructive, its ability to obtain sequential images in a predetermined plane at very close intervals (of the order of a few microns), enables researchers to describe the three-dimensional geometry of ligaments. Since no dissection is performed and the tissues can be frozen in their natural state, the anatomic integrity of the hard and soft tissue structures and their relative position will be saved [114].

A common method to derive ligament strain is measuring the crosshead displacement of the material testing machine and the initial length of the specimen. This method is prone to large errors because of the slack in the system, specimen slippage in the clamps, or inhomogeneities in the ligament strain field. Although it is simple to estimate the strain of ligament by this method, this has been exhibited to be a highly inaccurate method [115].

Some researchers have connected pins to the ligament insertion sites (the junction between the soft tissue of ligaments and the hard tissue of bones) and measured the distance between the pins at different joint orientations [116]. Hollis et al. [117] has used a similar technique to measure elongation in various specimens of the anterior cruciate ligament.

Another technique to measure the length of ligaments *in vivo* is Roentgenographic techniques. Also, researchers have used liquid metal strain gages [118,119] or Hall Effect Strain Transducers (HEST) [120,121,122] to measure strain in ligaments. These devices are attached to the tissue and measure displacement between attachment points. Liquid metal strain gages and HEST are shown to be more accurate than the earlier techniques of strain measurement [123,124], but they still have some problems. Despite their small size, they are still large enough to impinge on surrounding tissues during joint motion, changing normal ligament deformation.

Many researchers have used optical techniques such as Video Dimension Analyzer (VDA) [125] for the measurement of ligament strain [126,127].

Advances in video-based techniques with motion analysis software resulted in three-dimensional strain measurements [128,129]. Most motion analysis systems use a Direct Linear Transformation (DLT) to determine three-dimensional coordinate data from multiple two-dimensional views [130].

Video techniques are associated with many advantages compared with other strain measurement methods. Video-based techniques are less destructive than other techniques and can measure a three-dimensional strain at multiple locations on a single ligament. Despite their advantages, these techniques cause large errors in strain measurements of ligaments. For instance, in two-dimensional measurements, rotations will cause the markers to move out of the measurement plane and therefore, a large error occurs in measurement of strains [131,132].

Recently a new technique called photoelastic technique was developed to measure ligament strain [133,134,135]. In this method, the surface of a ligament is covered with a thin layer of polyurethane which is optically sensitive. When performing the test, fringe patterns are generated on the surface of ligament. The patterns can be recorded with a video system and analyzed to measure ligament strain. A remarkable advantage of this technique is the potential to measure strain inhomogeneities. Despite its benefits, researchers have found it highly difficult to find a photoelastic coating material that attaches well enough to the ligament without changing the material property of the tissues.

Forces in ligaments can be directly obtained by attaching devices such as buckle transducers [136,137] or implantable force transducers [138,139] to ligaments and also by strain gage attachment to bone near ligament insertion sites [140].

Fujie et al. [141] designed a six degree of freedom force-moment sensing robot to measure the magnitude and direction of ligament forces. The robot was used to measure both the six degree of freedom motion and applied forces and moments during kinematic testing. Ligaments were cut and the robot was used to recreate the kinematics determined before ligament transection. Using the principle of superposition and the alteration in the

measured forces and moments, the magnitude and direction of force present in the ligaments were determined.

4.2.3 Material Models for Ligaments

Numerous material models have been developed to represent biological soft tissues such as ligaments. These models assist researchers to understand how different tissue components affect the material behavior of the overall tissue. Also, material models can be used to anticipate the results of experimental tests. Additionally, the developed material models can represent the properties of tissue in a finite element analysis. The construction of accurate constitutive models is difficult because ligaments are nonlinear, anisotropic, inhomogeneous, viscoelastic, and undergo large deformations.

Material models of ligaments can be divided as either microstructural or phenomenological. Microstructural models are based on representation of the various components of the tissue. The characteristics of each component of the tissue are combined to define material behavior of the tissue. Phenomenological models present the material behavior of a tissue as a unit regardless of the responses of individual components of the tissue. The material coefficients obtained from phenomenological models generally do not have a direct physical interpretation.

In this section, a summary of the developed models presenting ligamentous tissues is presented.

4.2.3.1 Elastic Models

The material behavior of ligaments is not dependent on strain rate over several decades of variation. Also, ligaments reach a "preconditioned" state after cyclic loadings and a minimal amount of hysteresis introduced to the specimens. These features in ligaments

have motivated many researchers to neglect the viscoelastic property of ligaments and model them as nonlinear elastic materials.

There are two general approaches to develop microstructural models of ligaments. One of these approaches has employed sufficient elastic elements simulating the nonlinear elastic behavior of ligaments. The second approach describes the ligament behavior by developing the model of collagen fiber geometry [142].

Frisen et al. [142] represented the elastic model of ligaments using numerous individual linearly elastic components, each of which represented a collagen fibril of different initial length in its unloaded form. More fibrils were used to characterize the nonlinear behavior of ligaments.

Kastelic et al. [143] proposed a similar model as Frisen et al. [142]. They developed a model representing a tendon referred to as the sequential straightening and loading model. It was assumed that unfolded fibrils had not resisted in tension and only the elasticity of previously straightened fibrils showed tensile resistance.

Decraemer et al. [144] developed a similar model consisting of a large number of purely elastic fibers embedded in a gelatin-like liquid. Values for the modulus and cross-sectional area of each fiber were considered identical. Fibers with different lengths were used in the model.

Woo et al. [89] developed a model using a bilinear stress-strain curve for each individual fibril with various slopes for the low modulus and linear regions. Constitutive equation of each fiber was superposed those of the others to develop a single equation for the ligament.

Liao et al. [145] followed the earlier models of sequential recruitment [144,146,147] to include failure. In theses models, individual fibers exhibited linear elasticity until exceeding an ultimate strain where failure was introduced.

The uniaxial behavior of ligaments has also been investigated by modeling collagen fibril geometry. Diamant et al. [148] developed a microstructural model for ligaments and tendons considering the collagen crimp structure with straight elastic segments connected by rigid hinges.

Comninou et al. [149] employed a sinusoidal waveform to represent the collagen crimp structure. Constitutive equations for uniaxial extension were formulated for a single fiber as well as for a bundle of fibers embedded in a matrix. A constant crimp configuration was assumed that restricted this model to small strains.

In the model developed by Lanir [146,150] the collagen fibril crimp was represented by elastic fibers attached to each collagen fiber at numerous points along its length. In this model, initial tension was limited by the elastic fibers and with increasing the tension, the stiffer collagen fibrils began to straighten and bear more of the load.

All of the developed one-dimensional models are able to describe the uniaxial behavior of ligaments. However, since they are confined to only one dimension there is no independent measure to test their predictive value. These models cannot describe the three-dimensional, anisotropic behavior of ligaments, the contribution of the ground substance matrix to ligament material behavior, and shear or transverse loading.

Many researchers have developed three-dimensional models to represent the material behavior of ligaments. Beskos et al. [151] created a model representing a tendon as a

fiber-reinforced composite. Series of inextensible fibers were set in a helical pattern and were embedded in an incompressible, hollow circular cylinder.

Fung [88] developed a phenomenological model utilizing an exponential stress-strain relationship based on uniaxial experimental results obtained from rabbit mesentery. This formulation considered the nonlinearity and finite deformation associated with uniaxial tensile tests. Hildebrandt et al. [152] extended the model to two- and three-dimensional isotropic forms.

Ault et al. [153] proposed a three-dimensional model for soft connective tissues using a previously developed linearly elastic composite materials approach [154,155]. The cylindrical fibrils were assumed to be surrounded by a concentric cylinder of matrix material.

Using an energy approach, Lanir [147] proposed a continuum model for fibrous connective tissue. The energy of deformation was considered to increase from the tensile strain in the collagen fibers. In this model the matrix was performing only as a simple hydrostatic pressure. The model was represented as an incompressible composite of collagen fibers embedded in a fluid matrix. It was assumed that the collagen fibers buckled under a compressive load and the unfolding of the fibers during deformation compressed the matrix, resulting in an internal hydrostatic pressure.

Hurschler et al. [156] employed a similar approach as the one used by Lanir [147] to develop a three-dimensional model for tendon and ligament. It was assumed that the fibrils increased the strain energy when they were only in tension and the only contribution of the matrix was a hydrostatic pressure. Deformation of fibrils was considered to be incompressible and axisymmetric. Fibrils were modeled to deform only linearly.

Weiss et al. [95,157] proposed a model representing ligaments and tendons as incompressible, transversely isotropic, hyperelastic materials. Using a strain energy approach, they could apply the formulation to finite element applications. Additionally, the coefficients from material testing could be determined easily using the proposed formulation.

4.2.3.2 Viscoelastic Models

Although ligaments are almost independent of strain rate [158], tissue viscoelasticity is an important factor in the response of joints to high-rate loading or impact incidents [159]. Viscoelastic characteristics of ligaments are also important when considering cyclic loading [160] creep, or stress relaxation [99,100]. Viscoelastic models of ligaments may be divided into two categories of microstructural and phenomenological models.

Microstructural viscoelastic models of ligaments have a similar basis to some of the microstructural elastic models discussed before.

Frisen et al. [142] developed a microstructural viscoelastic model for parallel fibered tissues using a combination of spring and damper. Later, they modified the model to incorporate the nonlinearity of the elastic response [161].

Lanir [150] extended his previous microstructural elastic model by considering linearly viscoelastic fibers. This model was further modified to include three-dimensional viscoelasticity theory [147].

Decraemer et al. [162] included viscoelasticity in their model by considering internal friction between fibers and between fibers and the surrounding matrix. The damping was added by introducing linear viscoelastic properties to the fibers with a relaxation function.

Barbenel et al. [163] developed a phenomenological viscoelastic model of ligaments by including a logarithmic relaxation function in the spring and damper models. In another attempt to develop a phenomenological viscoelastic model, Sanjeevi et al. [164,165] formulated the viscoelastic behavior of biological soft tissues with an equation similar to that of a Voigt-type spring and damper model.

4.2.3.3 Poroelastic Models

Poroelastic models consider both solid and fluid phases of soft tissues to describe their material behavior. Poroelastic material models were originally introduced in the field of soil mechanics [166,167] and later used to describe the material behavior of ligaments [168] and interveterbral discs [169].

Experimental studies have demonstrated that the material behavior of ligaments and tendons is a function of tissue hydration [170,171], however, not so many researchers have incorporated fluid effects into their formulation.

Atkinson et al. [172] proposed a microstructurally based finite element model of a collagen fascicle including fluid effects. The model was formed by a water-based matrix surrounded by a fibrous outer ring with helically oriented fibrils.

4.2.3.4 Homogenization Models

Homogenization technique was developed specifically for the analysis of microstructured materials [173,174] and it has been extensively used in the study of composite materials [175,176]. Homogenization technique makes it is possible to conduct microstructural and continuum analyses independently and then combine the obtained results to define the stress-strain distribution on microstructural levels throughout a large region of material.

The analysis of large-scale systems is possible when implementing this method, as it is relatively inexpensive computationally [177].

4.3. Muscles

The primary function of skeletal muscles is to move and stabilize various parts of the body. The structure and function of each muscle varies, while the basic properties of the muscle cells are the same. Cyclic loading of the muscles will result in local alteration of tissue properties in the muscle, such as fiber diameter, maximum contraction force, etc.[178,179,180,181,182]. In the following sections the structure and the proposed models representing the material behavior of muscles are discussed.

4.3.1 Structure of Skeletal Muscles

The structure of a single connection muscle is illustrated in Figure 30. Muscle fibers and a connective tissue network are the main components of the muscle tissue. The blood and lymph vessels are considered as the mechanical structure of muscles. A network of connective tissue keeps the muscle components together. At different levels in the tissue, sheets of connective tissue are observed (Figure 31). The outer surface of the muscle is surrounded by the epimysium. The muscle is divided into bundles of muscle fibers. Each bundle contains a few to over a hundred muscle fibers, and is encapsulated by the perimysium. Within the bundle the individual fibers are held together by the endomysium.

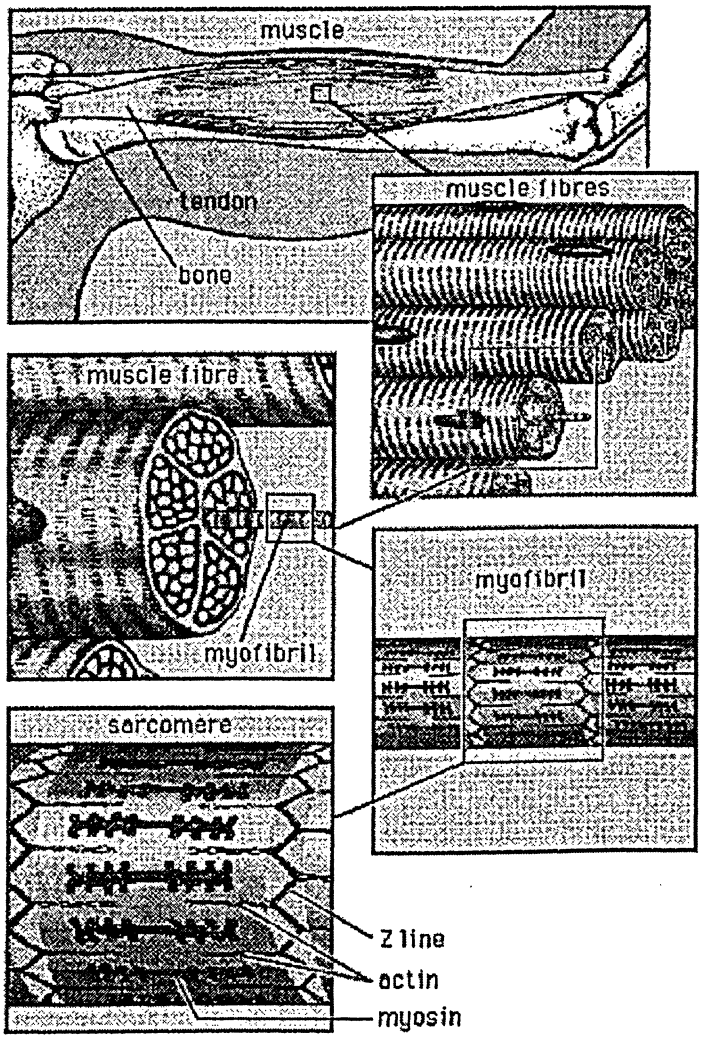

Figure 30: The muscle is attached to the bone by the tendons. The muscle consists of muscle fibers that are cells. In the muscle, cells are strands of myofibrils that are composed of sarcomeres repeating units of actin and myosin. Adapted from Encyclopaedia Brittanica, 1994.

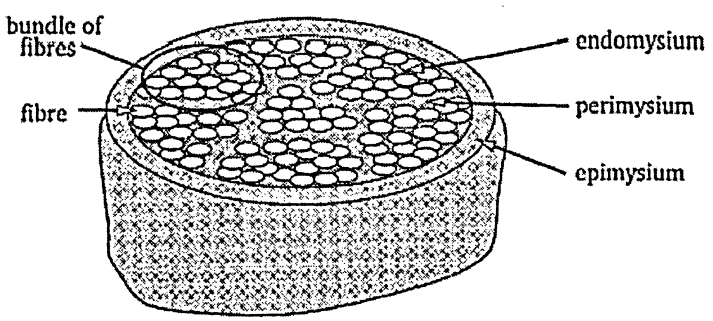

Figure 31: Location of the connective tissues, epimysium, permysium and endomysium. Adapted from Encyclopaedia Brittanica, 1994.

4.3.2. Material Models of Muscles

Similar to material models of ligaments, the models of material behavior for muscle fibers are divided into two major categories of phenomenological and microstructural models. In the following sections some of the models developed to represent the material behavior of muscles are discussed.

4.3.2.1 Hill Type Models

One of the first mathematical models of muscles was proposed by Hill [183]. This phenomenological model was developed from force-velocity measurements on a entire muscle. The obtained measurements resulted in an equation correlating the force of the muscle (F), the velocity of the contraction (v) and other muscle dependent parameters (Figure 32). The main advantage of the model is its simplicity and direct connection to macroscopic muscle experiments. The disadvantage of this model is the difficulty of incorporating the viscoelastic behavior of muscles to the underlying physiological mechanisms of muscle contraction.

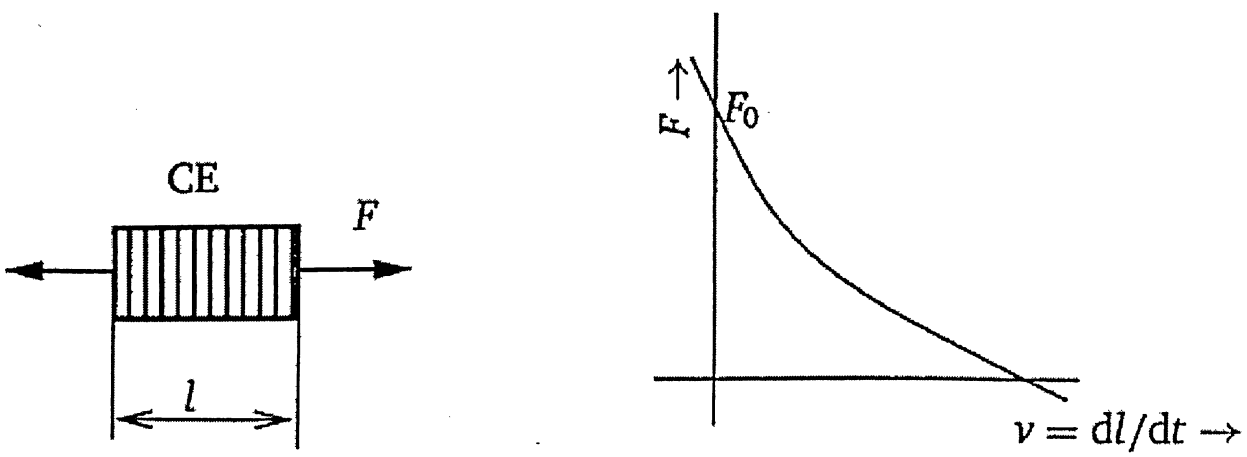

Figure 32: Graphical representation of the Hill model and Hill equation [183].

In Hill type muscle model, passive muscle (a muscle without neural input) behavior can be modeled similarly to the model of Deng [54] by the nonlinear stress-strain relation with strain defined as the elongation relative to the rest length of the muscle, the passive muscle stiffness and the strain asymptote. In this model the free length is defined as the length of a muscle at rest when it is removed from the body. A passive muscle experiences an initial stress at rest; therefore, the muscle at rest will shorten when it is removed from the body. This feature results in a smaller free length than the muscle length in its initial position. Assuming a linear relationship between sarcomere length and muscle length, the free length can be calculated as $l_{free} = l_{rest} \frac{s_{free}}{s_{rest}}$. Table 3 has summarized the required parameters to model the passive behavior of muscles.

Table 3: Model parameters for passive muscle behavior [55].

MUSCLE PARAMETER	SYMBOL	VALUE
Average sarcomere length of "free muscle	S_{free}	2.1 μm
length of sarcomere at rest	S_{rest}	Table 21-25
sarcomere length at muscle optimal length	S_{ref}	2.8 μm
length of "free" muscle	l_{free}	$l_{rest} \frac{s_{free}}{s_{rest}}$
length of muscle at rest	l_{rest}	Based on initial position of model
optimum length of muscle	l_{ref}	$l_{rest} \frac{s_{ref}}{s_{rest}}$
passive force-length stiffness	k	3.34 N/cm^2
passive force-length asymptote	a	0.7

4.3.2.2 Huxley Type Models

The primary Huxley type model was based on early ideas of how cross bridges behave [184]. This model assumes that a cross bridge has only two possible states: attached or detached. When it is attached it generates force that results in a shortening of the

sarcomere (the portion of a myofibril between two Z lines). This model was extended by adding more states and other features, such as length dependence of the attachment-detachment process, activation and metabolics [185,186].

It is shown that this is an exclusive model to describe the way muscles function mathematically [187,188,189]. Additionally, compared to Hill-type models, Huxley-type models describe more accurately the stiffness of the fibers [190,191]. A disadvantage of these models is their complexity leading to a high computational performance.

4.3.2.3 Myers Muscle Model

Myers et al. [192] modeled the muscles of the cervical spine as nonlinear spring elements with lines of action from muscle origin to insertion. For a particular muscle, an average origin and insertion was calculated and transferred to the local coordinate system of the vertebral bodies of origin and insertion, respectively. In this model, muscle force-length properties were measured by pulling stimulated rabbit tibialis anterior muscles [193]. Then, muscle force-displacement response was normalized. The data were fit with a bilinear response with an initial higher stiffness region followed by a lower stiffness region. The average stress-strain eccentric contraction response was used to formulate a force-displacement response for a typical neck muscle. The length of a neck muscle was assumed to be 70% of the origin to insertion length, and length of tendon was not considered.

Based on Myers et al. [193], the 0% strain length of Figure 33 corresponds to the human sarcomere length of approximately 2.9 μm. Since the pennation angles of neck muscles are small, fiber length and sarcomere length were assumed to change linearly with muscle length. Appendix 1 lists the origins and insertions of various muscles in cervical spine

region. Also the value of PCSA (physiological cross-sectional area (volume/Length)) for each muscle is noted.

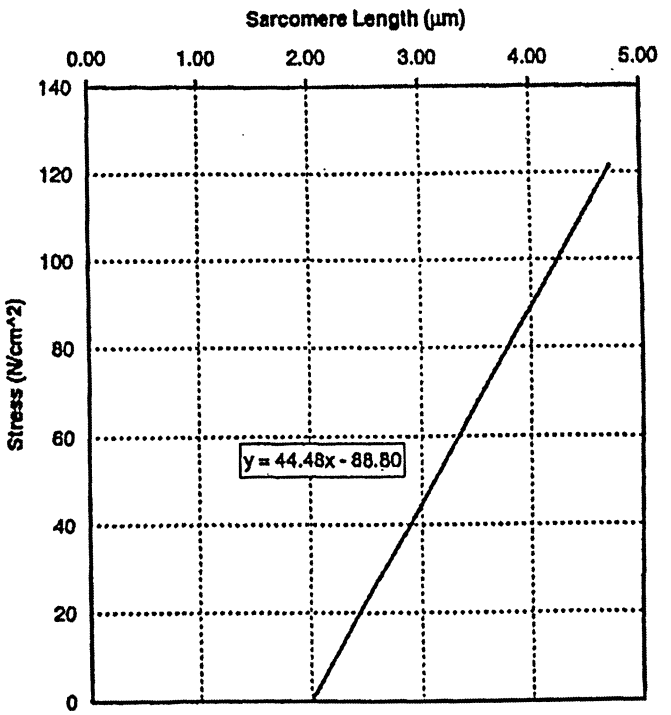

Figure 33: By setting the 0% strain position equal to a sarcomere length of 2.9 µm, a stress versus sarcomere length relation was defined. Neck muscle stress could then be defined based on resting sarcomere length [193].

4.3.2.4 Other Models of Contracting Muscles

Both the Huxley and Hill type models propose the contraction of an entire muscle. In these models, tendons can be included by adding an extra spring to represent the tendons. [194,195] (Figure 34A).

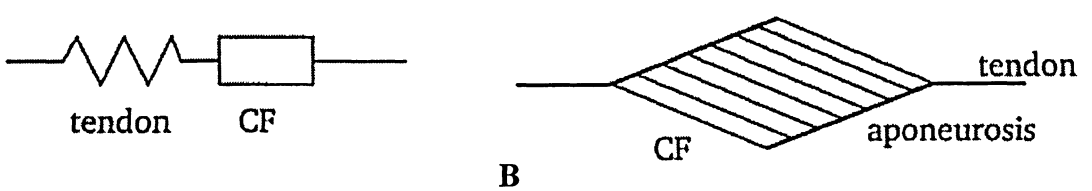

Figure 34: Models of muscle with tendons: (A) model with a spring to represent the tendon and contractile fibers (CF), (B) parallelogram model, with straight contractile fibers (CF) and a rigid aponeurosis [194].

To include some of the geometrical characteristics of muscles, planimetric or parallelogram models (Figure 34B) and 3D geometric muscle models were proposed [196]. These models assist researchers to understand the difference in the force length and force-velocity relationships of various unipennate muscles [197,198].

Kaufman et al. [199] included the most important geometric characteristics of the muscle by modifying the force-velocity and force-length relationships with geometric parameters proposed by Woittiez [196]. A disadvantage of the models developed by Woittiez and Kaufman is that the mechanical response is described by macroscopic geometric properties. Also, in their models, they considered homogeneous distributions of stress and strain, while it is essential to be able to describe inhomogeneous stress and strain distributions.

Otten [200] proposed a finite element model of skeletal muscle. He applied discrete elements; some elements represented connective tissue and the others contractile fibers.

A model developed by van der Linden [201,202] followed a similar approach. In this model, the contractile properties of the muscle were included as contractile fibers and closed fluid compartments (Figure 35).

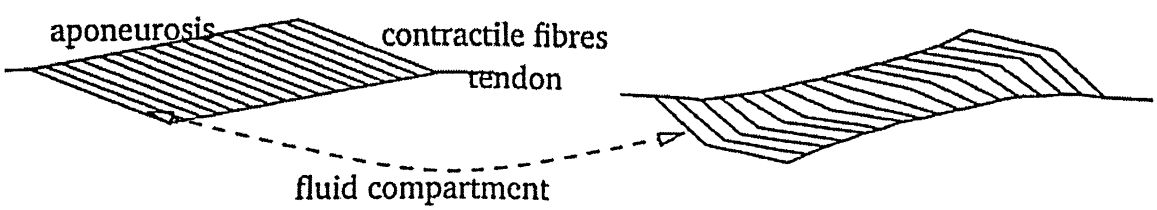

Figure 35: Finite element model of van der Linden in the reference (left) and contracted situation (right) [202].

Anton [203] proposed a two-dimensional continuum based finite element model of the skeletal muscle. In this model, an anisotropic Mooney-Rivlin elastic model was used to represent the behavior of the connective tissue network. The fibers are assumed to be embedded in a fluid matrix. The velocity dependency was assumed to be negligible.

4.4 Conclusion

Ligament and muscle injuries are common and in most cases lead to serious joint degeneration. Experimental studies of soft tissues have clarified the functions and mechanisms of injury; however, many aspects of their behavior are still unknown. Numerical models of soft tissues provide relatively accurate information regarding ligament and muscle mechanics that would be difficult or impossible to obtain experimentally. The complicated material properties of ligaments and muscles make the accurate modeling of their material behavior a challenge.

In this chapter, structure and function of the two main soft tissues in the cervical spine region, muscles and ligaments, were discussed and a brief review of the constitutive models was provided. These models were developed originally to describe one-dimensional behavior of soft tissues and later extended to models representing the three-dimensional anisotropic behavior of muscles and ligaments. In this review, the assumptions of each modeling approach as well as their benefits and drawbacks were discussed.

CHAPTER 5

FINITE ELEMENT MODELING OF THE CERVICAL SPINE

Development and analysis of the finite element model of the cervical spine can assist researchers to thoroughly study neck movements in real life. The results from the studies can provide important information to investigate the causes of cervical spine injuries and the methods of preventing such injuries. However, one of the major factors that can affect the accuracy of the results is the accuracy of the geometrical parameters defining the vertebrae. The anatomy of the cervical spine has been qualitatively documented in various textbooks and research [11, 45,46,48,59,204]. Because of the existing complication in the geometry of the cervical spine vertebrae, it is not possible to find all of the necessary parameters defining geometry of vertebrae in a single research. Therefore, to model the vertebrae it is essential to obtain the missing parameters from other reports [205,206].

Although the cervical spine contains seven vertebrae, no research has reported the quantitative parameters for all seven vertebrae in a single work. This is because the first two vertebrae of the cervical spine, Atlas and Axis, are completely different from the rest of vertebrae. Some quantitative studies have reported the required parameters to model Atlas and Axis [207,208,209,210,211].

The last parameter that has a significant contribution in the modeling of cervical spine is the height or relative location of the intervertebral discs to the adjacent vertebrae. In the simplified model of the intervertebral discs presented by Nissan et al. [212], the required parameters to locate adjacent vertebrae of the cervical spine can be found.

5.1 Parameters Defining Vertebrae in Cervical Spine

5.1.1 Parameters Defining Atlas

It is not possible to obtain all of the necessary parameters that describe the geometry of a vertebra in a single research study; therefore, the results of several published studies should be investigated to determine the essential parameters. To model the first vertebra in the cervical spine, except for parameters that describe facet joints, another six parameters (ARH, PRH, ART, PRT, FDL and ODS) must be determined. The research study by Doherty et al. [207] fully presents these parameters.

A quantitative study conducted by Dong et al. [209] has concentrated more on geometric parameters of lateral mass of Atlas. Therefore, the study by Dong et al. [209] and Panjabi et al. [205] are selected to determine the required parameters to model the facet joints of Atlas.

Inferior articular facet of Atlas and other vertebrae are mainly modeled as an elliptical area in the literature. The parameters presented by Panjabi et al. [205] fully define the facet joints of the cervical spine. Figure 36 illustrates the required parameters to describe the geometry of Atlas. All reported values for the geometrical parameters of Atlas are listed in Table 4.

Table 4: The reported values for geometrical parameters of Atlas.

Parameter	Mnemonic	Value (mm)
Anterior Ring Height (mm)	ARH	16.74
Posterior Ring Height (mm)	PRH	11.09
Anterior Ring Thickness (mm)	ART	11.84
Posterior Ring Thickness (mm)	PRT	12.77
Foramen Diameter Lateral (mm)	FDL	30.99
Overall Diameter Sagittal (mm)	ODS	47.98
Superior Facet Width (mm)	FCWS	14.30
Superior Facet Height (mm)	FCHS	25.25
Superior Facet Depth (mm)	FCDS	6.78
Superior Facet CAX* (°)	CAXS	32.65
Superior Facet CAY* (°)	CAYS	-59.41
Lateral Mass Height (mm)	LMH	18.82
Inferior Facet CAX* (°)	CAXI	-37.1
Inferior Facet CAY* (°)	CAYI	49.4
Inferior Facet Width (mm)	FCWI	16.4
Inferior Facet Height (mm)	FCHI	17.85

*Note: The parameters will be defined in section 3.

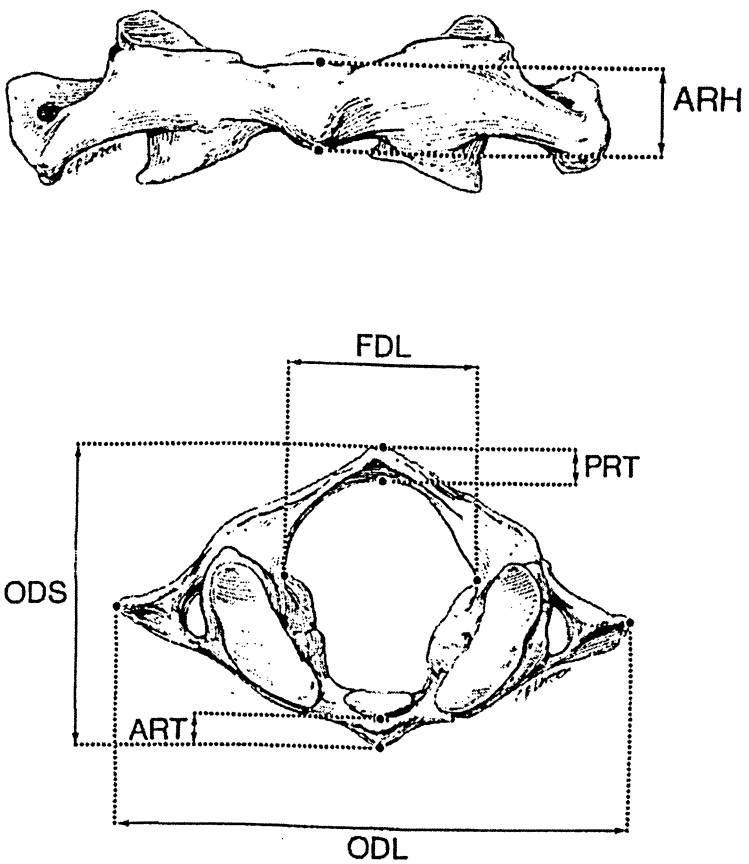

Figure 36: The parameters describing the geometry of Atlas [209].

5.1.2 Parameters Defining Axis

The second vertebra of the cervical spine (Axis) has 3 different regions. Although posteriorly Axis can be considered as one of the general vertebrae of cervical spine (C3 to C7), anteriorly it has a distinctive feature. Anteriorly, Axis can be divided into two sections: vertebral body and dens. The inferior endplate of Axis can be defined with the same parameters as the general vertebrae of the cervical spine, but seven parameters are required to describe the geometry of the dens and vertebral body of Axis. The parameters reported in a quantitative study conducted by Schaffler et al. [211] are used to model the anterior part of Axis. Figure 37 and Table 5 present the parameters and the values considered to model the anterior part of the second vertebra of the cervical spine. The posterior and geometry of the inferior endplate of Axis will be discussed with the remainder of the cervical vertebrae.

Table 5: The reported values for anterior region of Axis.

Parameter	Mnemonic	Value (mm)
Dens Height (mm)	DH	17.31
Angles of Dens in Sagittal Plane (°)	DASA	77.08
Lower Anterioroposterior Dens Diameter (mm)	APDL	13.24
Lower Transverse Dens Diameter (mm)	TDL	13.42
Upper Anterioroposterior Dens Diameter (mm)	APDU	13.44
Upper Transverse Dens Diameter (mm)	TDU	12.26
Vertebral Body Height (mm)	VBH	20.00

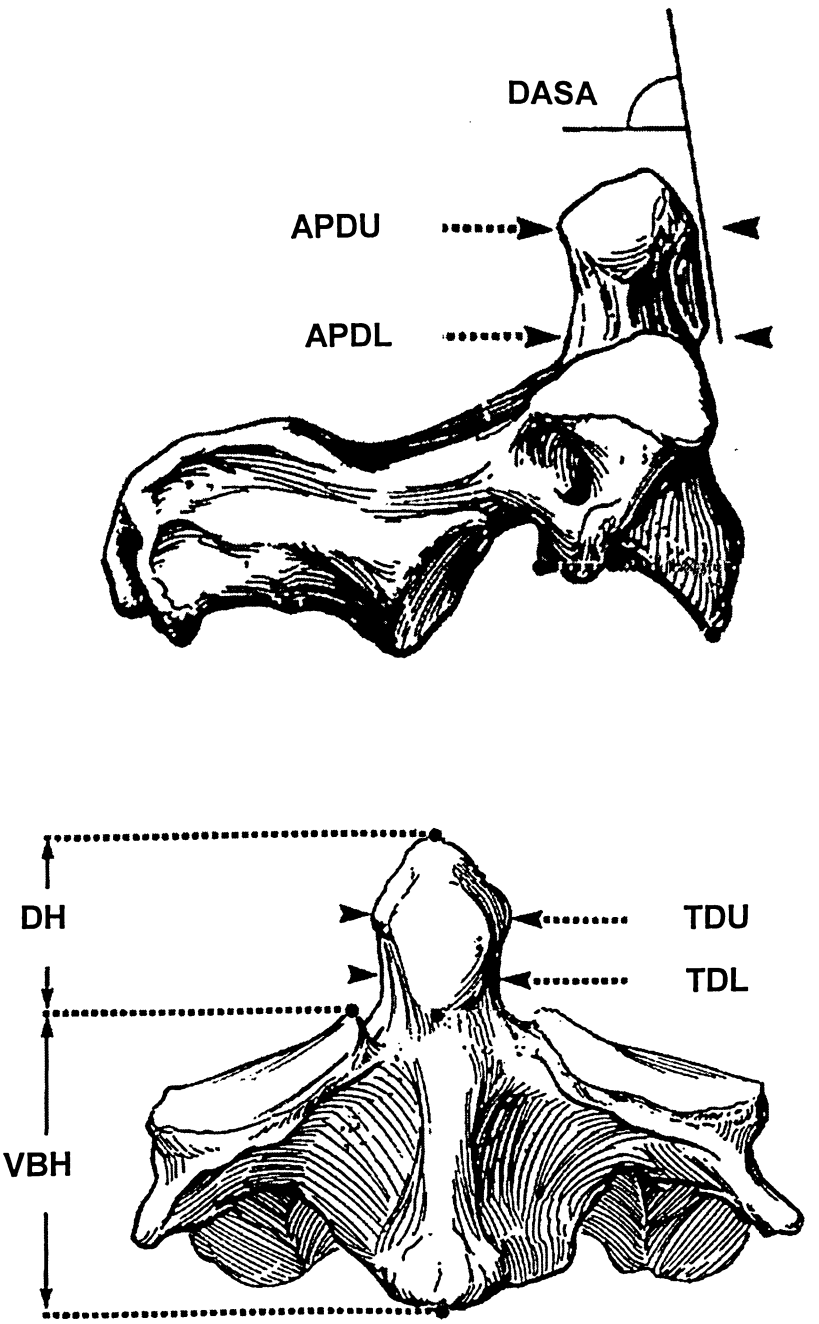

Figure 37: The parameters describing the geometry of Axis [211].

5.1.3 Parameters Defining Vertebrae of the Middle and Lower Regions (C3-C7)

Cervical vertebrae C3 through C7 are considered to be typical. They each have a vertebral body and are interconnected through intervertebral discs that help to distribute and absorb loading forces. The superior surface of the vertebral body is convex anteriorly and concave from side to side. The inferior surface of the vertebral body is concave anteriorly and convex from side to side. The anterior region of the vertebral disc is thicker than the posterior region. Some studies have reported the quantitative three-dimensional anatomy of C3 through C7 [213,214,204,215]. The most recent and comprehensive is the research done by Panjabi et al. [204]. Although many dimensions of vertebrae are measured in this study, they cannot fully describe the geometry of posterior elements and facet joints (Figure 38 and Table 6 and Table 7). Panjabi et al. [205] in a similar work have reported the quantitative three-dimensional anatomy of articular facets of the cervical spine. A summary of all measured dimensions for the articular facets is listed in Table 8 and Table 9. The linear and area measurements of facet joints and the facet orientations, in terms of planar and card angles, are shown in Figure 39. Another quantitative study by Xu [206] defines the required parameters to model the laminas of the cervical spine (Figure 40), which completes the list of required parameters to fully describe the geometry of vertebrae in the middle and lower regions of the cervical spine (Table 9 and Table 10). As previously mentioned, the posterior region of Axis can be described on the same fashion as the vertebrae in this area.

The goal of the present study is to model the cervical spine and the first vertebrae of the thoracic spine (T1); it is therefor essential to determine the required parameters to model T1. The study by Panjabi et al. [216] was used to define the parameters.

Table 6: Parameters describing the vertebral body of C2-T1.

Parameter	Mnemonic
End Plate Depth Upper	EPDU
End Plate Width Upper	EPWU
Uncovertebral Joint Inclination Frontal Plane Upper	UJIFU
Uncovertebral Joint Inclination Sagittal Plane Upper	UJISU
Uncovertebral Joint Area Upper	UJAU
End Plate Anterior Radius Upper	EPARU
End Plate Depth Lower	EPDL
End Plate Width Lower	EPWL
Uncovertebral Joint Inclination Frontal Plane Lower	UJIFL
Uncovertebral Joint Inclination Sagittal Plane Lower	UJISL
Uncovertebral Joint Area Lower	UJAL
End Plate Anterior Radius Lower	EPARL
Vertebral Body Height	VBHP

Table 7: Values for the parameters describing the vertebral body of C2-T1 [204,216].

Mnemonic	C2	C3	C4	C5	C6	C7	T1
EPDU (mm)	-	15	15.45	15.55	17.15	18.3	18.5
EPWU (mm)	-	15.8	17.2	17.25	18.95	21.9	24.5
UJAU (mm^2)	-	43.6	38.95	42.85	53.45	42.15	28.34
UJIFU (°)	-	76.6	78.9	83.1	94.45	110.9	113.40
UJISU (°)	-	38.7	40	34.5	40.8	47.3	0
EPARU (mm)	-	17	17	17	17	17	17
EPDL (mm)	15.3	15.45	15.55	17.15	18.3	17.65	19.7
EPWL (mm)	16.65	17.2	17.25	18.95	21.9	23.4	27.8
UJAL (mm^2)	18.75	22.45	24.5	28.85	24.7	21.2	32.55
UJIFL (°)	77.5	78.9	83.1	94.45	110.9	113.4	113.40
UJISL (°)	63.7	47.8	47.8	45	49.2	59.8	0
EPARL (mm)	17.16	17	17	17	17	17	17
VBHP (mm)	-	11.6	11.4	11.4	10.9	12.8	14.1

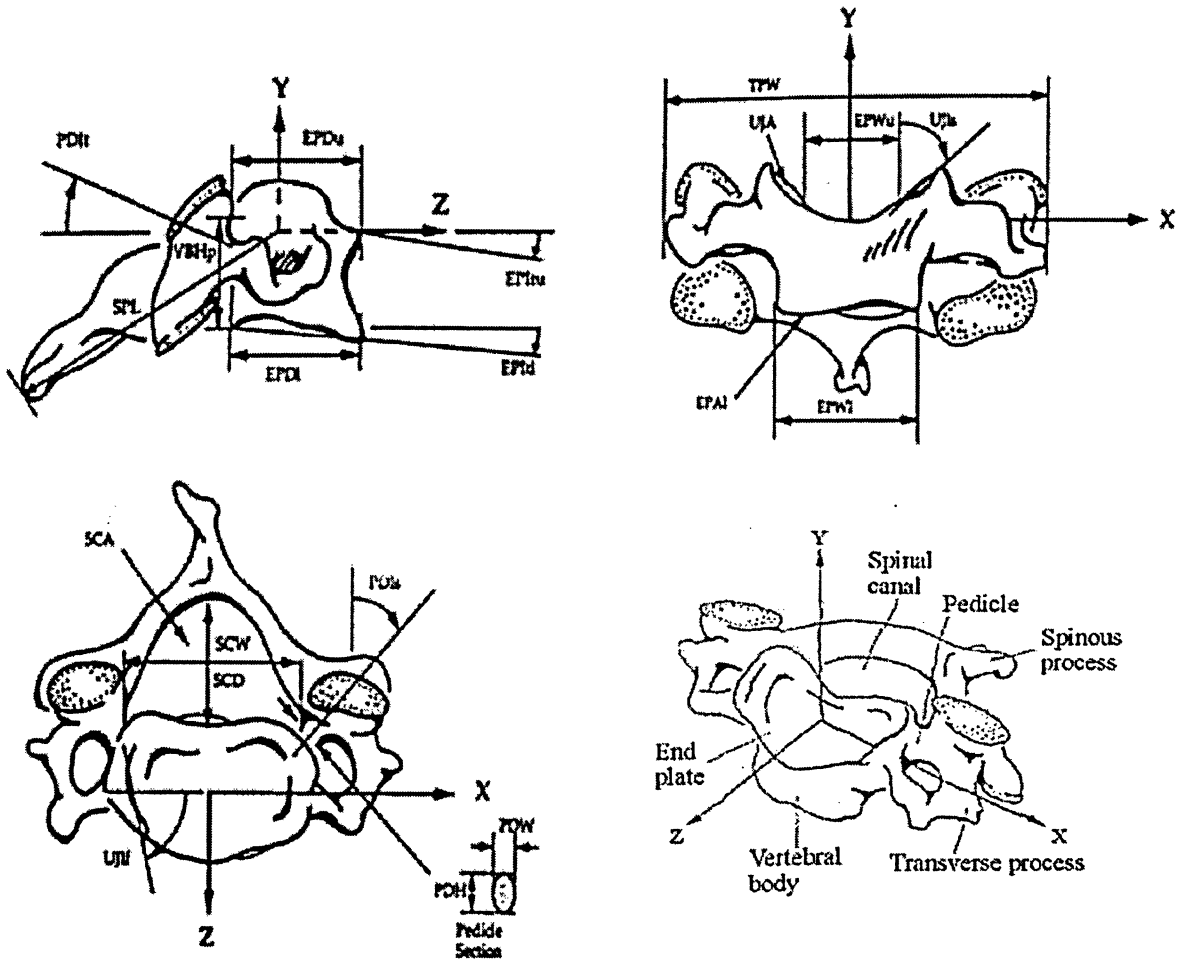

Figure 38: Four views, front, side, top and isometric, of a cervical vertebra [204].

Table 8: Parameters describing the articular facets of C2-T1.

Parameter	Mnemonic
Facet Width Superior	FCWS
Facet Height Superior	FCHS
Card Angle about X-axis Superior	CAXS
Card Angle about Y-axis Superior	CAYS
Interfacet Width Superior	IFWS
Interfacet Height Superior	IFHS
Facet Width Inferior	FCWI
Facet Height Inferior	FCHI
Card Angle about X-axis Inferior	CAXI
Card Angle about Y-axis Inferior	CAYI
Interfacet Width Inferior	IFWI
Interfacet Height Inferior	IFHI
Facet Line Distance to Vertebral Wall	FB

Table 9: Values for the parameters describing the articular facets of C2-T1 [205].

Mnemonic	C2	C3	C4	C5	C6	C7	T1
FCWS (mm)	16.4	11	11.425	11.85	12.075	12.725	13.45
FCHS (mm)	17.85	11.975	12.275	11.925	11.05	11.825	12.625
CAXS (°)	-37.1	-52	-48.60	-50.227	-53.453	-59.880	-53.465
CAYS (°)	49.4	-20.1	-13.17	14.7385	16.6788	9.09921	10.8672
IFWS (mm)	30.3	35.9	37.3	38.15	39.45	39.3	37.1
IFHS (mm)	*	6.3	8.25787	6.54713	7.44434	8.65	8.1258
FCWI (mm)	11	11.425	11.85	12.075	12.725	13.45	12.55
FCHI (mm)	11.975	12.275	11.925	11.05	11.825	12.625	12.9
CAXI (°)	-47.09	-41.40	-41.354	-45.807	-54.009	-49.45	-64.25
CAYI (°)	-21.69	-14.98	17.2129	18.7586	9.7334	11.5	16.2
IFWI (mm)	35.9	37.3	38.15	39.45	39.3	37.1	28.2
IFHI (mm)	*	6.3	7.59212	6.45286	6.25565	8.65	10.1742
FB (mm)	0.9637	0.8666	0.99895	0.91548	1.00830	1.09146	1.0459

*Note: IFHI+IFHS for C2 is 20.15 mm.

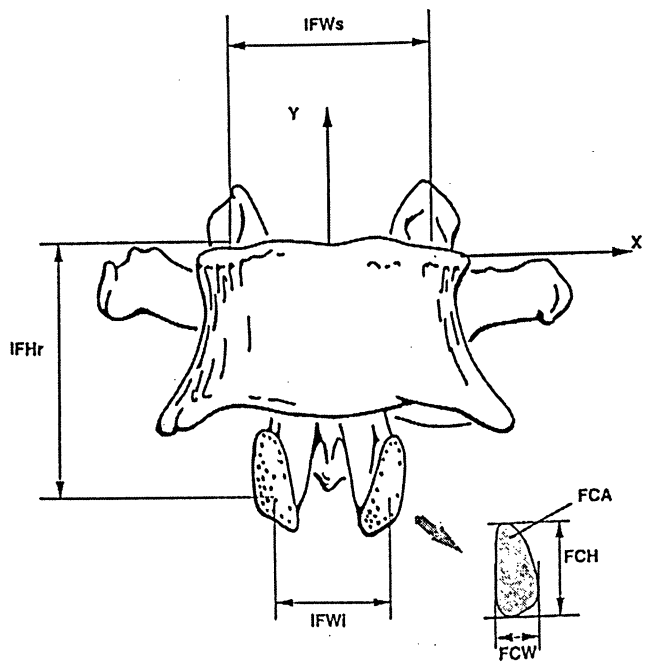

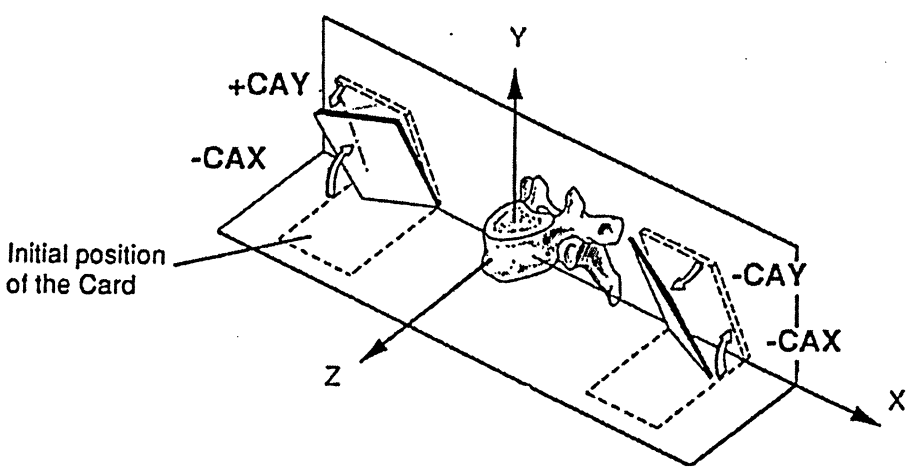

Figure 39: The linear and area measurements of facet joints and facet orientations, in terms of planar and card angles [205].

Table 10: Parameters describing the posterior region of vertebra C2-T1.

Parameter	Mnemonic
Spinal Process Length	SPL
Spinal Process Inclination	SPI
Spinal Canal Depth	SCD
Spinal Process Back Length	SPBL
Spinal Process Back Cut Length	SPBCL
Spinal Process Back Width	SPBW
Spinal Process Back Height	SPBH
Spinal Process Width	SPW
Spinal Process Height	SPH
Spinal Lamina Width	SLW
Spinal Lamina Angle	SLA
Pedicle Width	PDW
Pedicle Height	PDH
Pedicle Inclination Sagittal Plane	PDIS
Pedicle Inclination Transverse Plane	PDIT

Table 11: Values for the parameters describing the posterior region of vertebra C2-T1[204,206].

Mnemonic	C2	C3	C4	C5	C6	C7	T1
SPL (mm)	33.7	34.4	33.6	35.4	41.5	49.6	50.1
SPI (mm)	16.88	27.39863	25.27285	21.23229	17.02374	21.138	25.55
SCD (mm)	21	16.2	17.7	17.4	18.1	15.2	16.4
SPBL (mm)	1	1	1	1	1	1	1
SPBCL (mm)	4	4	4	4	4	4	4
SPBW (mm)	5	5	5	5	5	5	5
SPBH (mm)	5	5	5	5	5	5	5
SPW (mm)	9	9	9	9	9	9	9
SPH (mm)	7	7	7	7	7	7	7
SLW (mm)	4	3.31	3.44	3.08	2.92	3.10	3.44
SLA (°)	66.90	97.32	95.98	101.13	101.39	109.13	104.03
PDW (mm)	-	5.6	5.4	5.6	5.95	6.55	8.45
PDH (mm)	-	7.4	7.35	7	7.3	7.5	9.6
PDIS (°)	-	42.1	44.25	40.25	31.85	29.9	27.05
PDIT (°)	-	-8.15	-7.55	-6	6.5	11.3	7.55

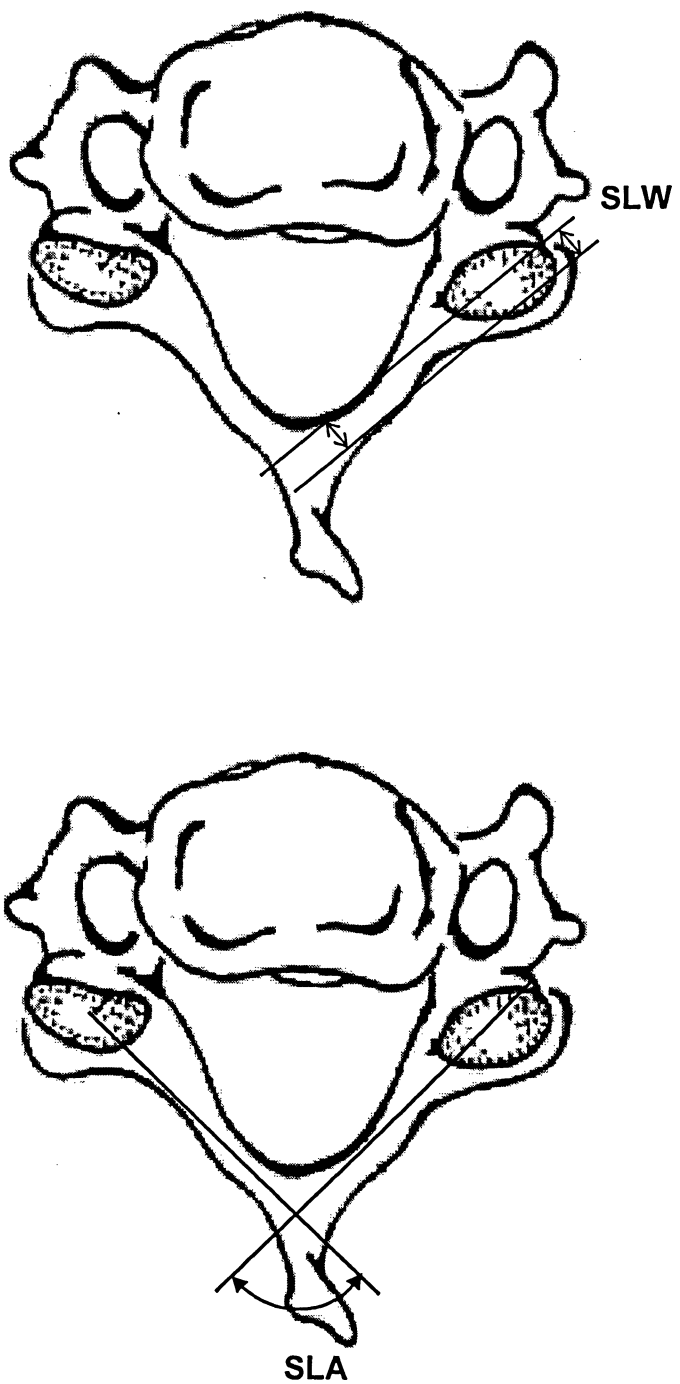

Figure 40: The various parameters defining the spinal lamina of vertebra [206].

The last parameters that should be determined to locate adjacent vertebrae of the cervical spine and to form the curvature of the cervical spine are the anterior and posterior heights of intervertebral discs. With these parameters, the relative angles of adjacent vertebrae can be calculated (Appendix 2). Nissan et al. [212] have presented these parameters for the cervical spine and the lumber spine. Figure 41 and Table 12 show discussed parameters and their values.

Table 12: Parameters determining the relative angles of adjacent vertebrae [212].

Parameter	C2-C3	C3-C4	C4-C5	C5-C6	C6-C7	C7-T1
Anterior Height of Disc, AHD (mm)	4.8	5.3	5.5	5.4	5.2	4.7
Posterior Height of Disc, PHD (mm)	3.4	3.3	3	3	3.3	3.5
Calculated Angle, Alpha (°)	5.24473	7.42233	9.22176	8.02486	5.95159	4.09354
Radius of Rotation, K (mm)	37.1560	25.4917	18.6594	21.4368	31.7832	48.9985

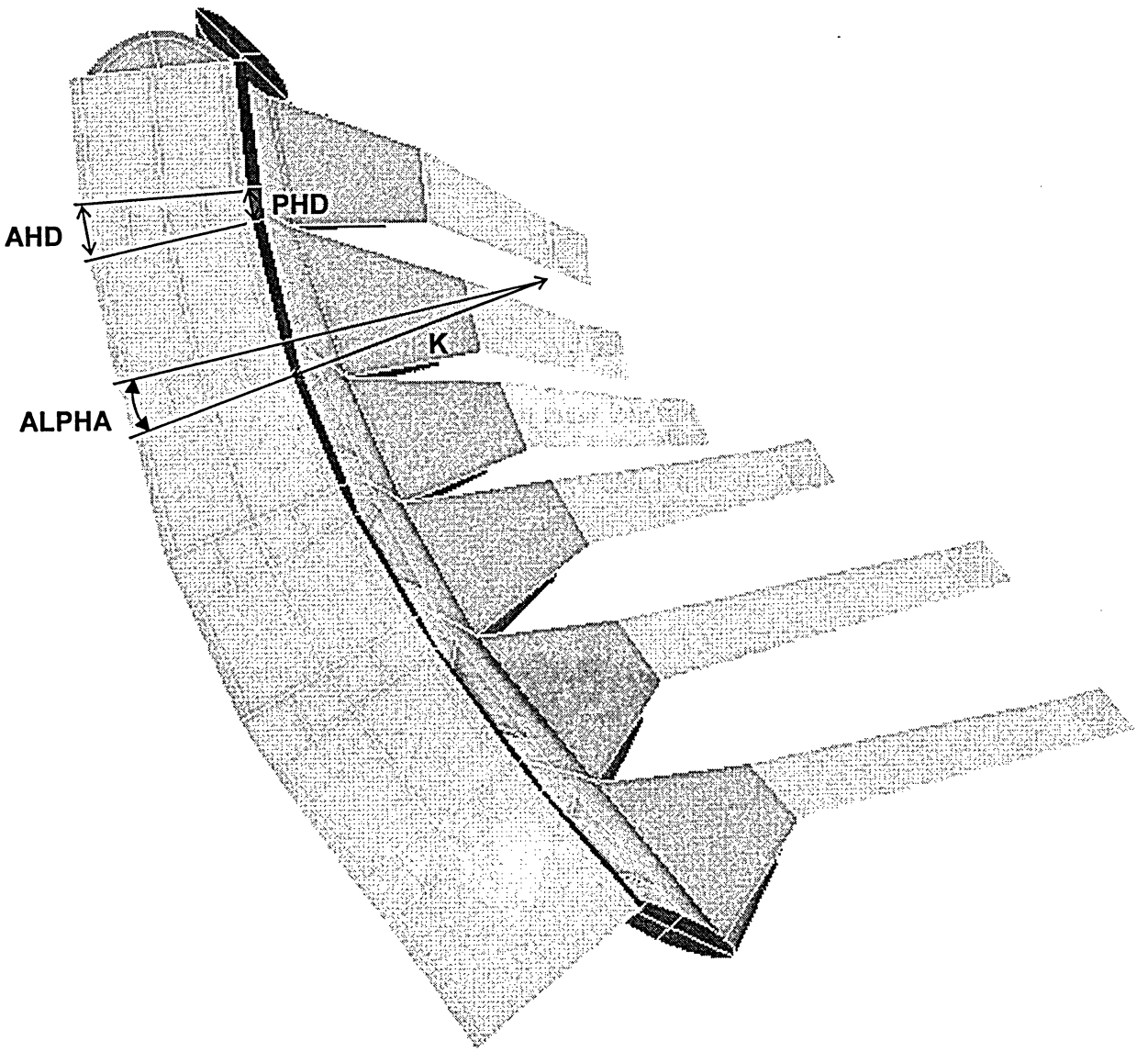

Figure 41: The relative location of adjacent vertebrae.

5.2 Modeling Vertebrae in Cervical Spine

5.2.1 Modeling Atlas

As shown in Table 4, sixteen parameters define the geometry of Atlas. Having the posterior and anterior thicknesses and heights of Atlas, midsagittal areas of posterior and anterior arches of Atlas can be constructed. Rectangular areas were chosen to model the aforementioned areas. Foramen Diameter Lateral and Overall Diameter Sagittal of Atlas define the overall width and length of Atlas and consequently the location of the mentioned areas (Figure 42).

Parameters defining the superior and anterior surfaces of articular facets and the height of the lateral mass of Atlas will assist to model facet joints. As the inferior facets of Atlas sit on superior facets, values presented in Table 9 determine the location of the lateral mass. Figure 43 compares the CAD model with the schematic model of Atlas.

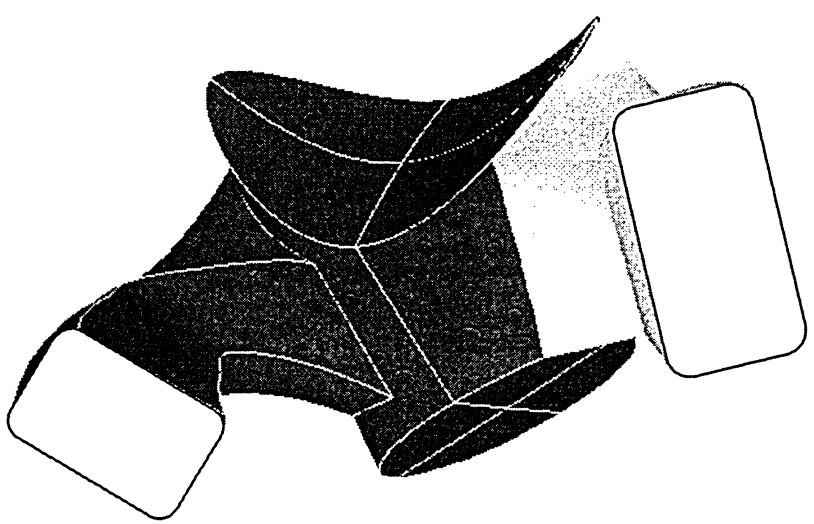

Figure 42: Anterior and posterior areas of Atlas.

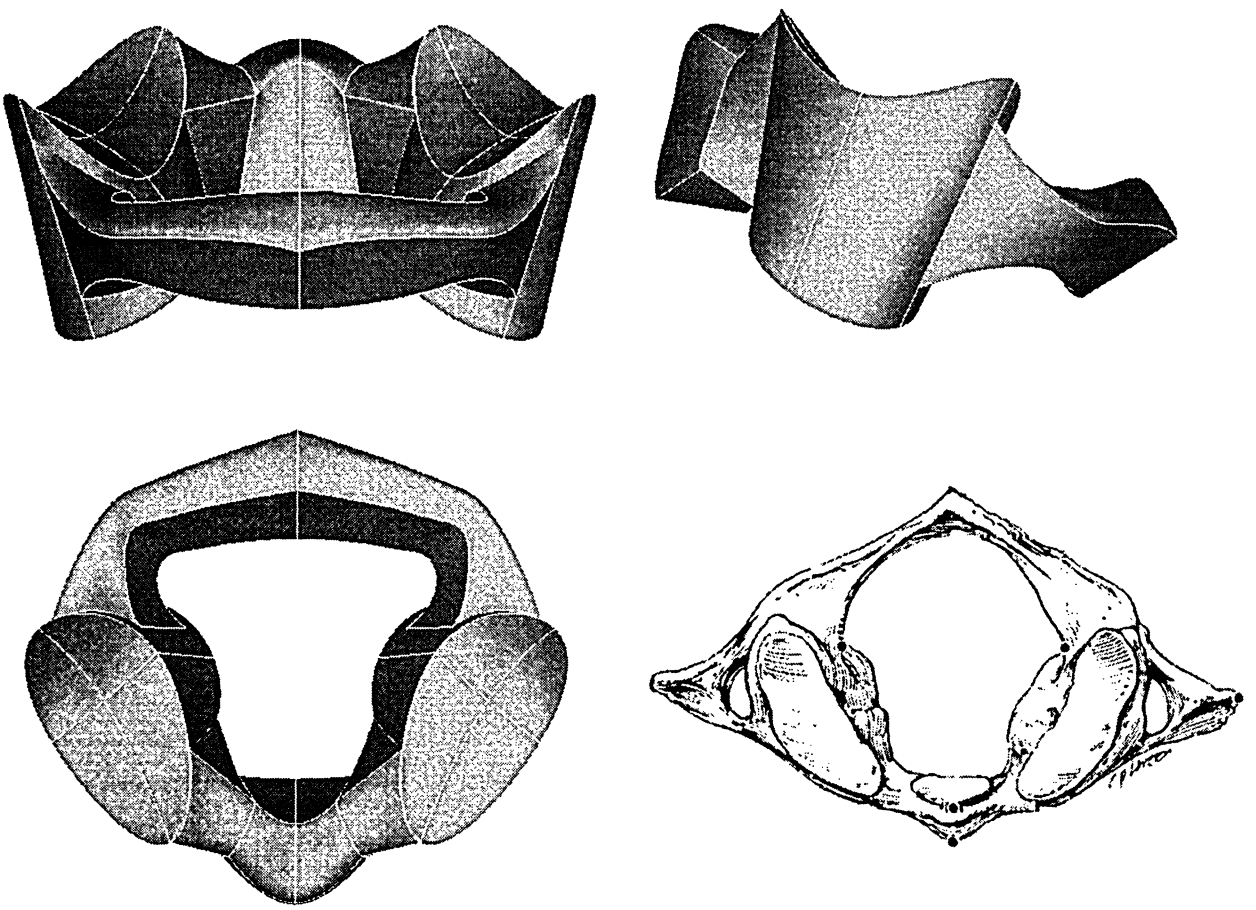

Figure 43: The comparison of the CAD model of Atlas with schematic model of Atlas.

5.2.2 Modeling Axis

The modeling of Axis consists of two sections, the anterior section, which demands parameters listed in Table 5, and posterior region, which can be modeled with the same parameters and methods implemented to model the posterior region of the general vertebrae of the cervical spine.

The inferior endplate of Axis was constructed according to the method elaborated in section 5.2.3. Later, the lower and upper elliptical cross-sections of dens were modeled and located according to the vertebral body height, dens height and angles of dens in the sagittal plane (Figure 44). The thickness of the cortical shell for the anterior region of Axis varies from inferior endplate to the top from 1.275 to 0.225 mm respectively.

The Posterior section of Axis consisting of the inferior and superior facet joints, spinal lamina and spinal process, was modeled the same as the posterior portion of vertebrae from C3 to T1, which will be explained in the next section. Figure 45 compares the CAD model with the schematic model of Axis.

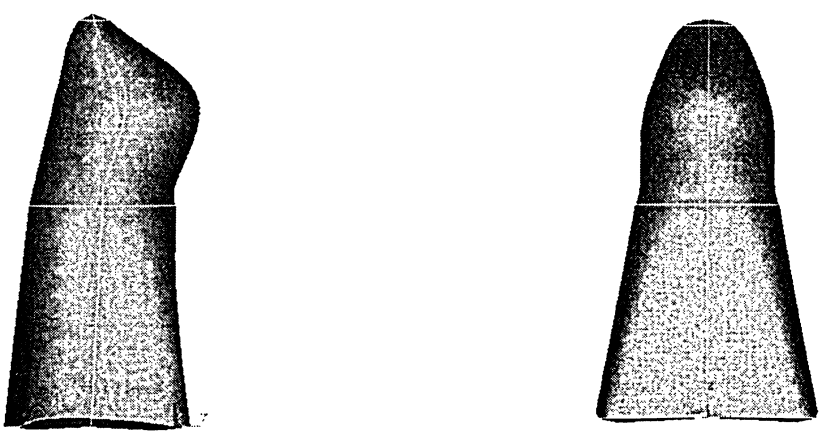

Figure 44: Lateral and posterior views of CAD model of den and vertebral body of Axis.

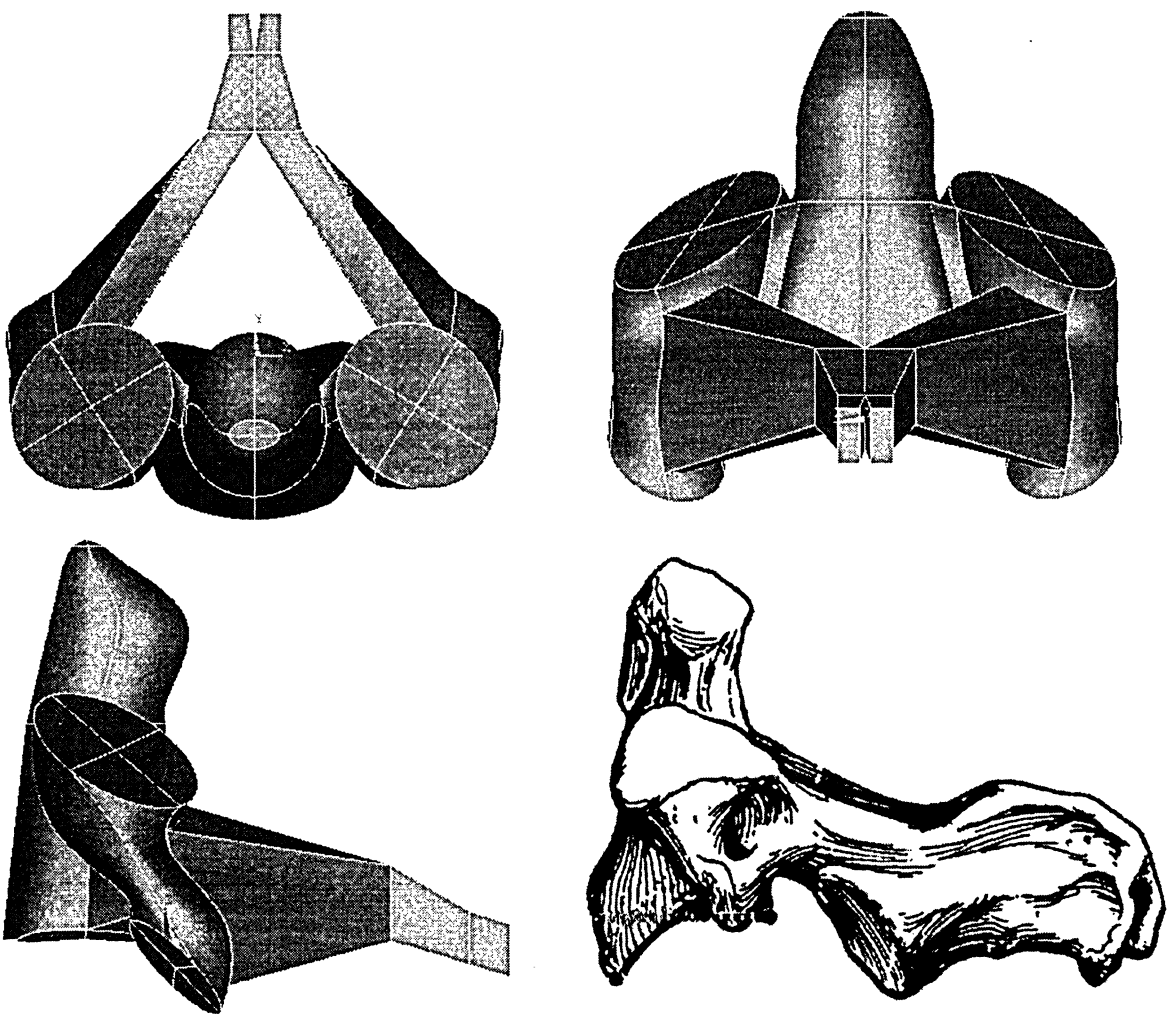

Figure 45: The comparison of the CAD model of Axis with schematic model of Axis.

5.2.3 Modeling the General Vertebrae of Cervical Spine (C3-C7) and T1

In the first step, the inferior and superior endplates of vertebrae were constructed. The necessary parameters to model endplates are EPDU, EPWU, EPDL and EPWL, which are the inferior and superior widths and depths of endplates. Also, UJAU, UJIFU, UJISU, UJAL, UJIFL and UJISL, which are the uncovertebral joint inclination with respect to frontal plane, uncovertebral joint inclination with respect to sagittal plane, and uncovertebral joint area, are needed to model the uncovertebral joint of endplates. Values listed in Table 7 are used to model the endplates. The posterior and anterior curvature of the vertebral body is not reported in literature. The value of the latter was set at 17 mm for all inferior and posterior endplates of the vertebrae to comply with the endplate area presented in the literature. The posterior curvature was determined in a way that the outer curve of the uncovertebral joint be tangent to the anterior curve of the endplate. The thickness of the cortical shell is reported as 1 mm by Panjabi et al. [217]; therefore, the outer border of the endplate was offset by 1 mm interiorly.

When the planar area of the endplate was modeled as the uncovertebral joint inclination with respect to sagittal plane, UJIS, should be applied to the right and left uncovertebral joints to form the proper three dimensional endplate. The distance between the inferior and superior endplates were determined by vertebral body height, VBH. Via this method, the vertebral body for C3 to T1 could be developed. Figure 46 demonstrates the step by step development of a vertebral body for a general cervical vertebra.

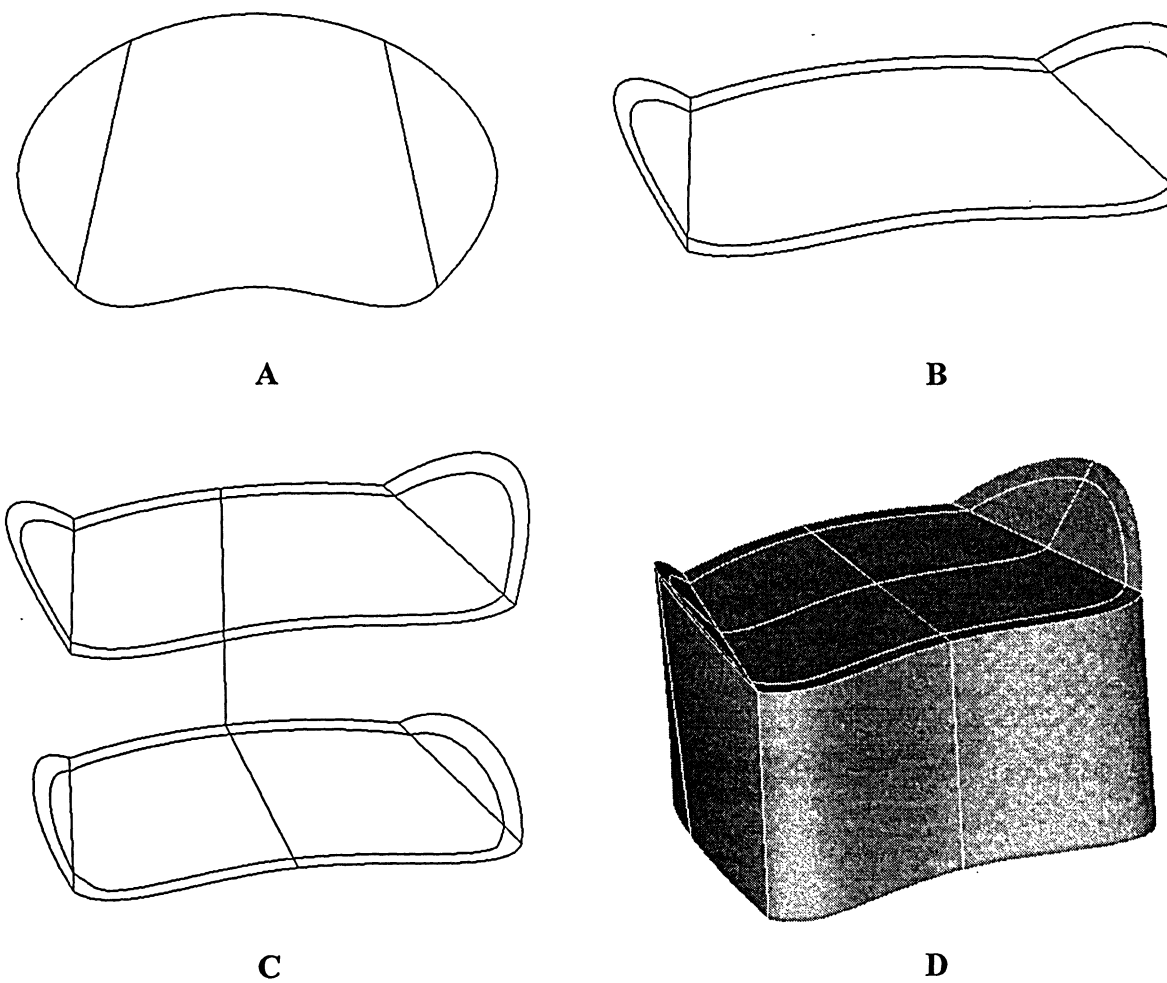

Figure 46: Various steps to model the vertebral body. A) Modeling the inferior and superior endplates. B) Applying uncovertebral joint inclination with respect to sagittal plane. C) Locating superior and inferior endplates of vertebra according to vertebral body height. D) CAD model of vertebral body.

The posterior part of vertebra consists of facet joints, spinous process and spinal lamina. To construct the facet joints, the centers of the facet joints should be located by IFWS, IFWI, IFHS, IFHI and FB. As suggested in the literature [205] the facet joints were defined as ellipse. According to the card angle about X-axis and card angle about Y-axis, the rotation of the facets will be applied in space (Figure 47). The width and height of each facet joint and values for other necessary parameters are listed in Table 9.

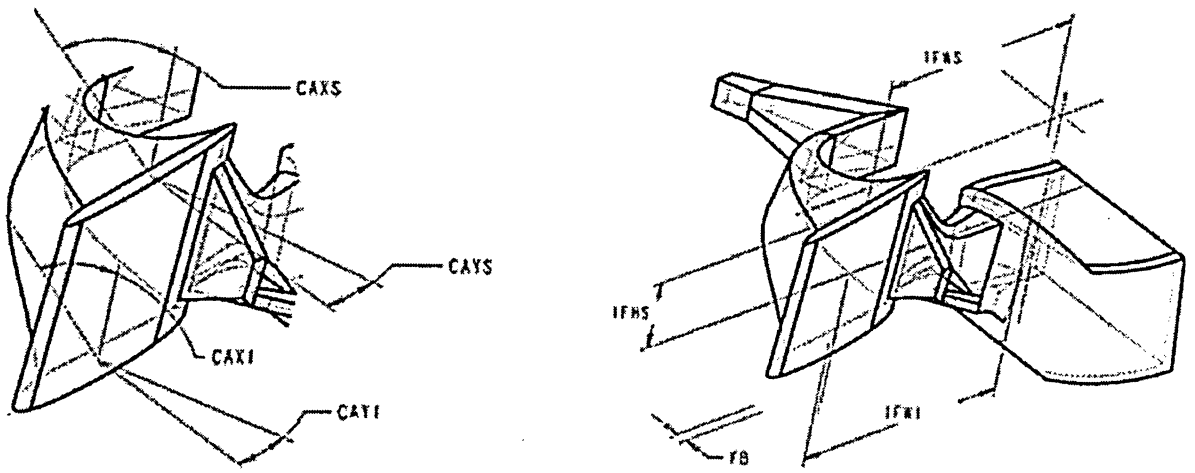

Figure 47: The various parameters defining facet joint of vertebra [218].

Table 11 and Figure 48 clearly illustrate the modeling of the spinal process. Using the two values of thickness and angle listed in Table 11, the spinal lamina can be modeled (Figure 49).

The posterior portion of the vertebra should be connected to the vertebral body by the pedicle. A connecting axis was defined from an interfacet point and using the angular parameters PDIS. PDIT and linear dimensions of pedicle were define by PDW and PDH (Table 11). The connection between the vertebral body and the posterior elements was particularly complex due to the requirements of the meshing.

Modeling the vertebral body, facet joints, spinous process, spinal lamina and pedicles will completed the modeling of a vertebra in the middle and lower region of the cervical spine. Figure 50 illustrates the CAD model of a general vertebra of the cervical spine from various views and compares it with a schematic model of the vertebra.

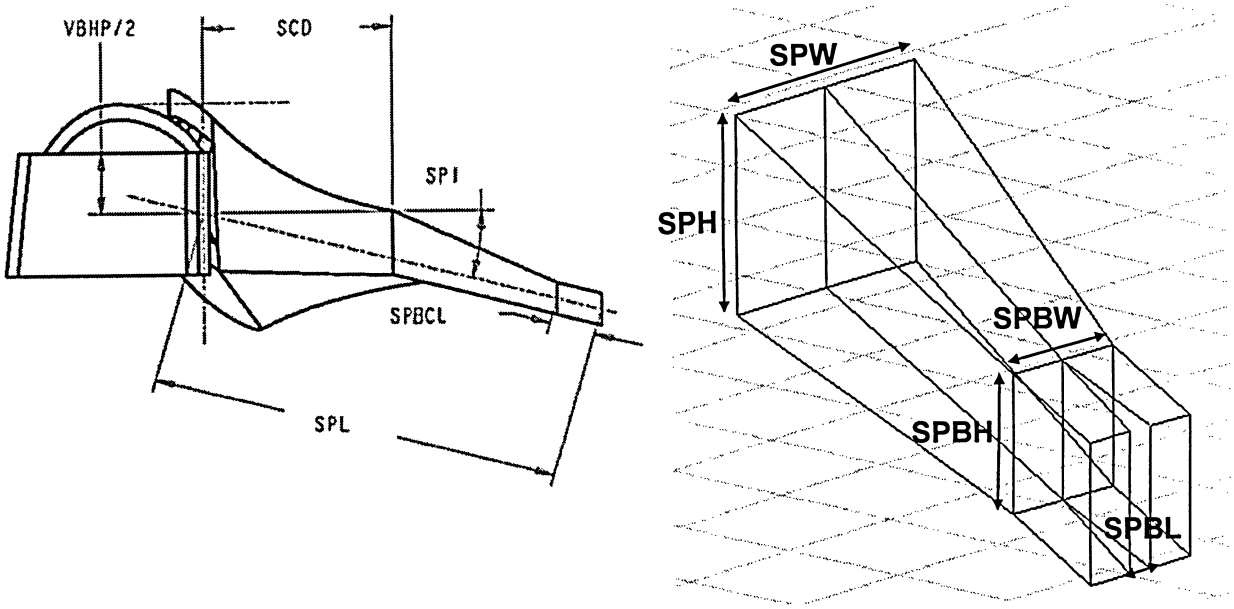

Figure 48: The various parameters defining spinous process of vertebra [218].

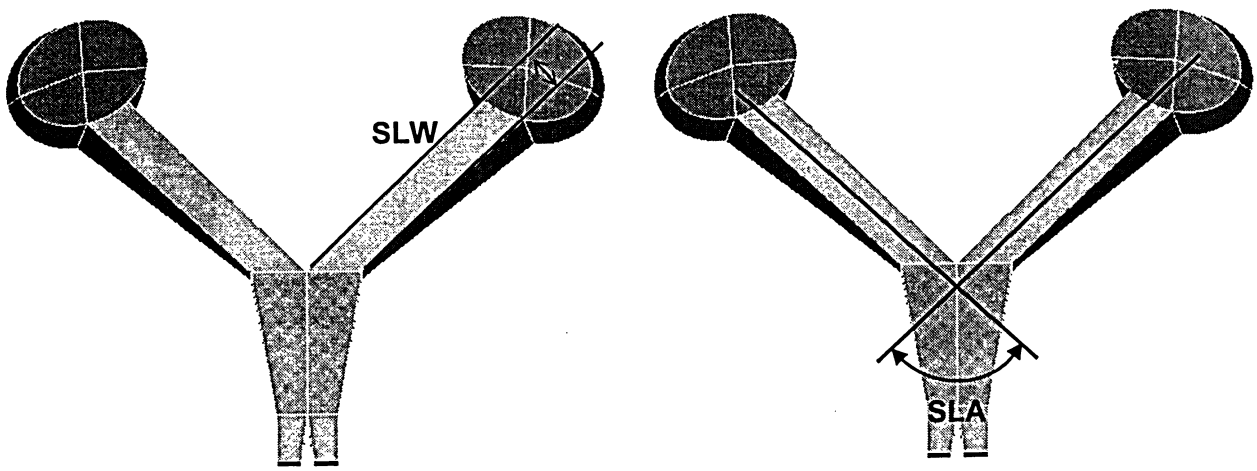

Figure 49: Modeling the spinal lamina based on the lamina thickness and angle.

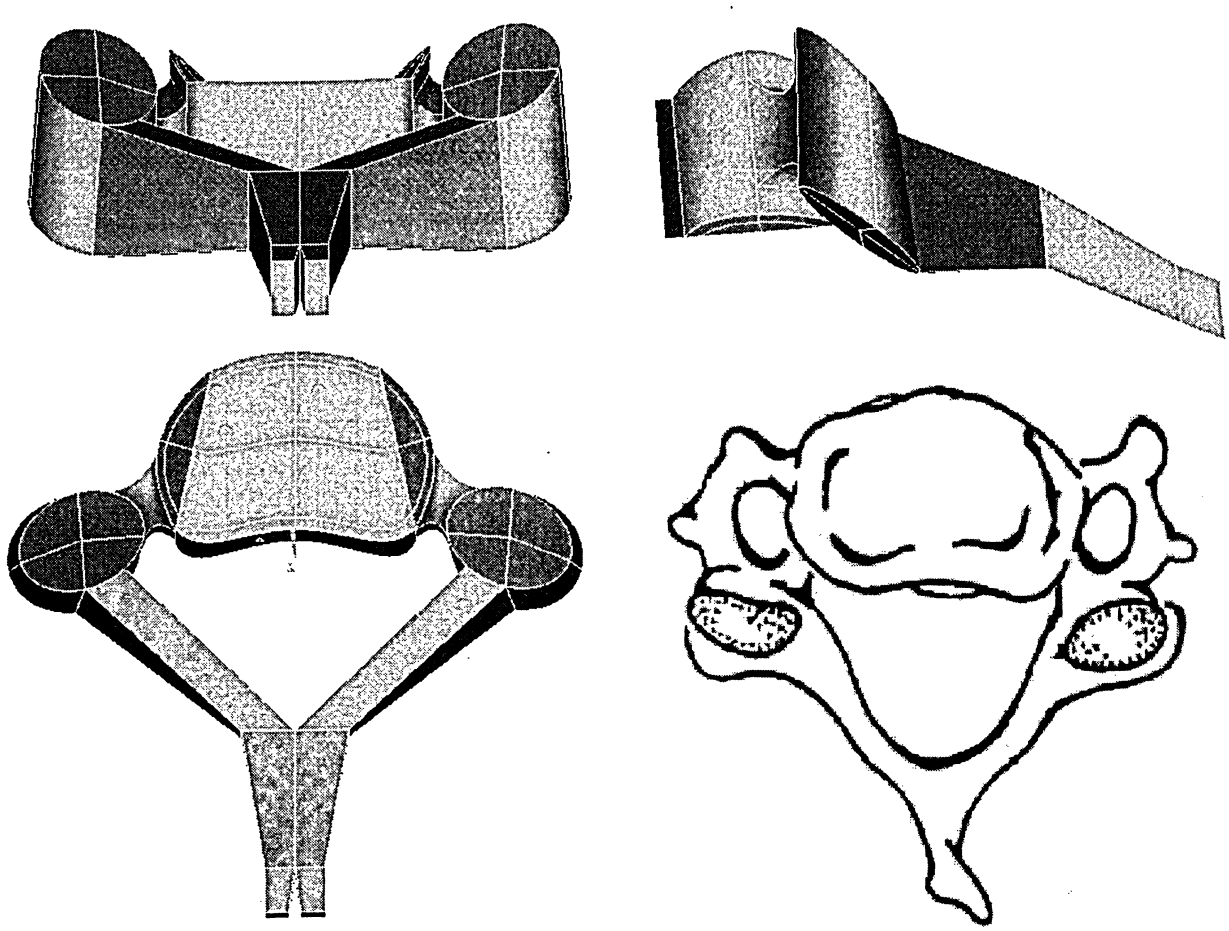

Figure 50: The comparison of the CAD model of a general vertebra of cervical spine with schematic model.

5.3 Assembly of Cervical Spine

The assembly of the cervical spine requires a fixed coordinate system. The inferior posterior midsagittal endplate of Axis was set as the location of the coordinate system. The direction of the Z-axis was selected parallel to the posterior wall of Axis, the Y-axis pointing to the right, and the X-axis was determined accordingly.

As previously mentioned, the calculated center and angle of rotation based on posterior and anterior heights of the intervertebral disc for each motion segment can accurately

place each vertebra in the appropriate location (Table 12). Afterward, Atlas was placed vertically above Axis in a way that the superior facet joints of Axis were parallel to the inferior facet joints of Atlas, maintaining the distance of 0.1 mm.

5.4 Modeling the Intervertebral Disc

Filling the spaces between adjacent vertebrae, the intervertebral discs were modeled. According to the anatomy of the intervertebral disc explained above, nucleus pulposus and annulus fibrosus are the two major components of intervertebral discs; the area of nucleus is half of the area of annulus [219]. Therefore, two volumes were constructed between each two vertebrae resembling the intervertebral disc (Figure 51). After meshing the intervertebral discs, the fibers of annulus were added to the model by Link10 element. The model of the middle and lower region of the cervical spine including intervertebral discs is presented in Figure 52.

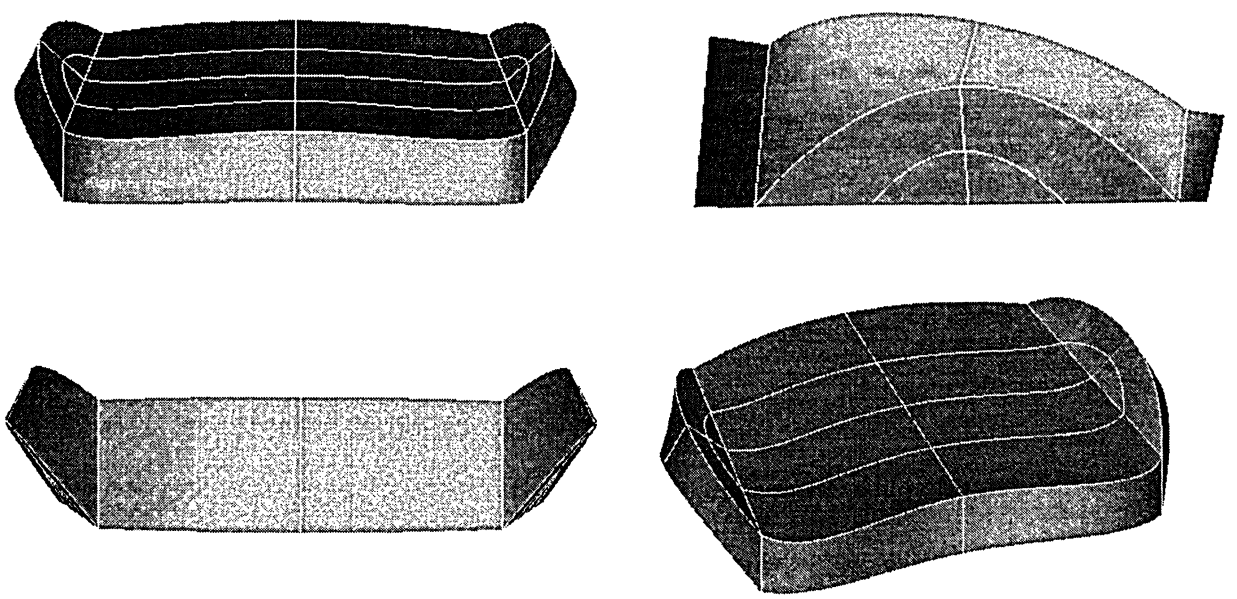

Figure 51: Intervertebral disc from various views.

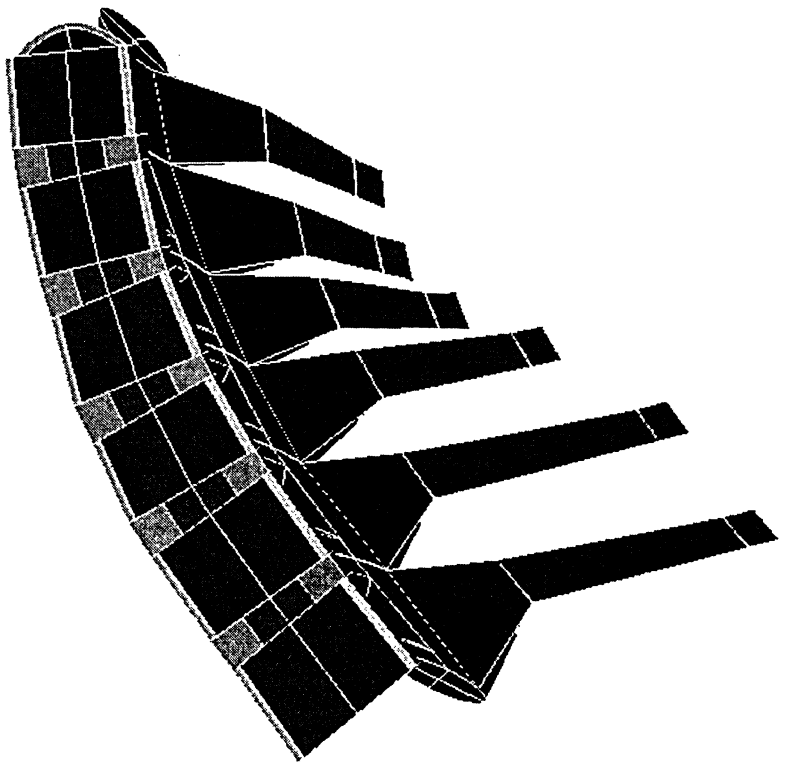

Figure 52: The model of middle and lower region of cervical spine including intervertebral discs.

5.5 Material Property Selection for Finite Element Model of Cervical Spine

In literature, various sets of material properties for the bony elements and soft tissues of the cervical spine are offered. Most of these studies show the same values for the material properties of bony parts. In contrast, there is no unique set of material properties for soft tissues. In some studies, linear values are presented for soft tissues and in the others non-linear values are offered. Although theses values vary from one study to another, one can select the common values repeated in various research.

To construct the finite element model of the cervical spine, the geometric characteristics and material properties of vertebrae, intervertebral discs and the main ligaments of the

lower and upper cervical spine are critical. Table 13 presents the essential components of the cervical spine to develop the finite element model.

Table 13: The various components of cervical spine.

Description	Components
Bony Elements	Cortical Bone
	Cancellous Bone
	Posterior Elements
Intervertebal Disc	Disc- Nucleus Pulposus
	Disc- Annulus Fibrosus
	Annulus Fibers
Lower Cervical Spine Ligaments	Anterior Longitudinal Ligament
	Posterior Longitudinal Ligament
	Interspinous Ligament
	Ligamentum Flavum
	Capsular Ligament
Upper Cervical Spine Ligaments	Alar Ligament
	Transverse Ligament

The two main sets of material properties for bony elements are presented by Maurel et al. [21] and Yoganandan et al. [25]. These values are listed in Table 14. In the available finite element models of the cervical spine developed by various researchers, one of these sets of material properties are predominently used.

Table 14: Material properties of bony elements of cervical spine.

Author	Components	E (Mpa)	Poisson's ratio
Maurel et al. [21]	Cortical Bone	12000	0.3
	Cancellous Bone	100	0.2
	Posterior Elements	6000	0.3
Yoganandan et al. [25]	Cortical Bone	10000	0.29
	Cancellous Bone	100	0.29
	Posterior Elements	3500	0.29

At each vertebral level, the intervertebral discs bind the adjacent vertebral bodies. The intervertebral disc has a special structure, therefore numerous models have been proposed for its material behavior. In the most common model of the intervertebral disc, fiber involvement in the annulus fibrosus was included by superimposing a homogeneous

isotropic material, representing the ground substance and tension only cable members, representing the fibers. In Table 15 some of the proposed material properties of intervertebral discs are compared.

Table 15: Material properties of intervertebral disc in cervical spine.

Author	Components	E (Mpa)	Poisson's ratio
Goel et al.[29]	Disc- Nucleus Pulposus	1.0	0.499
	Disc- Annulus Fibrosus	4.2	0.45
	Annulus Fibers	450	0.30
Yoganandan et al.[220]	Disc- Nucleus Pulposus	K - 1666.7	fluid
	Disc- Annulus Fibrosus	4.7	0.45
	Annulus Fibers	500	
Maurel et al. [21]	Disc- Nucleus Pulposus		
	Disc- Annulus Fibrosus	2.5	0.45
	Annulus Fibers (lateral)	10.0	
	Annulus Fibers (anterior and posterior)	110.0	
Ng et al. [221]	Disc- Nucleus Pulposus	1	0.499
	Disc- Annulus Fibrosus	4.2	0.45
	Annulus Fibers	450	
Lee et al. [32]	Disc- Nucleus Pulposus	1	0.499
	Disc- Annulus Fibrosus	3.4	0.4
	Annulus Fibers		

The final step is determining the material properties of ligaments. The bony elements of the cervical spine are connected by a variety of structures that are known as the soft tissues of the cervical spine. Different types of ligaments connect the vertebral bodies and the posterior elements of the cervical vertebrae, and cover one or more segments, depending on the type of ligament and vertebral level.

Capsular ligaments connect the articular facets of the neck. The other remaining ligaments connect various parts of the adjacent vertebrae. These soft tissues enable the movement of the cervical spine in general and between the cervical vertebrae. They are also responsible for limiting the range of many movements under normal conditions. In the case of external loading, they are essential to keep the integrity of the cervical spine.

Although the general functions of soft tissues are to enable and limit movement of the cervical spine, they differ in structure and contribution to these functions. Ligaments contain different amounts of collagen and elastin, and their main contribution is to resist tension [220]. The significant differences in the mechanical properties of the soft tissues compared to the bony parts, makes the roles of each type of soft tissues exclusive. Thus, it is crucial to consider the most appropriate set of material properties for ligaments in a finite element model of the cervical spine.

Various values for material properties of lower cervical spine ligaments are proposed in the literature. On the contrary, for the upper cervical spine ligaments, only a few references can be mentioned. In Table 16 and

Table 17, the linear and non-linear material properties of the main ligaments of the cervical spine are listed.

Table 16: Material properties of the lower ligaments of cervical spine.

Author	Components	E (Mpa)	Cross Section (mm^2)
Goel et al.[29]	Anterior longitudinal Ligament	15 (<12%) 30 >12	
	Posterior longitudinal Ligament	10 (<12%) 20 >12	
	Interspinous Ligament	4 (<20–40%) 8 >40	
	Ligamentum Flavum	5 (<25%) 10 >25	
	Capsular Ligament	7 (<12%) 30 >12	
Yoganandan et al. [220]	*C2-C5*		
	Anterior longitudinal Ligament	43.8 (<12.9) 26.3 (>12.9)	11.1
	Posterior longitudinal Ligament	40.9 (<) 22.2 (>11.1)	11.3
	Interspinous Ligament	4.9 (<26.1) 3.1 (>26.1)	13.0
	Ligamentum Flavum	3.1 (<40.7) 2.1(>40.7)	46.0
	Capsular Ligament	5(<56) 3.3(>56)	42.2
	C5-T1		
	Anterior longitudinal Ligament	28.2 (<14.8) 28.4 (>14.8)	12.1
	Posterior longitudinal Ligament	23.0 (<11.2) 24.6 (>11.2)	14.7
	Interspinous Ligament	5.0 (<27.0) 3.3 (>27.0)	13.4
	Ligamentum Flavum	3.5 (<35.3) 3.4 (>35.3)	48.9
	Capsular ligament	4.8(<576) 3.4(>57)	49.5
Maurel et al. [21]	Anterior longitudinal Ligament	10	0.5
	Posterior longitudinal Ligament	20	0.5
	Interspinous Ligament	3	3
	Ligamentum Flavum	50	0.4
	Capsular Ligament	20	0.5
Kumaresan et al. [28]	Anterior longitudinal Ligament	11.9	
	Posterior longitudinal Ligament	12.5	
	Interspinous Ligament	2.4	
	Ligamentum Flavum	7.7	
	Capsular Ligament	7.7	
Lee et al. [32]	Anterior longitudinal Ligament	12.0 (<17), 20.0 (>17)	
	Posterior longitudinal Ligament	10.0 (<12), 20.0 (>12)	
	Interspinous Ligament	4.0 (<40), 8.0 (>40)	
	Ligamentum Flavum	5.0 (<25), 10.0 (>25)	
	Capsular Ligament	7.0 (<30), 30.0 (>30)	

Table 17: Material properties of the upper ligaments of cervical spine.

Author	Components	E (Mpa)	Poisson's ratio
Yang et al. [30]	Alar Ligament	11.4	0.4
	Transverse Ligament	17.1	0.4
Lee et al. [32]	Alar Ligament	10	0.3
	Transverse Ligament	20	0.3

Studying the material properties of various parts of the cervical spine, the most common material properties used by other researchers were selected. The linear material properties of the cervical spine used to model the present finite element model of the cervical spine are listed in Table 18.

Table 18: The linear material properties of the cervical spine used to model the present finite element model of cervical spine.

Component	Material Property	Element
Cortical Bone	E=10,000 Mpa $\upsilon = 0.29$	Solid45
Cancellous Bone	E=1000 Mpa $\upsilon = 0.29$	Solid45
Posterior Elements	E=3500 Mpa $\upsilon = 0.29$	Solid45
Nucleus Pulposus	E=1 Mpa $\upsilon = 0.4999$	Solid45
Annulus Fibrosus	E=4.5 Mpa $\upsilon = 0.45$	Solid45
Annulus Fibers	E=450 Mpa Area 0.08 mm^2	Link10 Tension Only
Alar Ligament	E=10 Mpa $\upsilon = 0.3$	Solid185
Transverse Ligament	E=20 Mpa $\upsilon = 0.3$	Solid185
Facet Joints	Initial Gap=0.25 mm $\mu = 0.01$	Conta178
Anterior Arch of Atlas and Dens of Axis	Initial Gap=0.1 mm $\mu = 0.01$	Conta178
Transverse Ligament and Dens	Initial Gap=0.01 mm	Conta178

There were several options to select material properties for the ligaments. The common approach was to model the ligaments using cable elements with some slacking [21]. Another approach was to introduce the correct value for the cross-sectional area, in which little experimental data was available and then a mixed criterion for the area definition. The recent ligament study by Yoganandan [113] was the most appropriate approach for the development of the current model. The experimental results provide accurate force-deflection values that differ from those commonly used in other studies. In the present study, ligaments of the lower cervical spine area were modeled as a non-linear spring

using Combine39 element with a tension only option. The values of the force-deflection of each ligament are listed in Table 19.

Table 19: Force (N)-Deflection (mm) for the ligaments of lower cervical spine area [113].

ALL		PLL		LF		ISL		CL	
Deflection	Force	Deflection	Force	Deflection	Force	Deflection	Force	Deflection	Force
0	0	0	0	0	0	0	0	0	0
1.2	32	1.2	28	1.8	30	1.3	8.5	1.7	1.5
2.5	60	2.2	50	3.5	55	2.8	10	3.6	29
3.7	81	3.2	66	5.1	71	4.1	23	5	52
4.8	100	4.3	79	6.9	95	5.5	28	7.5	86
6	115	5	88	8	105	7	32	9.5	104

ALL = Anterior longitudinal Ligament
PLL = Posterior longitudinal Ligament
LF = Ligamentum Flavum
ISL = Interspinous Ligament
CL = Capsular Ligament

To distribute the effect of ligaments in the effective regions, each set of ligaments is divided into a number of elements. Therefore, the values of forces in Table 19 are divided into the number of elements chosen for each ligament. Table 20 presents the number of ligaments and force-deflection values for one element of each ligament.

Table 20: Force (N)-Deflection (mm) for the ligaments of lower cervical spine area.

ALL (n=13)		PLL (n=13)		LF (n=20)		ISL (n=7)		CL (n=16)	
Deflection	Force	Deflection	Force	Deflection	Force	Deflection	Force	Deflection	Force
0	0	0	0	0	0	0	0	0	0
1.2	2.461	1.2	2.153	1.8	1.5	1.3	1.214	1.7	0.093
2.5	4.615	2.2	3.846	3.5	2.75	2.8	1.428	3.6	1.81
3.7	6.230	3.2	5.076	5.1	3.55	4.1	3.285	5	3.25
4.8	7.692	4.3	6.076	6.9	4.75	5.5	4	7.5	5.375
6	8.846	5	6.769	8	5.25	7	4.571	9.5	6.5

5.6 Developing the Finite Element Model of Cervical Spine

Once the CAD model of the cervical spine was completed, it was exported into ANSYS 7.0 [222] using IGES format file. Using a bottom-up method, the produced lines of vertebrae and intervertebral discs in the CAD model formed the areas and then the volumes of the vertebrae and intervertebral discs. Except for the articular facet joints and dens volumes, almost all volumes in the model were six-sided; therefore, map meshing could properly create the desired meshes. As the volumes of articular facet joints and dens are cylindrical, their volumes were divided into 4 volumes and sweep meshing was applied to avoid meshes with wide-angle corners.

The volume of annulus fibrosus was divided into 6 layers and each layer of annulus was reinforced by criss-cross form elements using Link10 element to simulate the fibers of annulus fibrosus (Figure 53).

In each level the five ligaments of the cervical spine were introduced to the model (Figure 54). The ligaments were modeled by non-linear spring element, Combine39, with no effect in compression and with a tension behavior as presented in Table 19. It should be noted that the force-deflection table for Combine39 elements in ANSYS was filled by values listed in Table 20.

According to Panjabi et al. [52] and Dvorak et al. [223], the geometry of the alar ligament and transverse ligament were determined and Solid185 element was selected to mesh these two ligaments as suggested by Lee et al. [32] (Figure 55).

As the meshing in inferior and superior endplates of vertebrae is different from those of intervertebral discs, it was essential to introduce coupling equations to keep the adjacent areas connected. This coupling technique was applied to the elements in the surface of

the vertebral bone and to the nodes on the connecting surface of the disc in such a way that the coupling equations would guarantee the attachments of both areas.

Finally, to consider the existing contacts in facet joints, the anterior arch of Atlas and dens of Axis and the transverse ligament and dens of Axis node-to-node contact element, Conta178, was selected. In meshing of the contact areas, it was carefully considered that the nodes in adjacent areas be as close as possible to each other.

The finite element model of the entire cervical spine region is shown in Figure 56.

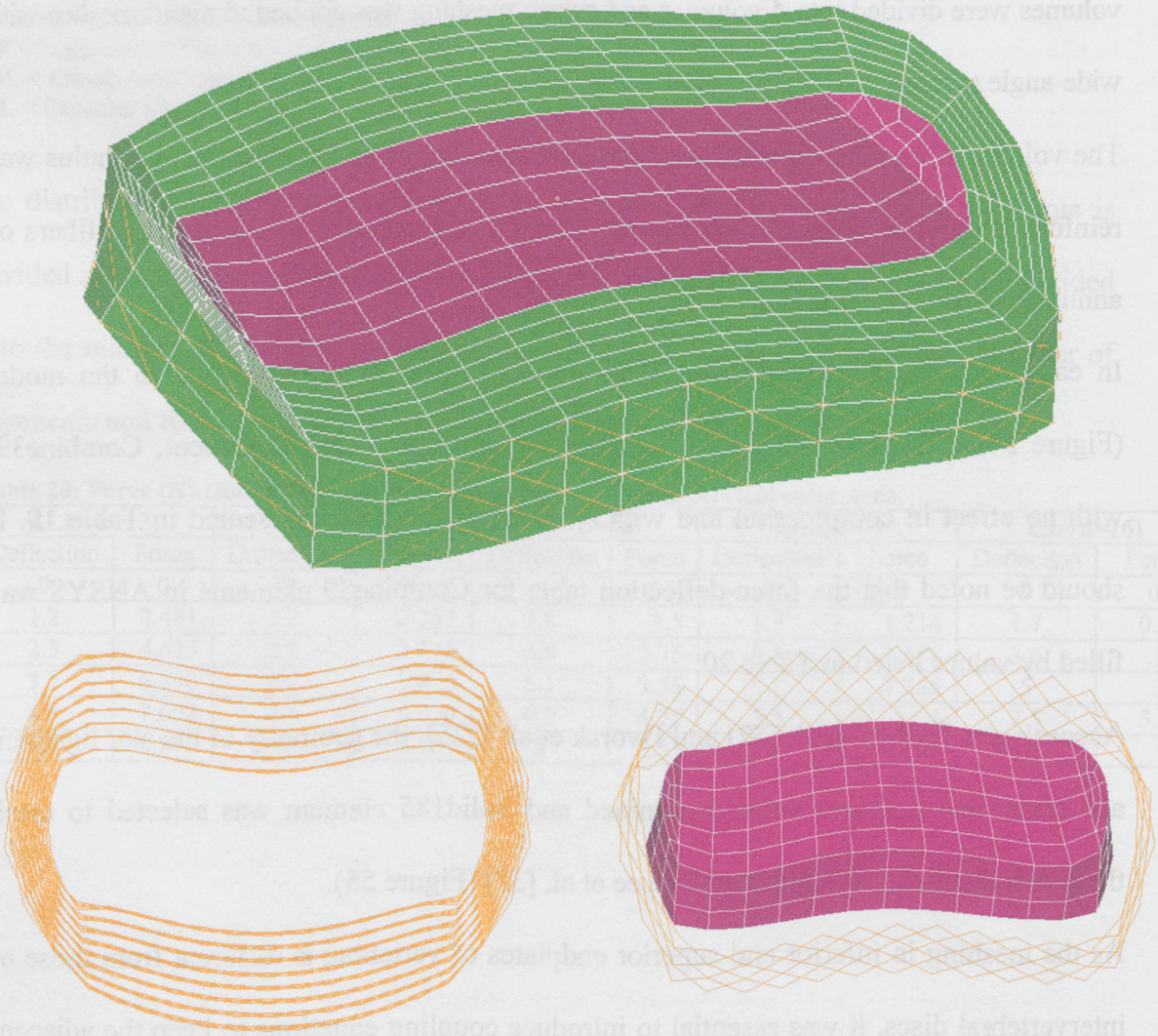

Figure 53: Finite element model of intervertebral disc model including the fibers, 6 layers of annulus surrounding the nucleus and 8 layers of criss-cross elements of fibers reinforce interior and exterior layers of annulus.

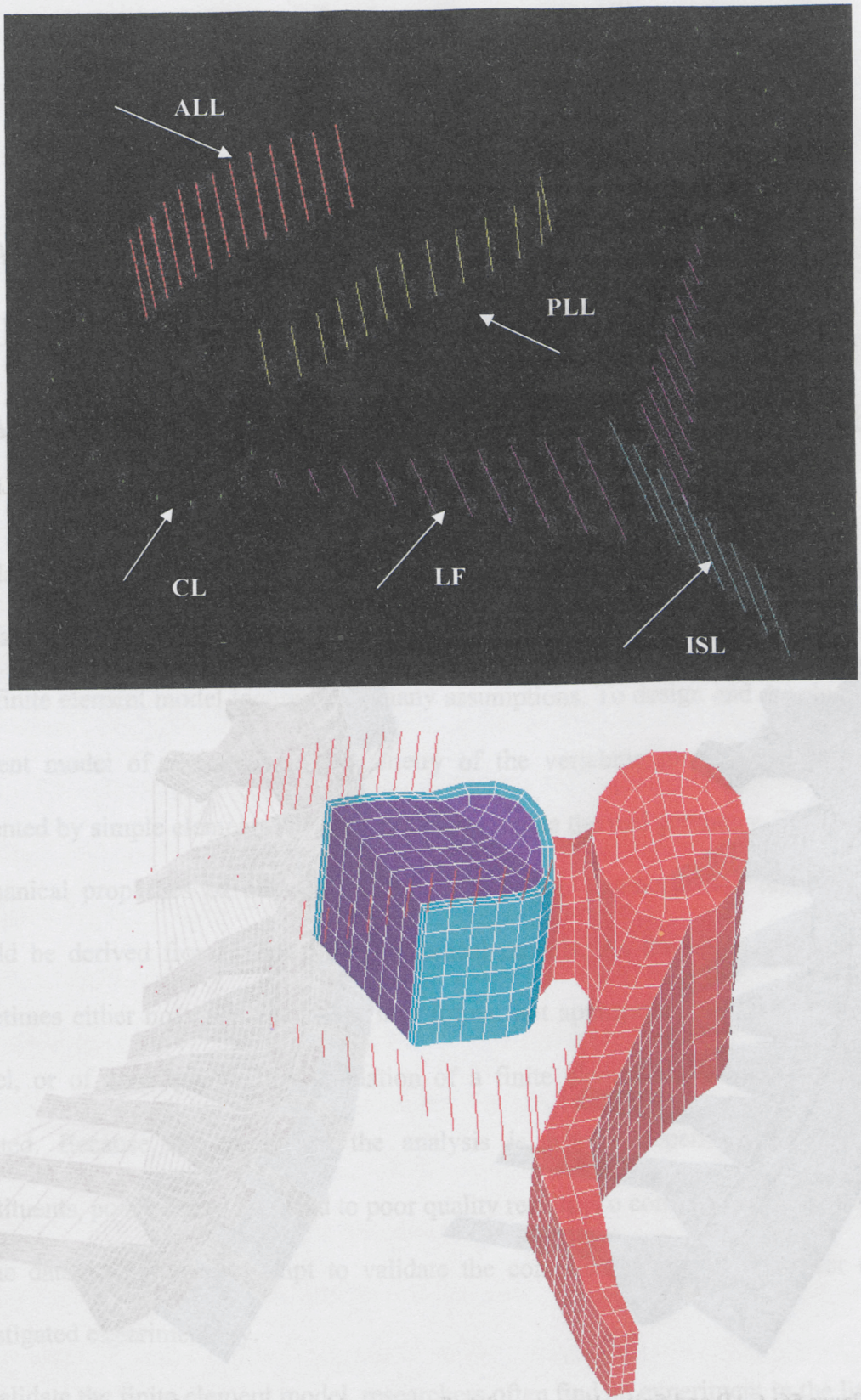

Figure 54: Five sets of ligaments used for middle and lower regions of cervical spine.

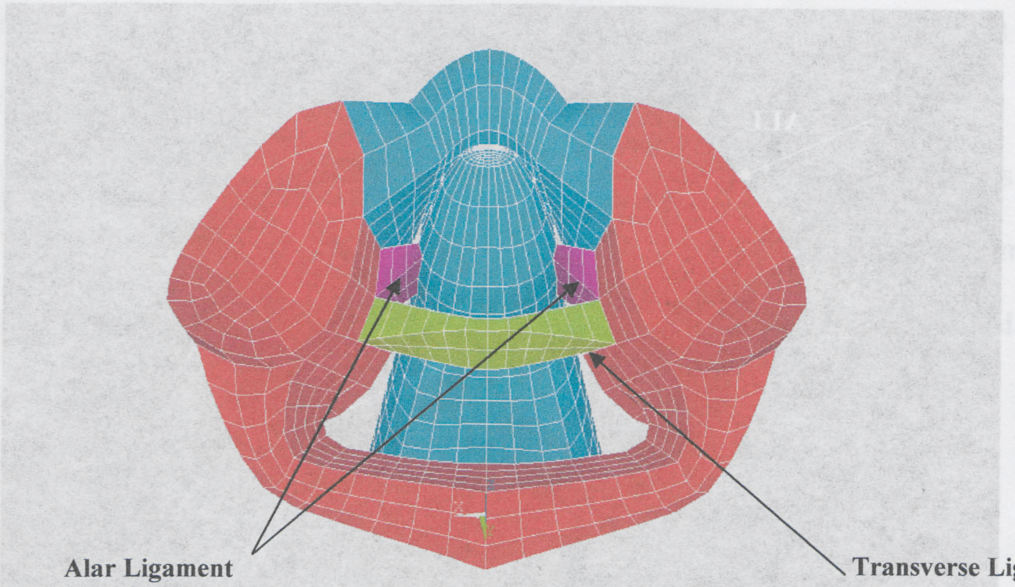

Figure 55: Ligaments of upper cervical spine.

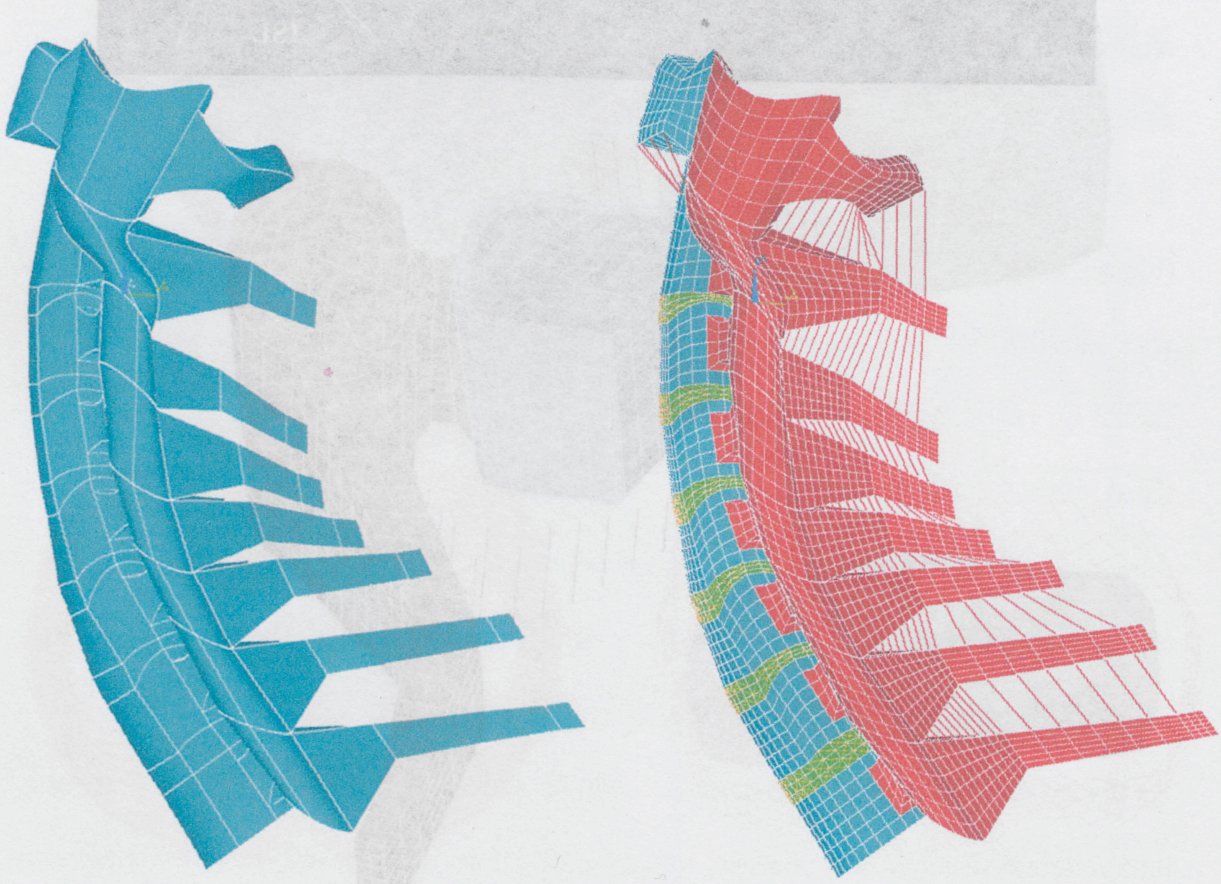

Figure 56: CAD and finite element model of upper and lower regions of cervical spine.

CHAPTER 6

VALIDATION, STRESS ANALYSIS AND MATERIAL SENSITIVITY OF CERVICAL SPINE

Validation of a finite element model is the most important part of the analysis. This critical issue is more difficult to achieve compared to the cadaveric and *in vivo* models. The finite element model incorporates many assumptions. To design and develop a finite element model of the spine, the geometry of the vertebrae must be simplified and presented by simple elements that together approximate the real geometry. To include the mechanical properties of the various soft tissues (e.g. ligaments and discs), the data should be derived from *in vitro* biomechanical models. As the experimental data are sometimes either not available at all, in a format not appropriate for the finite element model, or of poor quality, the validation of a finite element model can be seriously affected. Because the output of the analysis is wholly dependent on the model constituents, poor quality data lead to poor quality results. To compensate the imprecision of the data, researchers attempt to validate the computer model with similar models investigated experimentally.

To validate the finite element model, researchers often find an experiment in the literature suitable for validation, They compare the results of the experiment with those from the

computer model simulation of the experiment. A reasonably good agreement between the two is considered validation of the model. When the model is validated, it can be used for further prediction of behavior of the model in situations in which the model has not been validated. As the validity of the mathematical model is not universal, its use should be restricted to the domain of the experiment against which it was validated. Considering this point, the computer models could be used with advantage to provide basic understanding concerning the functioning of the spinal column. Validated computer models can simulate the effects of injury, degeneration, tumor, and trauma. They can help evaluate new spinal instrumentation without actually manufacturing it.

To validate the present finite element of the complete cervical spine, three types of validation were conducted. First the finite element model of a single motion segment, C5-C6 motion segment, of the cervical spine was validated by the experimental data of Moroney et al. [5]. Then, the finite element model of the cervical spine from C3-T1 was validated under four loading conditions of Extension, Flexion, Lateral Bending and Axial Torsion by the results of experiments published by Panjabi et al. [224]. Finally, the complete model of the cervical spine was validated by the same research work of Panjabi et al. [224]. To analyze the finite element model of the cervical spine, Trial Version of ANSYS 7.0 was used. To investigate the sensitivity of the model against the material properties, the model of the cervical spine from C3-T1 was used. Minimum and maximum values for material properties reported by Kumaresan et al. [28] for various components of the cervical spine were applied to the model and the effect of this variation in material properties was studied.

6.1 Validation of Finite Element Model of Cervical spine

6.1.1 Validation of Model of C5-C6 Motion Segment

To ensure that the process of modeling and assigning material properties to various components of the cervical spine were reliable and suitable for developing the complete model of the cervical spine, the finite element model of C5-C6 motion segment of the cervical spine, constructed according to the method mentioned in previous chapter, was validated by reported results in the literature. The model of C5-C6 motion segment of the cervical spine consists of C5 and C6 vertebrae, C5-C6 intervertebral disc and all five existing ligaments connecting the two vertebrae were developed and tested under four loading conditions (Figure 57). In the model 5220 elements of Solid45 for bony structure of vertebrae and annulus and nucleus of intervertebral disc, 1728 elements of Link10 for fibers of intervertebral disc, 85 elements of Combine39 for existing ligaments and 114 element of Contac178 for contacts of facet joints were used.

To define the loads applied to the model and the motions measured, setting a proper coordinate system is necessary. A three-dimensional coordinate system was defined for this purpose (Figure 58). The origin is located at the inferior-posterior wall of the body of the vertebra in the midsagittal plane. The positive x-axis is directed to the left and perpendicular to the sagittal plane. The positive y-axis is directed superiorly, and the positive z-axis is oriented anteriorly. The applied pure moments were defined as: flexion (+MX), extension (-MX), left axial rotation (+MY), right axial rotation (-MY), right lateral bending (+MZ), and left lateral bending (-MZ).

As the aim of this part of the study was to validate the model with the experimental data of Moroney et al. [5]; the boundary conditions were selected according to the values

reported in the paper. In all four tests, the inferior endplate of C6 was fully constrained. Then, the pure moment of 1.8 Nm (in extension, flexion, lateral bending and axial torsion) and axial load of 73.6 N was applied to the superior endplate of C5.

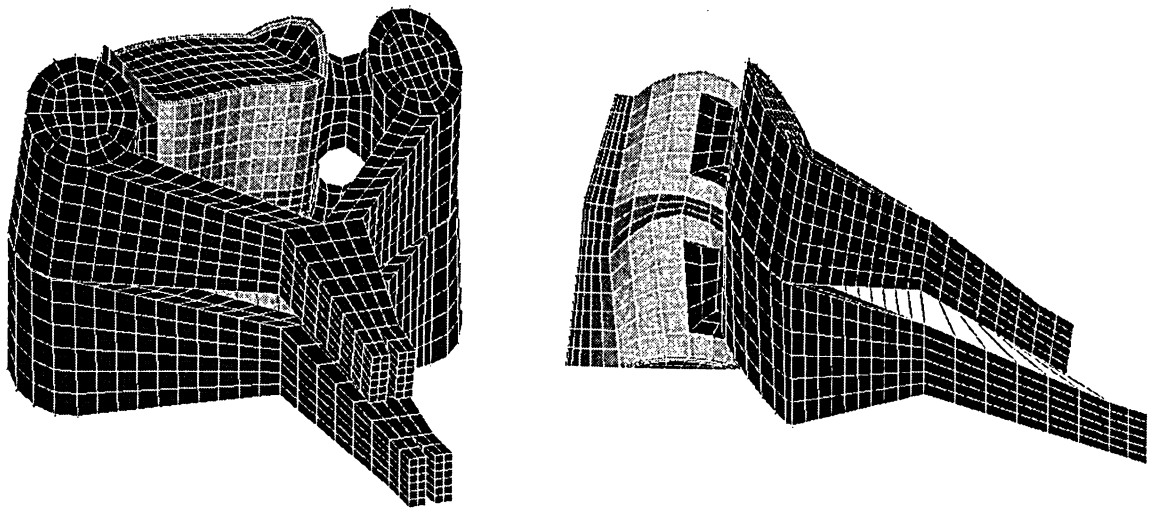

Figure 57: The finite element model of a single motion segment of C5-C6.

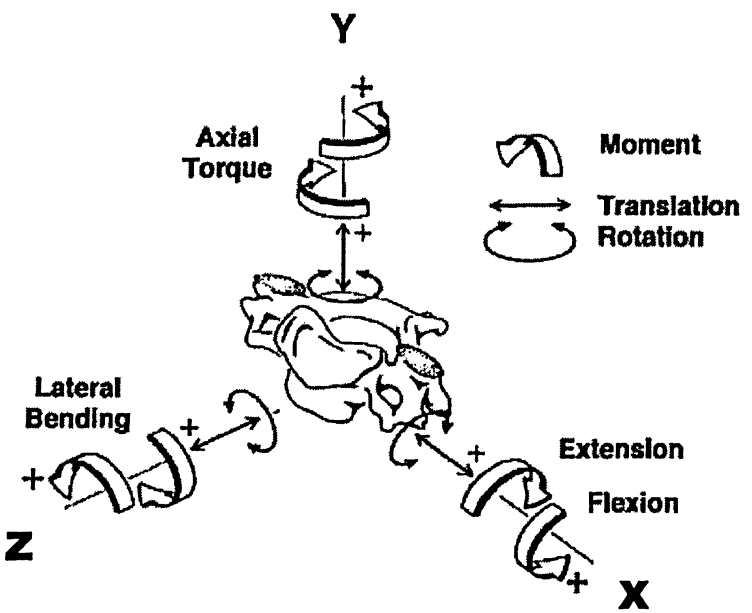

Figure 58: The three-dimensional coordinate system of a moving vertebra [224].

Based on the results of the finite element analysis, the rotation of the single motion segments for extension, flexion, lateral bending and axial torsion was calculated. Figure 59 shows the comparison of the finite element results with data reported by Moroney et al. [5]. The values obtained from the finite element analysis mainly fall in the range of motion observed in the experiment. Therefore, it can be concluded that the finite element results are in good agreement with the reported data in the literature.

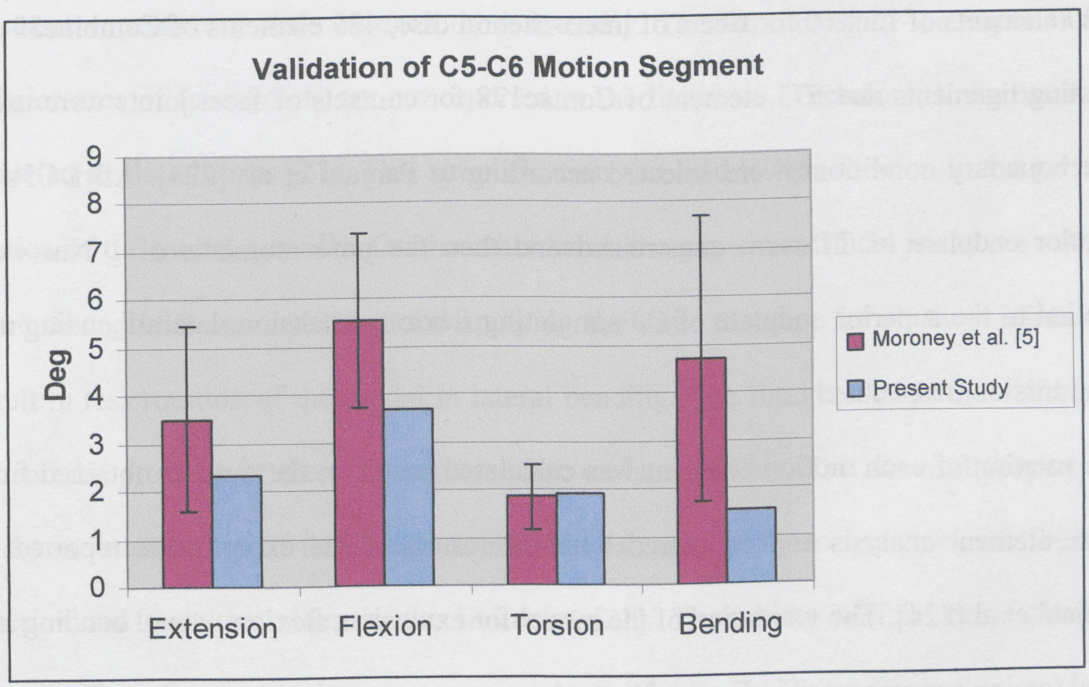

Figure 59: Validation of model of C5-C6 motion segment of cervical spine.

6.1.2 Validation of Model of C3-T1

Before investigating the validation of the complete finite element model of the cervical spine, C3-T1 model of the cervical spine was tested for four loading conditions of flexion, extension, lateral bending and axial torsion. In this study the results of experiments reported in research work of Panjabi et al. [224] were selected as a reference to validate the finite element model of the cervical spine.

This model consists of the vertebrae of C3 to T1, the intervertebral discs of this section of the cervical spine and the connecting ligaments (Figure 60). In the model 17748 elements of Solid45 for bony structure of vertebrae and annulus and nucleus of intervertebral disc, 9720 elements of Link10 for fibers of intervertebral disc, 425 elements of Combine39 for existing ligaments and 573 element of Contac178 for contacts of facet joints were used. The boundary conditions were selected according to Panjabi et al. [224]. All DOFs of inferior endplate of T1 were constrained and then the pure moments of 1 Nm were applied to the superior endplate of C3 simulating flexion, extension, lateral bending and axial torsion, respectively.

The rotation of each motion segment was calculated based on the outputs obtained from finite element analysis and compared with the results of the experiments reported by Panjabi et al [224]. The validation of the model for extension, flexion, lateral bending and axial torsion are presented in Figure 61.

The present finite element model of the cervical spine shows good agreement with the experimental results in flexion, extension and axial torsion. In the case of lateral bending the values of finite element analysis are lower than the experimental results in the first two motion segments. This discrepancy can be justified by several explanations; material

properties of the cervical spine vary in lower and upper regions [225] but material properties in literature are reported regadless of this variation. For the present finite element model of the cervical spine, material properties are applied to the model as they are reported in the literature with no alteration in lower and upper regions. Therefore, considering the same material properties for both regions makes the upper region of the cervical spine become stiffer and rotate less in lateral bending analysis. Another reason rises from the shape and gap distance of facet joints. Observing the anatomy of the facet joint of cervical spine carefully, it can be seen that the superior area of the facet joint is convex and the inferior area is concave. This special feature will allow the adjacent vertebrae to slide on each other laterally. The curvatures of the superior and inferior area of facet joints are not reported in the literature. Therefore, the areas were modeled as flat ellipses [21]. This simplification can lead to less rotation in the general motion of the model laterally. On the other hand, the gap size of facet joints are not the same through the cervical spine and applying the same distance for all facet joints can result in less rotation of the model in lateral bending. The final reason is the difference in material property of the intervertebral disc on lateral sides. The material property of fibers in lateral sides of the intervertebral disc is reported up to one tenth of fibers in anterior and posterior sides in the literature [21]. The model will be more flexible laterally if a softer material property were selected for lateral fibers of annulus.

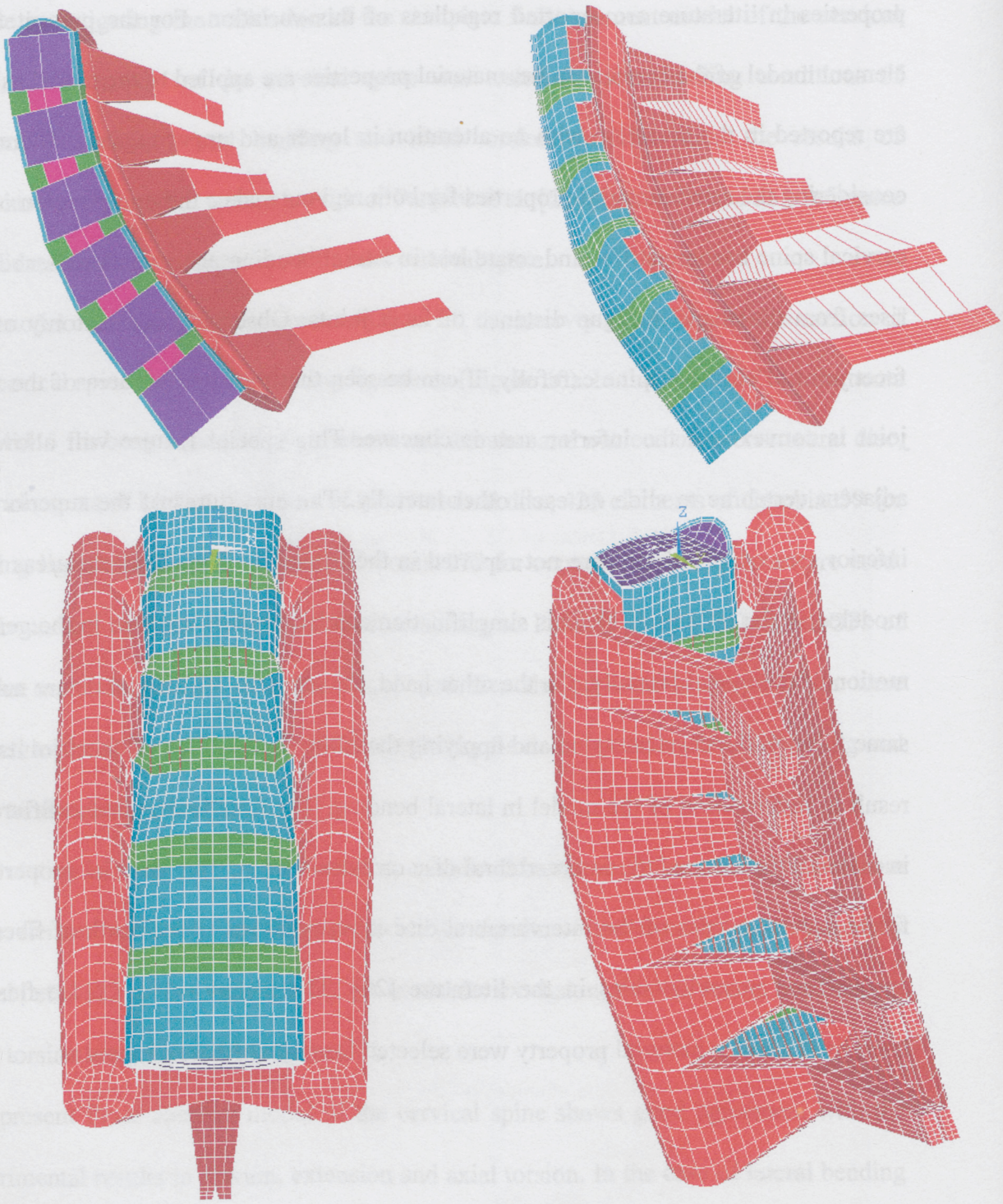

Figure 60: The model of cervical spine from C3 to T1.

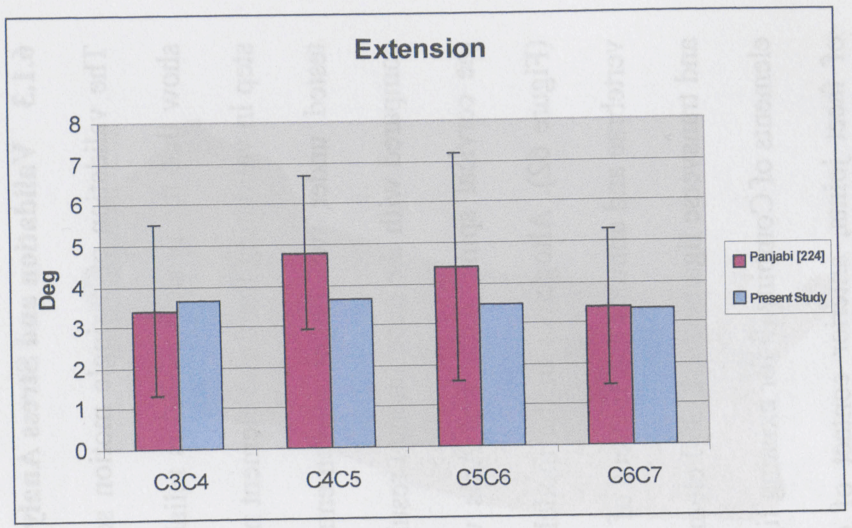

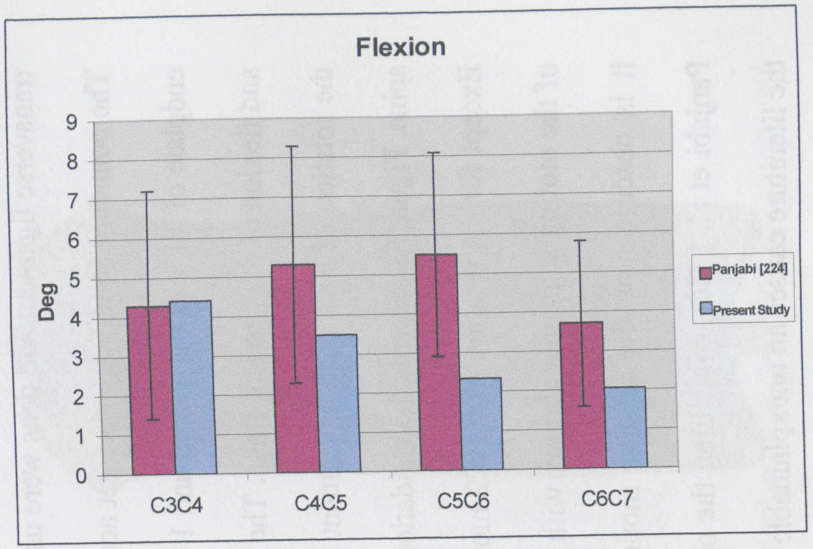

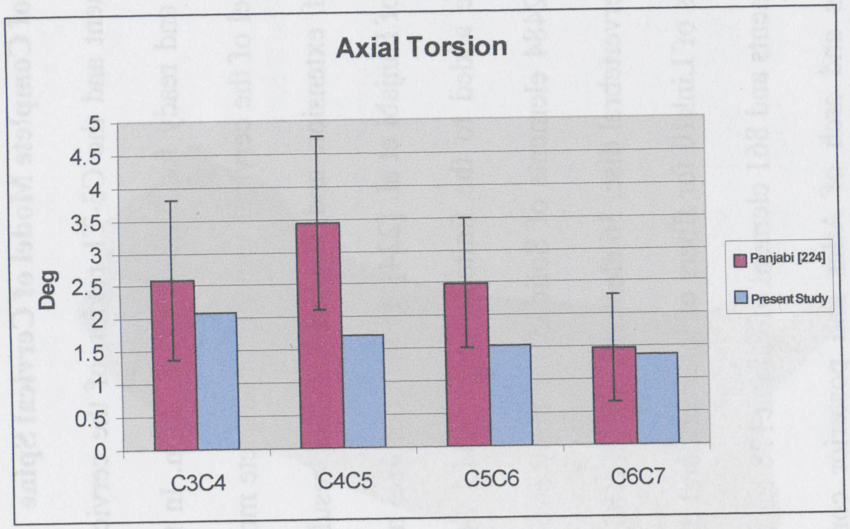

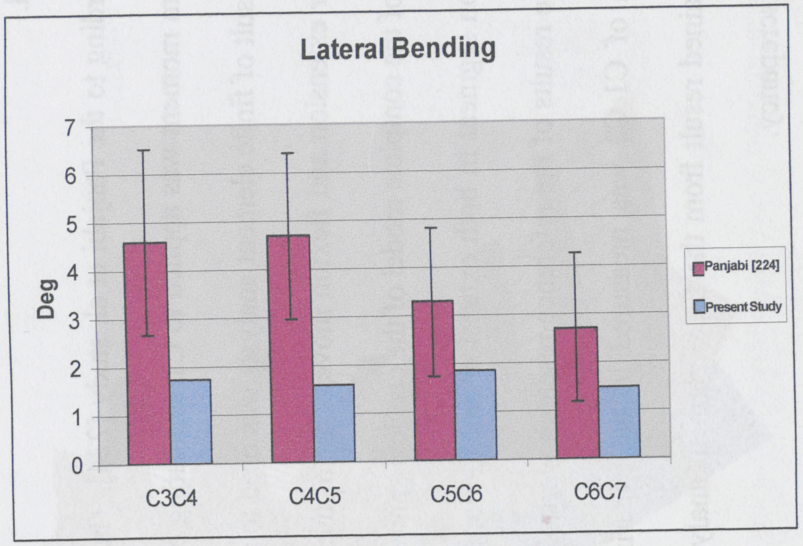

Figure 61: Validation of C3-T1 finite element model of cervical spine in extension, flexion, axial torsion and lateral bending.

6.1.3 Validation and Stress Analysis of Complete Model of Cervical Spine

The validation of a single motion segment and the C3-T1 region of the cervical spine show that the present model is reliable and ready for further investigation. In the final step in validating the finite element model of the cervical spine, the complete model was tested under two major movements of extension and flexion and the results were compared with the experimental results of Panjabi et al. [224]. In the complete model of the cervical spine, Atlas and Axis were added to the finite element model of C3-T1 (Figure 62). Altogether in the model, 22484 elements of Solid45 for bony structure of vertebrae and annulus and nucleus of intervertebral disc, 36 elements of Solid185 for alar and transverse ligaments, 11390 elements of Link10 for fibers of intervertebral disc, 563 elements of Combine39 for existing ligaments and 861 element of Contac178 for contacts of facet joints, anterior contact of dens and arch of Atlas and posterior contact of transverse ligament and dens were used.

The boundary conditions were set according to the Panjabi et al. study [224]. The inferior endplate of T1 was fully fixed and 1 Nm moment was applied to C1 simulating extension and flexion of the cervical spine. The result of finite element analysis was used to calculate the rotation of each motion segment for extension and flexion movements of the cervical spine. Figure 63 presents the validation of the complete model of the cervical spine.

Except for the rotation of C1-C2 motion segment in both extension and flexion, the rest of the motion segments comply with the results of the reference research work [224]. As it is obscure how the relative motion of C1-C2 was measured in the experiment of Panjabi et al. [224], comparing the obtained result from the finite element analysis with the literature causes an unexplainable discrepancy.

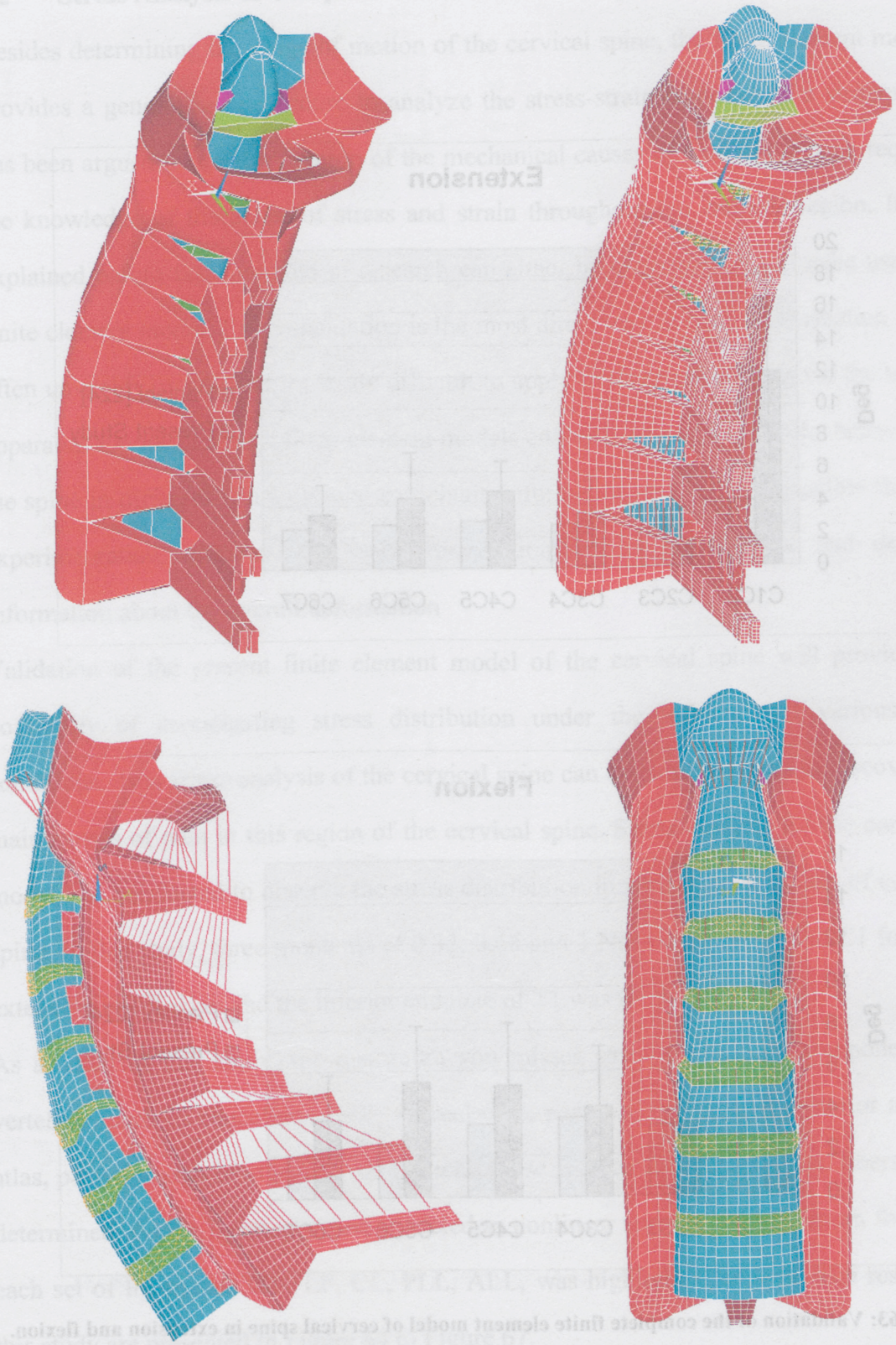

Figure 62: The finite element model of complete cervical spine.

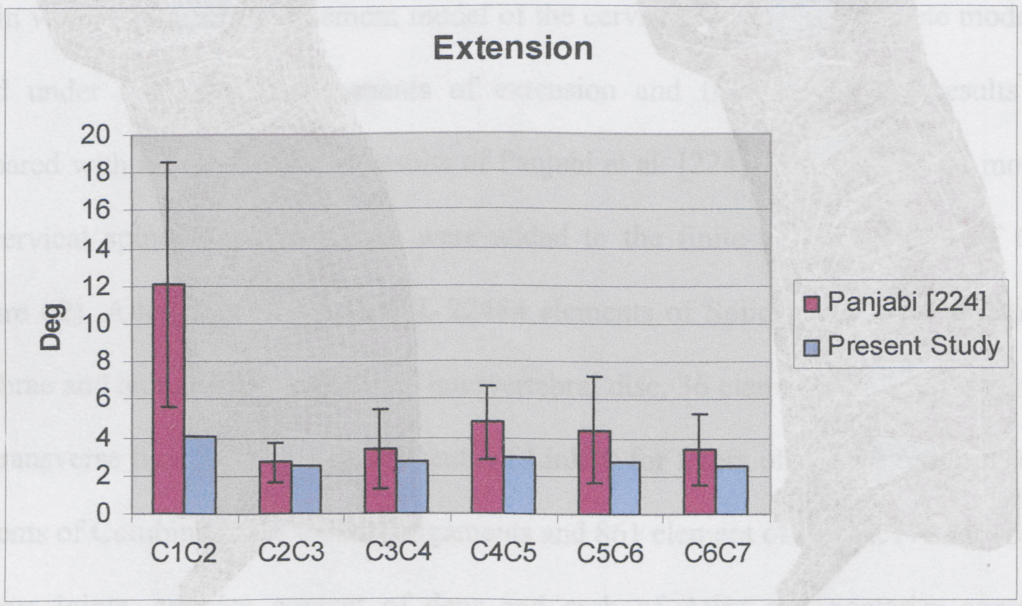

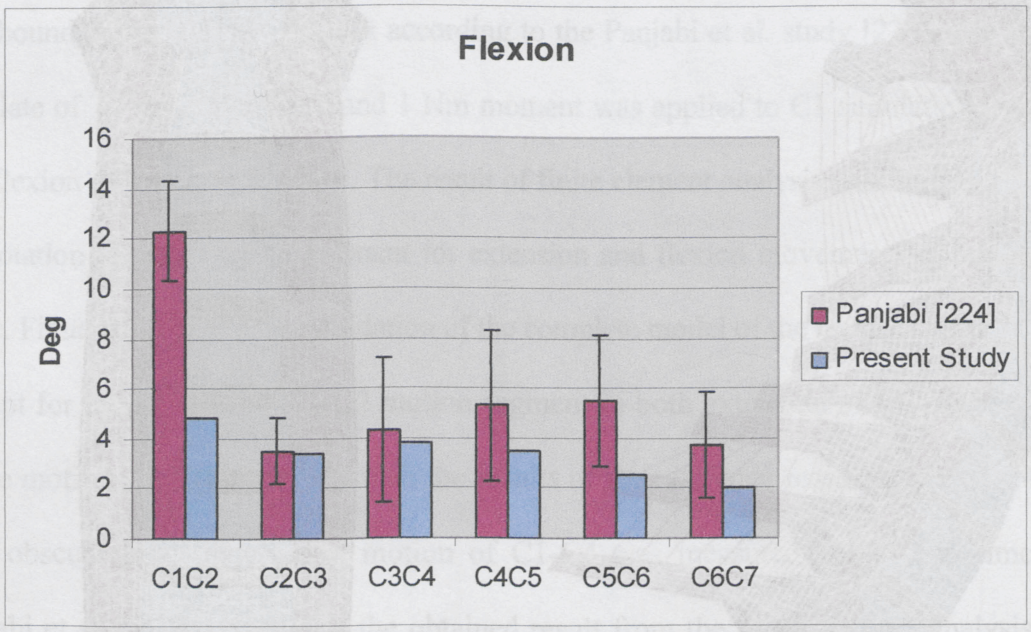

Figure 63: Validation of the complete finite element model of cervical spine in extension and flexion.

6.2 Stress Analysis of Complete Model of Cervical Spine

Besides determining the range of motion of the cervical spine, the finite element method provides a generalized procedure to analyze the stress-strain response of a structure. It has been argued that a clarification of the mechanical causes of pain in the neck requires the knowledge of the states of stress and strain throughout the cervical region. It was explained before that this kind of research can either be experimental, or make use of a finite element model. Experimentation is the most direct way to obtain information but is often unwieldy, costly and loads are difficult to apply in three dimensions via the testing apparatus. On the contrary, finite element models enable the simulation of the behavior of the spine in different situations and can obtain information that is not accessible through experimentation, such as the stress distribution inside the vertebra and detailed information about the overall deformation

Validation of the present finite element model of the cervical spine will provide the possibility of investigating stress distribution under the influence of various load conditions. This stress analysis of the cervical spine can assist researchers to discover the main causes of pain in this region of the cervical spine. Stress analysis for the complete model was conducted to observe the stress distribution in various components of cervical spine. In this study, three moments of 0.33, 0.66 and 1 Nm where applied to C1 for both extension and flexion and the inferior endplate of T1 was fully constrained.

As a result of this study, the maximum von misses stress for various components of vertebrae, such as cancellous shell, cortical core, pedicles, facets, dens, anterior arch of atlas, posterior arch of atlas and intervertebral disc such as annulus, nucleus, fibers, were determined. As the ligaments were modeled as nonlinear springs, the maximum force for each set of ligaments, ISL, LF, CL, PLL, ALL, was highlighted as well. The results of this study are presented in Figure 64 to Figure 67.

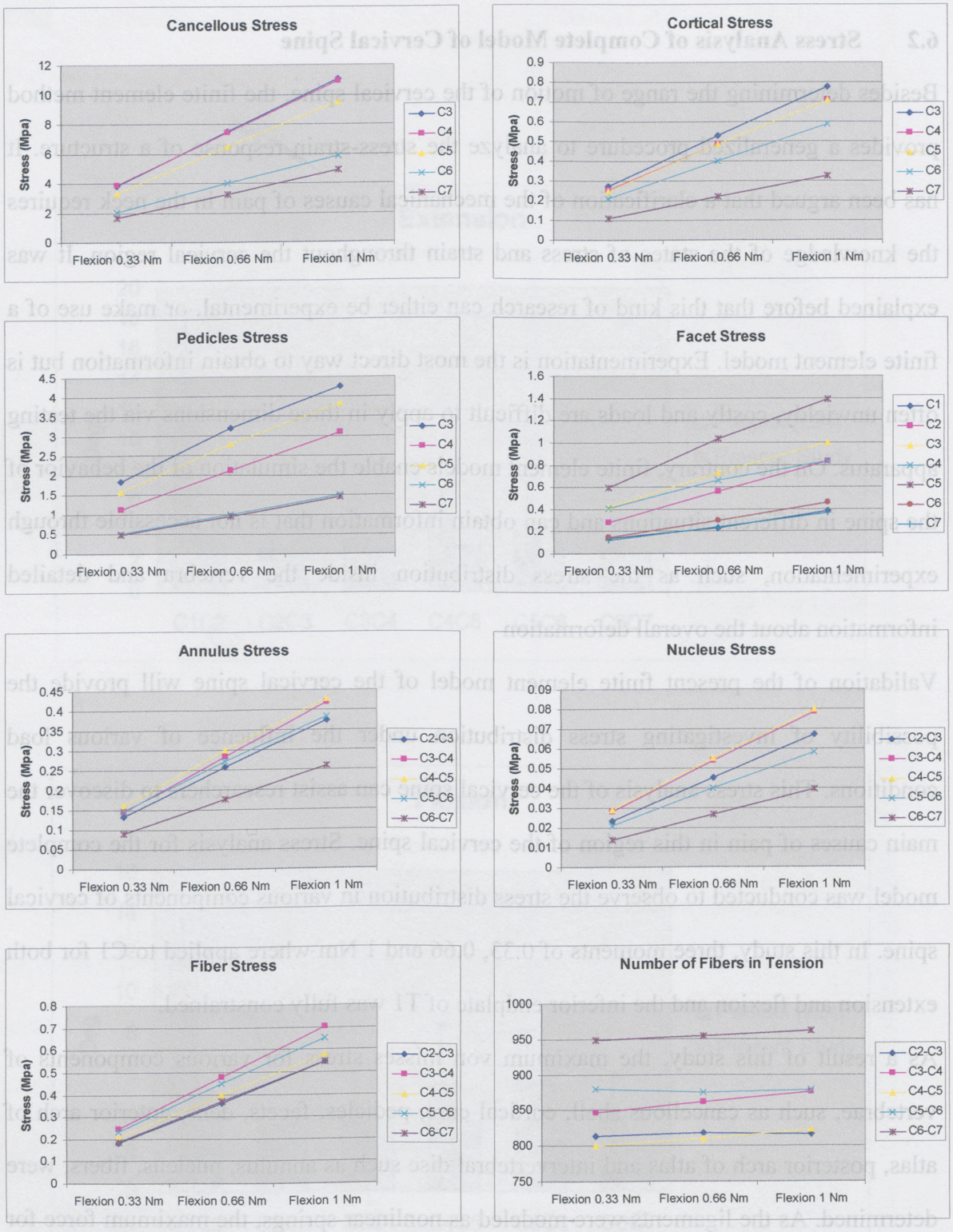

Figure 64: Stress analysis of complete model of cervical spine under flexion movement.

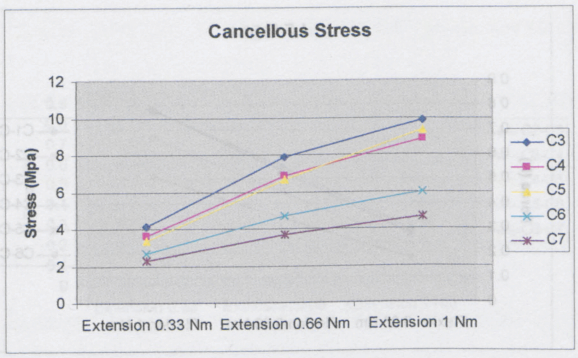

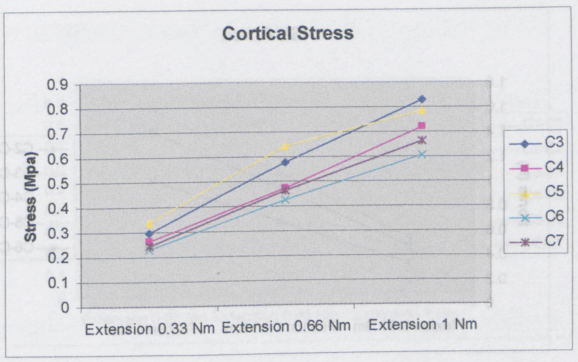

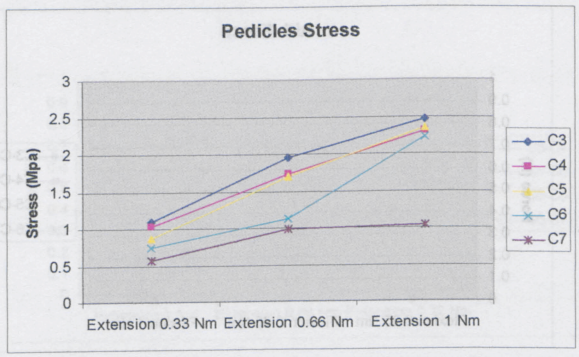

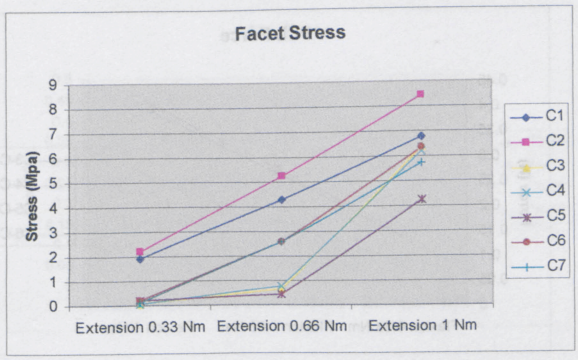

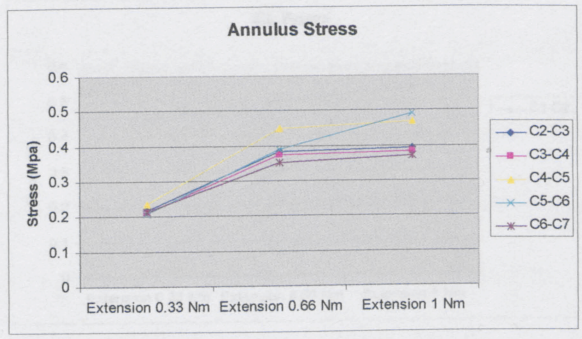

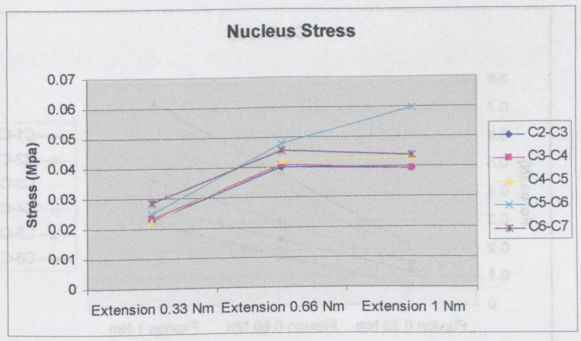

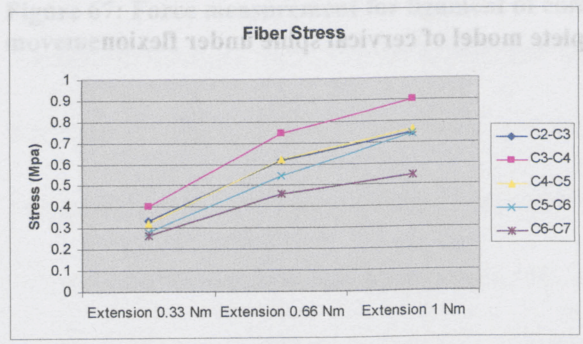

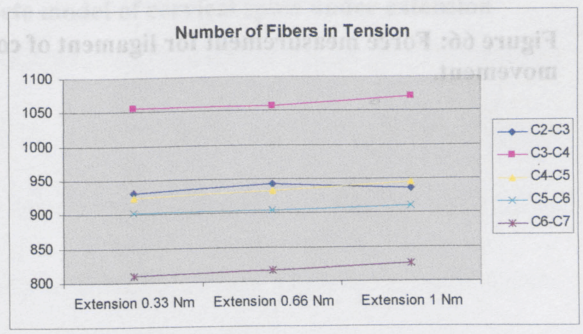

Figure 65: Stress analysis of complete model of cervical spine under extension movement.

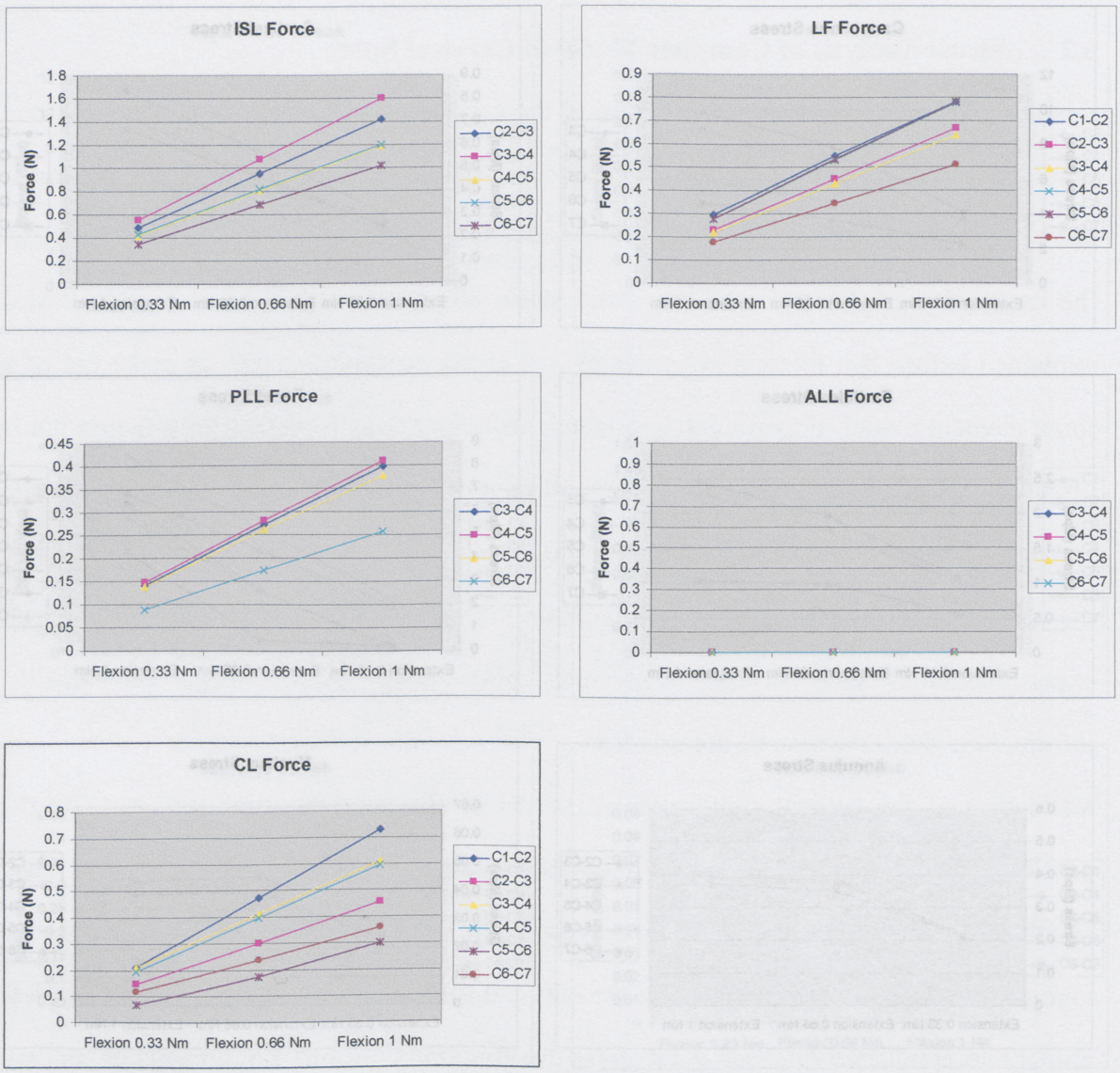

Figure 66: Force measurement for ligament of complete model of cervical spine under flexion movement.

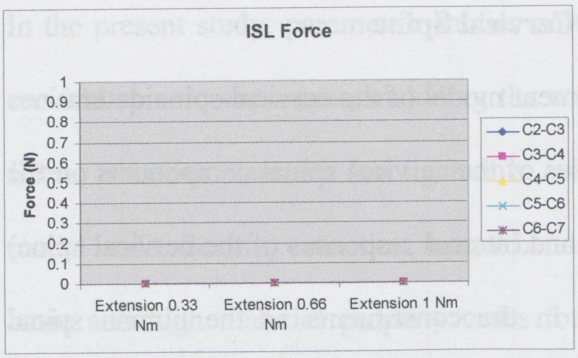

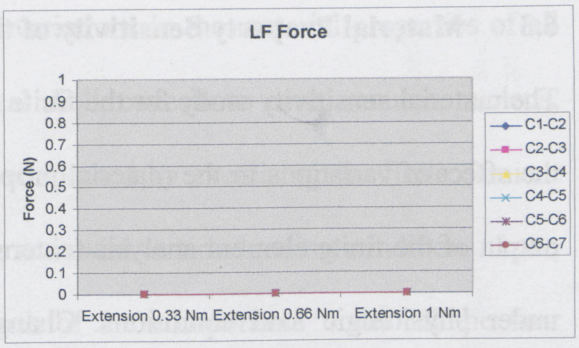

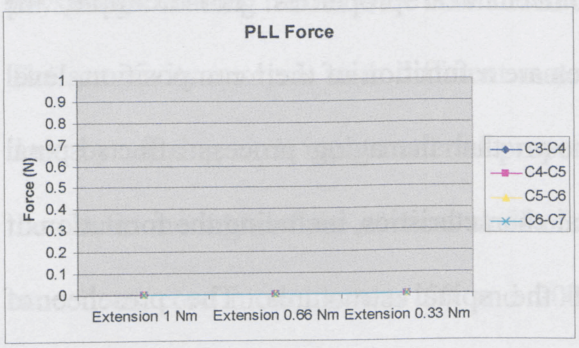

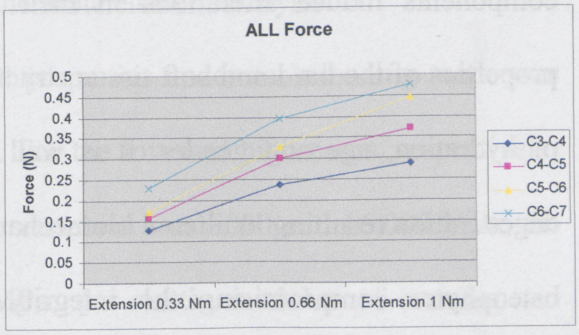

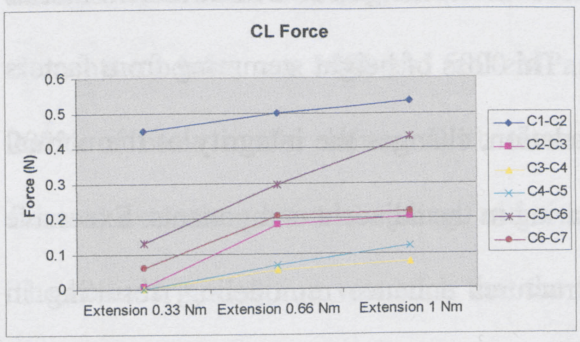

Figure 67: Force measurement for ligament of complete model of cervical spine under extension movement.

6.3 Material Property Sensitivity of the Cervical Spine

The material sensitivity study for the finite element model of the cervical spine determines the effect of variations in the material properties of the cervical spinal components on the output of the finite element analysis (external and internal responses of the cervical spine) under physiologic load conditions. Changes in the constituents of the human spinal components induce alterations in their biomechanical properties. For example, the properties of the hard and soft tissue structures are a function of their composition, level of hydration, age and gender. It is well known that the aging process affects spinal degeneration resulting in altered biomechanical characteristics, including the formation of osteophytes compromising the integrity of the spinal structures. The presence of osteophytes has been correlated with a decrease in disc height. It is well known that as the disc degenerates, a loss in height follows. This loss of height stemming from factors such as desiccated nucleus and annular degradation, changes the integrity of the normal spinal structure and alters the internal load sharing in the adjacent components. Excessive stresses placed on the neighboring bony structures enhance remodeling, resulting in overgrowths of abnormal calcifications or osteophytes. This phenomenon can be explained by the present study, wherein increased stress states were found in the bony components due to increased material properties in the intervertebral disc structures. A systematic biomechanical analysis can be carried out if these variations, in terms of the mechanical properties, can be quantified and used as input into finite element models.

The effect of material property variations of spinal components on the cervical spine is rarely investigated in the literature [28].

In the present study, parametric studies on the variations in the material properties of all cervical spine components, including the cortical shell, cancellous core, annulus, nucleus, fibers, posterior elements and ligaments, were conducted by exercising the finite element model under flexion, extension, lateral bending and axial torsion loading conditions. Low, basic and high material property cases for each of the components under all the four physiologic loading modes were considered in the finite element analysis.

The sensitivity analysis with different material properties under each loading mode was done by varying each input material property. For the low and high cases, respectively, the elastic modulus of the cortical shell of the vertebrae was 8000 and 16,000 MPa; the cancellous core modulus was 50 and 200 MPa; the elastic modulus of annulus and nucleus were 1 and 10 MPa; fibers modulus was 110 and 550 MPa, the bony posterior elements modulus was 1000 and 5000 MPa; the values for all the ligaments were 50 and 200% of basic model values. With these variations, the model was exercised under flexion, extension, lateral bending, and axial torsion loading modes at a level of 1 Nm. The boundary condition was such that the inferior endplate of T1 was fully constrained under all degrees of freedom.

The result of the finite element analysis was used to calculate the rotation of each motion segment under each load condition for low and high material properties. The effect of variation in material property was studied by comparing the obtained results with those determined by basic material properties and experimental results. Figure 68 presents the comparison results from the finite element analysis of the cervical spine utilizing low, basic and high material properties with experimental results.

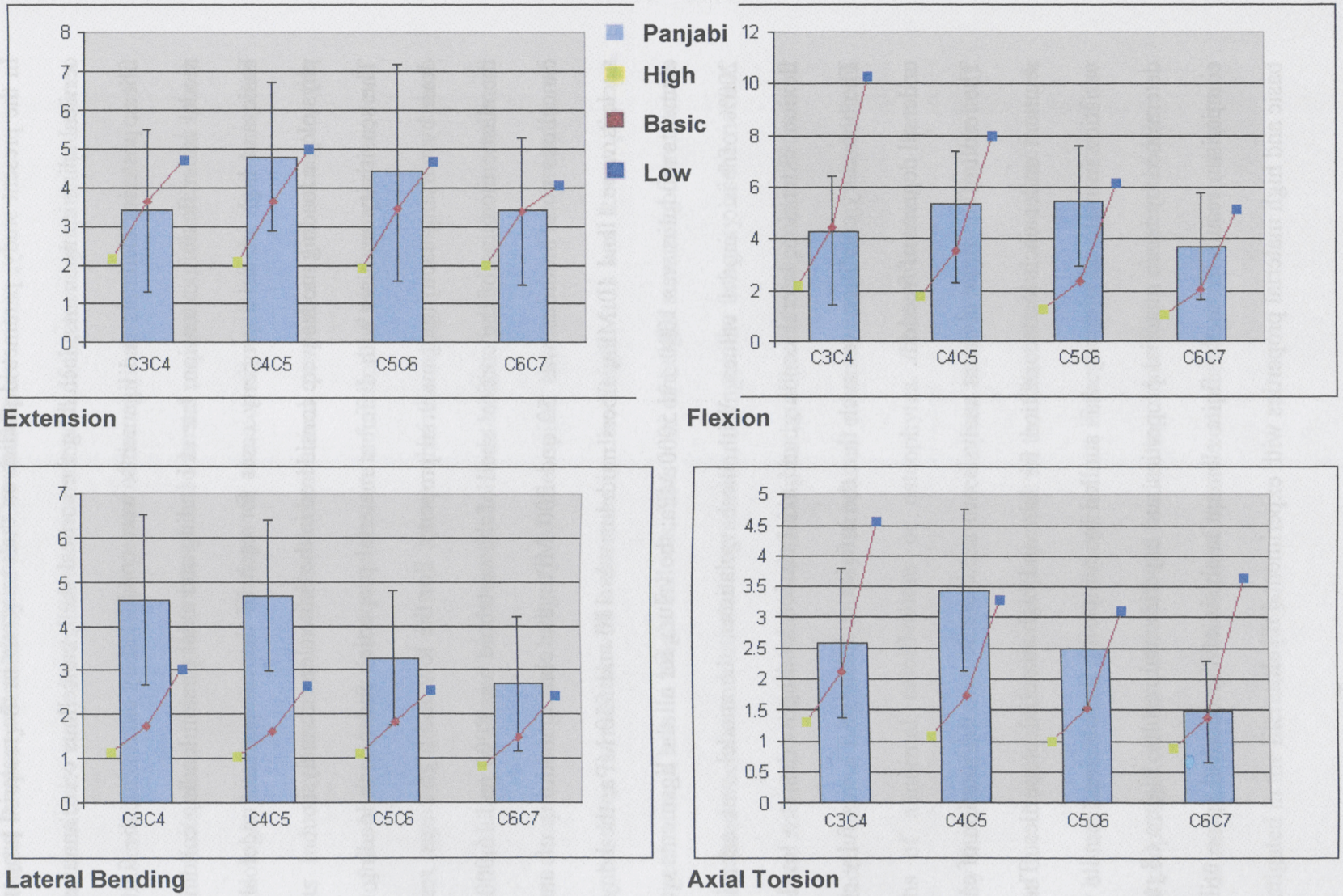

Figure 68: The comparison results from finite element analysis of cervical spine utilizing low, basic and high material properties with experimental results.

CHAPTER 7

CONCLUSION AND FUTURE WORK

7.1 Conclusion

The main purpose of the present study was to develop and validate the finite element model of the cervical spine. To achieve this goal, numerous research works related to the area of the cervical spine were examined.

Biomechanical models of the cervical spine can assist researchers to investigate the mechanisms of cervical spine injury. The four categories of biomechanical models of the cervical spine were studied to understand the advantages and disadvantage of the various models. The history of development and progress in the biomechanical methods, particularly the numerical models, can assist researchers to employ the best method to develop the finite element of the cervical spine. To validate the model of the cervical spine, knowledge of *in vitro* biomechanical models and related research works are necessary.

It is understood that the biomechanical models are to investigate the various parameters causing injury and pain in the area of the cervical spine. Therefore, it is essential to study the different cervical spine injuries to become familiar with the mechanism of injuries.

Among other biomechanical models, the numerical model is the best method to investigate the mechanisms of injury in the cervical spine, but it is not reliable unless it is validated. The finite element method can determine if the cervical spine is at risk of injury by determining the stress in various components of the cervical spine. This exclusive feature in finite element analysis has motivated researchers to utilize the numerical method to find the causes of injury in the cervical spine.

In the current study, the anatomy of various components of the cervical spine such as vertebrae, intervertebral discs, ligaments and joints were studied to understand the structure of the cervical spine in detail.

The three-dimensional parametric model of the cervical spine was developed using available parameters in literature. In all cases, the average values for various parameters were selected. The developed model differs from previous models as it presents a complete 3D parametric model of the cervical spine, including the first thoracic vertebra.

Modeling the cervical spine using CT-scan data will limit the researcher to the specific scanned cervical spine, while the present method uses the average values presented in the literature. Therefore, the results obtained from the analysis of the present model can be generalized for a wide range of cervical spines.

The current study was more focused on the development of a flexible model in terms of the geometry. The parametric approach has led to the selection of a limited number of measurements that allow the reconstruction of the cervical spine. The importance of

having a parametric model is its flexibility; therefore, the model can be modified to simulate injuries for different groups representing different patients with different morphologies. The advantage of the developed method and procedures for the cervical spine for finite element analysis is its simplicity, and the possibility of variation of the material properties for sensitivity studies.

To use the current model of the cervical spine for further study, it should be validated. Using the material properties listed in Table 18 and Table 19, the present finite element model was validated in three different levels under flexion, extension, lateral bending and axial torsion to ensure the model is accurately constructed and selection of material properties is done properly. In all three levels of validation, the model was constrained at the inferior region of the inferior-most vertebra, and the above mentioned four physiologic load vectors were applied to the superior surface of the superior-most vertebra. The selected moment level under each loading mode was based on the papers, with which the model was validated. The resulting angular rotation from the model correlated well with experimental data. Therefore, the model could be used for future finite element studies, with a reasonable accuracy.

Observing the results obtained from the stress analysis of the cervical spine, it can be concluded that increasing the moments will increase the stress in various components of the cervical spine linearly. In both flexion and extension the state of stress is approximately the same for the cancellous shell, cortical core, annulus, nucleus and fibers. The stress is higher for the cancellous shell compared to other components, due to its higher Young's modulus.

As in extension, facet joints come closer to each other and begin to contact, facet joints bear higher stress in extension rather than flexion. On the contrary, in flexion pedicles show higher stress compared with state of stress of pedicles in extension.

The maximum number of fibers in tension occurs in the intervertebral disc of C3-C4 during extension. It is interesting to notice that the number of fibers in tension rapidly increases for small loads, and then remains almost constant.

As could be predicted, in flexion except for ALL, the other ligaments will be in tension. All ligaments of the cervical spine are modeled as nonlinear spring elements with a tension only option; therefore, under compression, the elements bear no force and don't show any change in length. It can be seen in Figure 66 that as the moment increases the force for ALL is zero. In contrast, in extension ISL, LF and PLL are under compression and the force is zero but the ALL and CL are pulled and their length increase under tension.

In the material sensitivity study, the validated model of C3-T1 was used to determine the effects of the variations in the material properties of the spinal components on the external and internal responses of the model under four physiologic loading modes.

The material property variations considered in this investigation are limited to changes only in the Young's modulus values. Changes in Poisson's values are excluded for the following two reasons; firstly, it increases the computational effort since the size of the parametric test matrix increases considerably; secondly, the alterations in the Poisson's ratio of the spinal elements, particularly the cancellous bone, cortical shell, and endplates, have been shown to have little influence on the finite element stress analysis results [28].

The present study evaluated the effects of varying the material property in two steps. In the first step the effects of varying the material property of one component at a time, while

maintaining the material properties of all other components at their basic levels was studied. Then variation of material properties of all components to lower and higher limits was investigated. The first procedure exhibits the effects of a particular component on the biomechanics of the cervical spine.

The results of the finite element analysis show that changes in the material properties of the hard tissues such as the cancellous bone, cortical shell and posterior elements, affect only the internal response of the hard tissues, and the changes in the material properties of the soft tissues, such as the intervertebral discs and ligaments, affect the external and the internal response of both the hard and soft tissue components.

As expected, angular motions increased with a decrease in the stiffness of the material properties of the intervertebral disc and the ligaments, and decreased with an increase in their corresponding values. Variations in material properties of the intervertebral disc components had a larger effect on external response of the cervical spine compared to the ligaments. The variations in the modulus of the cancellous core, cortical shell, endplate and posterior elements (hard tissues) had little effect on the internal stresses of the adjacent intervertebral discs. However; the variations in the Young's modulus of the intervertebral disc and ligaments influenced the stresses in both intervertebral discs and hard tissues.

In the next step the effect of changing the material properties for all componenets to the low and high level at the same time was investigated. It can be seen in Figure 68 that using low and high material properties for all the components affects the external angular motion of the cervical spine considerably. As was previously explained, changes in material property of soft tissues significantly influences the range of motion of the cervical spine in

all four physiologic loading modes. Changing the material properties to a lower level causes a maximum increase of 36.61% in angular motion of C4-C5 in extension, 162.12% in angular motion of C5-C6 in flexion, 63.97% in C4-C5 in lateral bending and 163.76% in C6-C7 in axial torsion. Considering the change of material properties to a higher level, the model undergoes a maximum decrease of 44.21% in angular motion of C5-C6 in extension, 50.45% in angular motion of C3-C4 in flexion, 44.66% in C6-C7 in lateral bending and 38.09% in angular motion of C3-C4 in axial torsion.

The present finite element model can be employed to study common cervical spine injuries by modifying the geometric parameters used to develop the model. This model can be improved in the future by eliminating the simplifications assumed in the modeling and analysis of the model. This issue is discussed in the next chapter.

7.2 Future work

The present finite element modeling of the cervical spine can be continued by eliminating the simplifications assumed in the modeling and analysis of the cervical spine in the current model and by making the model as close as possible to the real human cervical spine.

It is discussed earlier that in the present model, ligaments are modeled by nonlinear spring elements as reported in the literature. To model the laminated structure of annulus, each layer of annulus is reinforced by criss-cross form elements. These assumptions are accurate enough for a static analysis of the cervical spine but for a dynamic analysis and stress analysis of cervical spine over a long period of time, different type of material properties for ligaments, muscles and annulus are required to reflect the effect of time. In other words, viscoelasticity of soft tissues should be taken into account.

The ligaments and muscles of the cervical spine are biological tissues and to consider all characteristics, they should be modeled as quasi-incompressible, non-homogeneous, anisotropic, non-linear viscoelastic materials. Besides, the modeling of muscles involves the passive and active characteristics of muscles and both should be considered in the modeling of the cervical spine.

To consider viscoelastic material properties for soft tissues, required experiments should be run to fully describe material properties of more than the 10 ligaments and 25 major muscles in the area of the cervical spine. Furthermore, multiaxial experiments should be conducted in order to model the laminated structure of the outer section of the intervertebral disc (annulus fibrous). Then, results obtained from these experiments can be applied to the present finite element model of the cervical spine to analyze the model under various loading conditions.

Another issue that can be investigated in future research work is fatigue in the laminated structure of annulus fibrous. Because of the special structure of annulus, everyday activity causes fatigue in this area, more than any other region of neck. Therefore, the nerves' roots and spinal cord will be pinched as a result of extra bulging of the intervertebral disc. This important issue is not investigated in detail in the literature, and hence, requires serious consideration.

The other goal of future research can be to design a protective device to support the cervical spine in case of sudden and strong force. Based on stress analysis of the finite element model of the cervical spine and careful study of the obtained results, the regions at high risk of injury can be located and then essential supportive devices to protect the cervical spine in a high-acceleration environment can be designed and manufactured.

REFERENCES

[1] Panjabi M., Cholewicki J., Nibu K., Grauer J., Babat L. and Dvorak J., Critical Load of the Human Cervical Spine; an in vitro Experimental Study, Clinical Biomech., 1998, 13, pp. 11-17.

[2] Lysell E. Motion in the Cervical Spine, Acta Orthop. Scand., 23 (suppl.), 1969.

[3] Panjabi M., Summers D., Pelker R., Videman T., Friedlaender G., Southwick W., Three-dimensional Load Displacement Curves of the Cervical Spine, J. Orthop. Research, 1986, 4, pp. 152.

[4] Panjabi M., Dvorak J, Duranceau J, Yamamoto I, Gerber M, Rauschning W, and Bueff HU. Three-dimensional movements of the upper cervical spine, Spine, 1988, 13 (7), pp. 726-730.

[5] Moroney S., Schultz A., Miller J., and Andersson G., Load-displacement Properties of Lower Cervical Spine Motion Segments. J. Biomech., 1988, 21(9), pp. 769.

[6] Goel VK, Winterbottom JM, Schulte KR et al. Ligamentous Laxity Across the C0-C1-C2 Complex: Axial Torque-Rotation Characteristics until Failure, Spine, 1990, 15, pp. 990-996.

[7] Penning L. Normal Movements of the Cervical Spine, Am. J. Roentenol., 1979, 130, pp. 317.

[8] Dvorak J, Hayek J, and Zehnder R. CT-functinal Radiographic Diagnosis of the Rotary Instability of the Upper Cervical Spine, Part 2: An Evaluation on Healthy Adults and Patients with Suspected Instability, Spine, 1987,12 (8), pp.726.

[9] Penning L. and Wilmink JT. Rotation of the cervical spine. Spine, 1987, 12 (8), pp. 732.

[10] Dvorak J., Fröhlich D., Penning L., Baumgartner H., Panjabi M.., Functional Radiographic Diagnosis of the Cervical Spine: Flexion/Extension, Spine, 1988, 13 (7), pp. 748-755.

[11] Dvorak J., Panjabi M., Novotny J. E., Antinnes J. A., In vivo Flexion/Extension of the Normal Cervical Spine. J. Orthop Res., 1991, 9, pp. 828 - 834.

[12] Yoganandan N, Myklebust JB, Ray G, Mathematical and finite element analysis of spinal injuries, CRC Review Biomed Eng., 1987, 15, pp 29-93.

[13] Merrill. T., Goldsmith W. and Deng, Y. C., Three-dimensional Response of a Lumped Parameter Head-Neck Model Due to Impact and Impulsive Loading, Journal of Biomechanics, 1984, 17, pp. 81-85.

[14] Li Y., Bishop P. J., Wells R. P., McGill S. M., A Quasi-static Analytical Sagittal Plane Model of the Cervical Spine in Extension and Compression, 1991, SAE 912917, pp. 2066-2080.

[15] De Jager M, Sauren A, Thunnissen J, Wismans J., A Three-dimensional Head-Neck Model: Validation for Frontal and Lateral Impacts, SAE 942211, 1994, pp. 1660-1676.

[16] De Jager M, Sauren A, Thunnissen J, Wismans J., A Global and Detailed Mathematical Model for Head-Neck Dynamics, SAE 962430, 1996, pp. 1899-1911.

[17] Teo EC, Paul JP, Evans JH., Finite Element Stress Analysis of a Cadaver Second Cervical Vertebra, Med. & Biol. Eng. & Comput., 1994, 32, pp. 236-38.

[18] Graham R.S., Oberlander E.K., Stewart J.E., Griffiths D.J., Validation and Uuse of Finite Element Model of C2 for Determination of Stress and Fracture Patterns of Anterior Odontoid Loads, J. Neurosurg, 2000, 93, pp. 117-125.

[19] Teo EC, Ng HW., First Cervical Vertebra (Atlas) Fracture Mechanism Studies Using Finite Element Method, J. Biomechanics, 2001, 34, pp. 13-21.

[20] Bozic KJ, Keyak JH, Skinner HB, Bueff HU, Bradford DS., Three-dimensional Finite Element Modeling of a Cervical Vertebra: An Investigation of Burst Fracture Mechanism, J. Spinal Disorders, 1994, 7 (2), pp. 102-110.

[21] Maurel N, Lavaste F, Skalli W., A Three-dimensional Parameterized Finite Element Model of the Lower Cervical Spine, Study of the Influence of the Posterior Articular Facets, J Biomechanics, 1997;30, pp. 921–931.

[22] Yoganandan N, Kumaresan S, Voo L, Pintar FA., Finite Element Model of the Human Lower Cervical Spine: Parametric Analysis of the C4-C6 Unit, J. Biomechanical Engineering, 1997, 119 (1), pp. 87-92.

[23] Ng H., Teo E., Nonlinear Finite-Element Analysis of the Lower Cervical Spine (C4-C6) Under Axial Loading, J. Spinal Disorders, 2001, 14 (3), pp. 201-210.

[24] Teo E.C., Ng H.W., Evaluation of the Role of Ligaments, Facets and Disc Nucleus in Lower Cervical Spine under Compression and Sagittal Moments Using Finite Element Method, Medical Engineering & Physics, 2001, 23, pp. 155–164.

[25] Yoganandan N., Kumaresan S.C., Voo Liming, Pintar F.A. and Larson S. J., Finite element modeling of the C4-C6 cervical spine unite, Med. Eng. Phys. 1996, 18, pp. 569-574.

[26] Kumaresan S., Yoganandan N., Pintar F., Finite Element Analysis of Anterior Cervical Spine Interbody Fusion, Bio-medical mat. and engineering, 1997, 7, pp. 221-230.

[27] Wheeldon J, Khouphongsy P, Kumaresan S, Yoganandan N, Pintar FA., Finite Element Model of Human Cervical Spinal Column, Biomedical Sciences Instrumentation, 2000, 36, pp. 337-342.

[28] Kumaresan S., Yoganandan N, Pintarh F.A., Finite Element Analysis of the Cervical Spine: A Material Property Sensitivity Study, Clinical Biomechanics, 1999, 14, pp 41-53.

[29] Goel V. K., Clausen J. D., Prediction of Load Sharing among Spinal Components of a C5-C6 Motion Segment Using the Finite Element Approach, Spine, 1998, 23, pp. 684-691.

[30] Yang K, Zhu F, Luan F, Zhao L, Begeman P. Development of a FE model of the human neck. In: Proceedings of the 42nd Stapp Car Crash Conference. Ft. Lauderdale, FL, 1998, pp. 195-205.

[31] Jost R., Nurick G., Development of a Finite Element Model of the Human Neck Subjected to High G-level Deceleration, Int. J. Crashworthiness, 2000, 5, pp. 259-267.

[32] Lee V. S., Neo L. D., Seng K. Y., Teo E. C., Ng H. W. and Zhang Q. H., Biomechanical Analysis of the Human Upper Cervical Spine, ICBME: "The Bio-Era: New Challenges, New Frontiers", 2002, 4 – 7 December, Singapore.

[33] Brolin K., Halldin P., Development of a Finite Element Model of the Upper Cervical Spine and a Parameter Study of Ligament Characteristics, Spin, 2004, 29 (4), pp. 376–385.

[34] Kleinberger M., Application of Finite Element Techniques to the Study of the Cervical Spine, 1993, SAE 933131.

[35] Stemper BD, Kumaresan S, Yoganandan N, Pintar FA., Head-neck Finite Element Model for Motor Vehicle Inertial Impact: Material Sensitivity Analysis, Biomedical Sciences Instrumentation, 2000, 36, pp. 331-335.

[36] Kumaresan S., Yoganandan N., Pintar F., Voo L., Cusick J., Larson S., Finite Element Modeling of Cervical Laminectomy with Graded Facetectomy, J. Spinal Disorders, 1997, 10 (1), pp. 40-46.

[37] Kumaresan S., Yoganandan N., Pintar F., Age-Specific Pediatric Cervical Spine Biomechanical ones: Three-Dimensional Nonlinear Finite Element Models, 1997, SAE 973319.

[38] Nataranjan R., Chen B., An H., Andersson G., Anterior Cervical Fusion - A Finite Element Model Study on Motion Segment Stability Including the Effect of Osteoporosis, Spine, 25(8), pp. 955-961.

[39] Pitzen T., Matthis D., Barbier D., Steudel W., Initial Stability of Cervical Spine Fixation: Predictive Value of a Finite Element Model, J. Neurosurg (Spine 1), 2002, 97, pp. 128-134.

[40] Puttlitz CM, Goel VK, Traynelis VC, Clark CR, A Finite Element Investigation of Upper Cervical Instrumentation, Spine, 2001, 26 (22), pp. 2449-2455.

[41] Voo LM, Kumaresan S, Yoganandan N, Pintar FA, Cusick JF., Finite Element Analysis of Cervical Facetectomy, Spine, 1997, 22 (9), pp. 964-969.

[42] Tan K.W., Lee V.S., Teo E.C., Zhang Q.H., Ng H.W. , Seng K.Y., A C2–C3 Finite Element Model to Determine the Stress Patterns of Odontoid Loads, Bioengineering Conference, 2003, June 25-29, Sonesta Beach Resort in Key Biscayne, Florida.

[43] Sadegh A., Tchako A., Vertebral Stress of a Cervical Spine Model Under Dynamic Load, Technology and Health Care 8, 2000, pp. 143–154.

[44] Ng H.W., Teo E.C., Leeb V.S., Statistical Factorial Analysis on the Material Property Sensitivity of the Mechanical Responses of the C4–C6 under Compression, Anterior and Posterior Shear, Journal of Biomechanics, 2004, 37, pp. 771–777.

[45] Sherk H.H., Dunn E.J., Eismont F.J., The Cervical spine, second edition, Lippincott Co., 1989.

[46] Johannes L., Verlag G. T., Clinical anatomy of the cervical spine, 1993.

[47] http://hal.bim.msu.edu/cmeonline/cervical/start.html

[48] Goel V. K., Biomechanics of the Spine: Clinical and Surgical Perspective, CRC Press, 1990.

[49] http://connection.lww.com/products/stedmansmedict/primalpictures.asp

[50] Myklebust JB, Pintar F, Yoganandan N, Cusick JF, Maiman D, Myers TJ, Sances A., Tensile Strength of Spinal Ligaments, Spine, 1988, 13, pp. 526-531.

[51] Brolin K., Cervical Spine Injuries - Numerical Analyses and Statistical Survey, Doctoral Thesis, Royal Institute of Technology, Sweden, 2002.

[52] Panjabi M., Oxland T., Parks E., Quantitative Anatomy of Cervical Spine Ligaments, Part I: Upper Cervical Spine, J. Spinal Disord., 1991, 4(3), pp. 270-27.

[53] Saldinger P., Dvorak J., Rahn B., Perren S.., Histology of the Alar and Transverse Ligaments, Spine, 1990, 15, pp. 257-261.

[54] Deng Y. C. and Goldsmith W., Response of a Human Head/Neck/Upper-torso Rreplica to Dynamic Loading II: Analytical/Numerical Model, Journal of Biomechanics, 1987, 20, pp. 487-497.

[55] Horst M. J., Human Head Neck Response in Frontal, Lateral and Rear End Impact Loading: Modeling and Validation, Masters Thesis, Eindhoven : Technische Universiteit Eindhoven, 2002.

[56] Warfel J. H., The Head, Neck, and Trunk. Muscles and Motor Points. Lea & Febiger, Philadelphia, 1973.

[57] Myers BS, Winkelstein BA. Epidemiology, Classification, Mechanism, and Tolerance of Human Cervical Spine Injuries, Critical Reviews in Biomedical Engineering, 1995, 23, pp. 307-409.

[58] Roberge RJ, Samuels JR., Cervical Spine Injury in Low-Impact Blunt Trauma, Am. J. Emergency Medicine, 1999, 17 (2), pp. 125-129.

[59] Lowery D., Wald M., Browne B., Tigges S., Hoffman J., Mower W., Epidemiology of Cervical Spine Injury in Victims, Ann. Emergency Medicine, 2001, 38 (1), pp. 12-16.

[60] Holly L., Kelly D., Counelis G., Blinman T., McArthur D., Cryer H., Cervical Spine Trauma Associated with Moderate and Severe Head Injury: Incidence, Risk Factors, and Injury Characteristics, J Neurosurg., 2002, 96(3 Suppl.), pp. 285-291.

[61] Thorson J., Neck Injuries in Road Accidents, Scand. J Rehab Med, 1972, 4, pp. 110-113.

[62] Huelke D., O'Day J., Mendelsohn R., Cervical injuries suffered in automotive crashes, J. Neurosurg., 1981, 54, pp. 316-322.

[63] Krantz P., Head and Neck Injuries to Motorcycle and Moped Riders with Special Regard to the Effect of Protective Helmets, Injury, 1985, 16, pp. 253-258.

[64] Yoganandan N., Pintar F., Butler J., Reinartz J., Sances A., Larson S, Dynamic Response of Human Cervical Spine Ligaments, Spine, 1989, 14 (10), pp. 1102-1109.

[65] Brolin K., Von Holst H., Cervical Injuries in Sweden, a National Survey of Patient Data from 1987 to 1999, Injury Control and Safety Promotion, 2002, 9 (1).

[66] International Classification of Diagnosis version 10.

[67] Larson S.J., Vertebral Injury and Instability, Spinal Instability, New York, Springer, 1993, pp. 101–137.

[68] Larson S.J., Maiman D.J., Surgery of the Lumbar Spine, New York, NY: Thieme; 1999, pp. 334.

[69] Denis F., Three-Column Spine and Its Significance in Classification of Acute Thoracolumbar Spinal Injuries, Spine, 1983, 8, pp. 817–831.

[70] Holdsworth H., Fractures, Dislocations and Fractures-Dislocations of the Spine, J. Bone Joint Surg. Br., 1963, 45, pp. 6–20.

[71] Louis R., Spinal Stability as Defined by Three-Column Spine Concept, Anat. Clin., 1985, 7, pp. 33–42.

[72] White A., Panjabi M., Clinical Biomechanics of Spine, 2nd edition, Philadelphia, PA: JB Lippincott, 1990, pp. 722.

[73] White A., Johnson R., Panjabi M., Biomedical Analysis of Clinical Stability in Cervical Spine. Clin. Orthop., 1975, 109(III), pp. 85– 95.

[74] Cusick J. F., Yoganandan N., Biomechanics of the Cervical Spine 4: Major Injuries, Clinical Biomechanics, 2002, 17, pp. 1–20.

[75] McElhaney J., Myers B., Biomechanical Aspects of Cervical Trauma, Accidental Injury: Biomechanics and Prevention / Nahum A, Melvin J. (editors), 1993, ch.14, pp. 311-361.

[76] Lee TT, Green BA, Petrin DR., Treatment of Stable Burst Fracture of the Atlas (Jefferson Fracture) with Rigid Cervical Collar, Spine, 1998, 23 (18), pp. 1963-1967.

[77] Oda T, Panjabi MM, Crisco III JJ, Oxland TR., Multidirectional Instabilities of Experimental Burst Fractures of the Atlas, Spine, 1992, 17(11), pp. 1285-1289.

[78] Lee TT, Green BA, Petrin DR., Treatment of Stable Burst Fracture of the Atlas (Jefferson Fracture) with Rigid Cervical Collar, Spine, 1998, 23 (18), pp. 1963-1967.

[79] An H.S., Cervical Spine Trauma, Spine, 1998, 23 (24), pp. 2713-2729.

[80] Greene KA, Dickman CA, Marciano FF, Drabier JB, Hadley MN, Sonntag VK., Acute Axis Fracture: Analysis of Management and Outcome in 340 Consecutive Cases, Spine, 22 (16), pp. 1843-1852.

[81] Wilcox R, Allen D, Barton D, Hall R, Limb D, Dickson R. (2002) An investigation of the burst fracture mechanism using a combined experimental and finite element approach, IV World Congress of Biomechanics, Calgary, August 5-9.

[82] Fujimura Y, Nishi Y, Kobayashi K., Classification and Treatment of Axis Body Fractures, J. Ortopaedic Trauma, 1996, 10 (8), pp. 536-540.

[83] Carter J. W., Mirza S. K., Tencer A. F., Ching R. P., Canal Geometry Changes Associated with Axial Compressive Cervical Spine Fracture, Spine, 2000, 25 (1), pp. 46-54.

[84] Maiman D., Sances Jr A., Myklebust J., Larson S., Houterman C., Chilbert M., El-Ghatit A., Compression Injuries of the Cervical Spine: A Biomechanical Analysis. Neurosurgery, 1983, 13 (3), pp. 254-260.

[85] Brolin K., Finite Element Analyses of Spinal Stability and Instability due to Ligament Ruptures, IV World Congress of Biomechanics, Calgary, 2002, August 5-9.

[86] http://www.spineuniverse.com/displayarticle.php/article435.html

[87] Maurel W., 3D Modeling of the Human Upper Limb Including, the Biomechanics of Joints, Muscles And Soft Tissues, PhD Thesis, Ecole Polytechnique Federale De Lausanne, 1998.

[88] Fung Y. C., Perrone N., Aliker M., Stress-Strain History Relations of Soft Tissues in Simple Elongation, Englewood Cliffs, N. J. Prentice-Hall, 1972.

[89] Woo S L-Y., Kwan M.K., A Structural Model to Describe the Non-Linear Stress-Strain Behavior for Parallel-Fibered Collagenous Tissues, Journal of Biomechanical Engineering, 1989.

[90] Daniel D.M., Akeson W.H., O'Connor J.J., Knee Ligaments: Structure, Function, Injury and Repair, New York, Raven Press, 1990.

[91] Amiel D., Frank C., Harwood F., Fronek J., Akeson W., Tendons and ligaments: A Morphological and Biochemical Comparison, J. Orthop. Res., 1984, 1, pp.257–265.

[92] Kastelic J., Palley I., and Baer E., The Multicomposite Ultrastructure of Tendon, Conn. Tiss. Res., 1978, 6, pp. 11–23.

[93] Quapp K. M., Weiss J. A., Material Characterization of Human Medial Collateral Ligament, ASME J. Biomech. Eng., 1998, 120, pp. 757–763.

[94] Weiss J., Gardiner J., Computational Modeling of Ligament Mechanics, Critical Reviews in Biomedical Engineering, 2001, 29, pp. 1–70

[95] Weiss J. A., A Constitutive Model and Finite Element Representation for Transversely Isotropic Soft Tissues, PhD Thesis, Department of Bioengineering, University of Utah, 1994.

[96] Gardiner J. C., Cordaro N., Weiss J. A., Elastic and Viscoelastic Shear Properties of the Medial Collateral Ligament, Trans. 46th Meeting Orthop. Res. Soc., 2000, 25, pp. 63.

[97] Gardiner J. C., Weiss J. A., Simple Shear Testing of Parallel-Fibered Planar Soft Tissues, ASME J. Biomech. Eng., 2001, April.

[98] Yahia L. H., Drouin G., Study of the Hysteresis Phenomenon in Canine Anterior Cruciate Ligaments, J. Biomedical Eng., 1990, 12, pp. 57–62.

[99] Hughes D. W., Kirby M. C., Sikoryn T. A., Apsden R. M., Cox A. J., Comparison of Structure, Mechanical Properties, and Functions of Lumbar Spinal Ligaments, Spine, 1990, 15(8), pp. 787–795.

[100] Kwan M. K., Lin T. H., Woo S. L. Y., On the Viscoelastic Properties of the Anteromedial Bundle of the Anterior Cruciate Ligament, J. Biomechanics, 1993, 26 , pp. 447–452.

[101] Weiss J., Lai A., Loui S., and Nisbet J., Behavior of Human Medial Collateral Ligament in Unconfined Compression, Trans. 46th Meeting Orthop. Res. Soc., 2000, 25, pp. 781.

[102] Liggins A. B., Shemerluk R., Hardie R., Finlay J. B., Technique for the Application of Physiological Loading to Soft Tissue in vitro, J. Biomed. Eng., 1992, 14(5), pp. 440–441.

[103] Powell E. S., Trail I. A., Noble J., Non-Suture Repair of Tendons, J. Biomed. Eng., 1989, 11(3), pp. 215–218.

[104] Sharkey N. A., Smith T. S., Lundmark D. C., Freeze Clamping Musculo-Tendinous Junctions for in vitro Simulation of Joint Mechanics, J. Biomechanics, 1995, 28(5), pp. 631–635.

[105] Chuong C. J., Sacks M. S., Johnson R. L., Reynolds R., On the Anisotropy of the Canine Diaphragmatic Central Tendon, J. Biomechanics, 1991, 24, pp. 563–576.

[106] Lee T. Q., Woo S. L. Y., A New Method for Determining Cross-Sectional Shape and Area of Soft Tissues, ASME J. Biomech. Eng., 1988, 110, pp. 110–114.

[107] Allard P., Thirty P. S., Bourgault A., Drouin G., Pressure Dependence of the Area Micrometer Method in Evaluation of Cruciate Ligament Cross-Section, J. Orthop. Res. 1979, 1, pp. 265–267.

[108] Iaconis F., Steindler R., Marinozzi G., Measurements of Cross-Sectional Area of Collagen Structures (Knee Ligaments) by Means of an Optical Method, J. Biomechanics, 1987, 20(10), pp. 1003–1010.

[109] Przybylski G., Patel P., Carlin G., Woo S., Quantitative anthropometry of the subatlantal cervical longitudinal ligaments, Spine, 1998, 23, pp. 893-898.

[110] Mercer S., Bogduk N., The Ligaments and Annulus Fibrosus of Human Adult Cervical Intervertebral Discs, Spine, 1999, 24, pp. 619-628.

[111] Pintar F., Yoganandan N., Myers T., Elhagediab A., Sances Jr A., Biomechanical properties of human lumbar spine ligaments., J. Biomech., 1992, 25, pp.1351-1356.

[112] Rauschning W., Surface cryoplaning, a Technique for Clinical Anatomical Correlations, Ups J. Med. Sci., 1986, 91, pp. 251-255.

[113] Yoganandan N., Kumaresan S., Pintar F., Geometric and Mechanical Properties of Human Cervical Spine Ligaments, J. Biomech. Eng., 2000, 122, pp. 623-629.

[114] Pech P., Bergstrom K., Rauschning W., Haughton W., Attenuation Values, Volume Changes and Artifacts in Tissue due to Freezing, Acta. Radiol., 1987, 28, pp.779-782.

[115] Butler D. L., Grood E. S., Noyes F. R., Zernicke R. F., Brackett K., Effects of Structure and Strain Measurement Technique on the Material Properties of Young Human Tendons and Fascia, J. Biomechanics, 1984, 17(8), pp. 579–596.

[116] Wang C. J., Walker P. S., Wolf B., The Effects of Flexion and Rotation on the Length Patterns of the Ligaments of the Knee, J. Biomechanics, 1973, 6, pp. 587–596.

[117] Hollis J. M., Takai S., Adams D. J., Horibe S., Woo S. L. Y., The Effects of Knee Motion and External Loading on the Length of the Anterior Cruciate Ligament (ACL): A Kinematic Study, ASME J. Biomech. Eng., 1991, 113(2), pp. 208–214.

[118] Bach J. M., Hull M. L., Patterson H. A., Direct Measurement of Strain in the Posterolateral Bundle of the Anterior Cruciate Ligament, J. Biomechanics, 1997, 30(3), pp. 281–283.

[119] Monahan J. J., Grigg P., Pappas A. M., Leclair W. J., Marks T., Fowler D. P., Sullivan T. J., In vivo Strain Patterns in the Four Major Canine Knee Ligaments, J. Orthop. Res. 1984, 2, pp. 408–418.

[120] Arms S. W., Boyle J., Johnson R. J., Pope M. H., Strain Measurement in the Medial Collateral Ligament of the Human Knee: An Autopsy Study. J. Biomechanics, 1983, 16, pp. 491–496.

[121] Beynnon B., Howe J. G., Pope M. H., Johnson R. J., Fleming B. C., The Measurement of Anterior Cruciate Ligament Strain in vivo, Int. Orthop., 1992, 16(1), pp. 1–12.

[122] Fleming B. C., Beynnon B. D., Nichols C. E., Johnson R. J., Pope M. H., An in vivo Comparison of Anterior Tibial Translation and Strain in the Anteromedial Band of the Anterior Cruciate Ligament, J. Biomechanics, 1993, 26(1), pp. 51–58.

[123] Beynnon B., Howe J. G., Pope M. H., Johnson R. J., Fleming B. C., The Measurement of Anterior Cruciate Ligament Strain in vivo, Int. Orthop., 1992, 16(1), pp. 1–12.

[124] Renstrom P., Arms S. W., Stanwyck T. S., Johnson R. J., Pope M. H., Strain within the Anterior Cruciate Ligament during Hamstring and Quadriceps Activity, Amer J. Sports Med., 1986, 14(1), pp. 83–87.

[125] Yin F. C., Tompkins W. R., Peterson K. L., Intaglietta M., A Video-Dimension Analyzer, IEEE Tans. Biomed. Eng., 1972, 19, pp. 376–381.

[126] Woo S. L. Y., Mechanical Properties of Tendons and Ligaments: I. Quasi-static and Nonlinear Viscoelastic Properties, Biorheology, 1982, 19, pp. 385–396.

[127] Woo S. L. Y., Gomez M. A., Seguchi Y., Endo C. M., Akeson W. H., Measurement of Mechanical Properties of Ligament Substance from a Bone-Ligament-Bone Preparation, J. Orthop. Res. 1983, 1, pp. 22–29.

[128] Gardiner J. C., Weiss J. A., Strain in the Human Medial Collateral Ligament During Valgus Loading, Trans. 46th Meeting Orthop. Res. Soc., 2000, 25, pp. 774.

[129] Runco T. J., A Study of the Nonuniform in situ Strains on the Surface of the Anterior Cruciate Ligament, M.Sc. Dissertation, Department of Mechanical Engineering, University of Pittsburgh, 1996.

[130] Sharma M., Langrana N.A., Rodriguez J., Role of Ligaments and Facets in Lumbar Spinal Stability, Spine, 1995, 20, pp. 887-900.

[131] Derwin K. A., Soslowsky L. J., Green W. D., Elder S. H., A New Optical System for the Determination of Deformations and Strains: Calibration Characteristics and Experimental Results, J. Biomechanics, 1994, 27(10), pp. 1277–85.

[132] Lam T., Frank C., Shrive N., Calibration Characteristics of a Video Dimension Analyzer System, J. Biomechanics, 1992, 25(10), pp. 1227–31.

[133] Hirokawa S., Yamamota K., Kawada T., A Photoelastic Study of Ligament Strain, IEEE Trans. Rehabil. Eng., 1998, 6(3), pp. 300–308.

[134] Kawada T., Abe T., Yamamoto K., Hirokawa S., Soejima T., Tanaka N., Inoue A., Analysis of Strain Distribution in the Medial Collateral Ligament Using a Photoelastic Coating Method, Med. Eng. Phys., 1999, 21, pp. 279–291.

[135] Yamamoto K., Hirokawa S., Kawada T., Strain Distribution in the Ligament Using Photoelasticity, A Direct Application to the Human AGL, Med. Eng. Phys., 1998, 20, pp. 161–168.

[136] Komi P., Relevance of in vivo Force Measurements to Human Biomechanics, J. Biomechanics, 1990, 23, pp. 23–34.

[137] Lewis J. L., Lew W. D., Schmidt J., A Note on the Application and Evaluation of the Buckle Transducer for Knee Ligament Force Measurement, ASME J. Biomech. Eng., 1982, 104, pp. 125–128.

[138] Glos D. L., Butler D. L., Grood E. S., Levy M. S., In vitro Evaluation of an Implantable Force Transducer (IFT) in a Patellar Tendon Model, ASME J. Biomech. Eng., 1993, 115, pp. 335–343.

[139] Holden J. P., Grood E. S., Korvick D. L., Cummings J. F., Butler D. L., Bylski-Austrow D. I., In vivo Forces in the Anterior Cruciate Ligament: Direct Measurements during Walking and Trotting in a Quadruped, J. Biomechanics, 1994, 27(5), pp. 517–526.

[140] France E. P., Daniels A. U., Goble E. M., Dunn H. K., Simultaneous Quantitation of Knee Ligament Forces, J. Biomechanics, 1983, 16(8), pp. 553–564.

[141] Fujie H., Mabuchi K., Woo S. L. Y., Livesay G. A., Arai S., Tsukamoto Y., The Use of Robotics Technology to Study Human Joint Kinematics: A New Methodology, ASME J. Biomech. Eng., 1993, 115, pp. 211–217.

[142] Frisen M., Magi M., Sonnerup L., Viidik A., Rheological Analysis of Soft Collagenous Tissue, Part I: Theoretical Considerations, J. Biomechanics, 1969, 2, pp.13–20.

[143] Kastelic J., Palley I., Baer E., A Structural Mechanical Model for Tendon Crimping, J. Biomechanics, 1980, 13, pp. 887–893.

[144] Decraemer W. F., Maes M. A., Vanhuyse V. J., An Elastic Stress-Strain Relation for Soft Biological Tissues Based on a Structural Model, J. Biomechanics, 1980, 13, pp. 463–468.

[145] Liao H., Belkoff S. M., A Failure Model for Ligaments, J. Biomechanics, 1999, 32(2), pp. 183–188.

[146] Lanir Y., A Structural Theory for the Homogeneous Biaxial Stress-Strain Relationships in Flat Collagenous Tissues, J. Biomechanics, 1979, 12, pp. 423–436.

[147] Lanir Y., Constitutive Equations for Fibrous Connective Tissues, J. Biomechanics, 1983, 16(1), 1–12.

[148] Diamant J., Keller A., Baer E., Litt M., Arridge R. G. C., Collagen: Ultrastructure and Its Relation to Mechanical Properties as a Function of Ageing., Proc. R. Soc. Lond., 1972, 180, pp. 293–315.

[149] Comninou M., Yannas I.V., Dependence of Stress-Strain Nonlinearity of Connective Tissues on the Geometry of Collagen Fibers, J. Biomechanics, 1976, 9, pp. 427–433.

[150] Lanir Y., A Microstructure Model for the Rheology of Mammalian Tendon, ASME J. Biomech. Eng., 1980, 102, pp. 332–339.

[151] Beskos D. E., Jenkins J. T., A Mechanical Model for Mammalian Tendon, J. Appl. Math., 1975, 42, pp. 755–758.

[152] Hildebrandt J., Fukaya H., Martin C. J., Simple Uniaxial and Uniform Biaxial Deformation of Nearly Isotropic Incompressible Tissues, Biophysical J., 1969, 9, pp. 781–791.

[153] Ault H. K., Hoffman A. H., A Composite Micromechanical Model for Connective Tissues: Part I, Theory, ASME J. Biomech. Eng., 1992, 114(1), pp.137–141.

[154] Hashin Z., Rosen B. W., The Elastic Moduli of Fiber-Reinforced Materials, ASME J. Appl. Mech., 1964, 31, pp. 223–232.

[155] Hill R., Theory of Mechanical Properties of Fibre-Strengthened Materials: I. Elastic Behavior, J. Mech. Phys. Solids, 1964, 12, pp. 199–212.

[156] Hurschler C., Loit-Ramage B., Vanderby R., A Structurally Based Stress-Stretch Relationship for Tendon and Ligament, ASME J. Biomech. Eng., 1997, 119, pp. 392–399.

[157] Weiss J. A., Maker B. N., Govindjee S., Finite Element Implementation of Incompressible, Transversely Isotropic Hyperelasticity, Comp. Meth. Appl. Mech. Eng., 1996, 135, pp. 107–128.

[158] Fung Y. C., Biomechanics: Mechanical Properties of Living Tissues, 2nd Edition, New York, Springer-Verlag, 1993.

[159] Danto M. I., Woo S. L. Y., The Mechanical Properties of Skeletally Mature Rabbit Anterior Cruciate Ligament and Patellar Tendon over a Range of Strain Rates, J. Orthop. Res., 1993, 11(1), pp. 58–67.

[160] Yahia L. H., Drouin G., Study of the Hysteresis Phenomenon in Canine Anterior Cruciate Ligaments, J. Biomedical Eng., 1990, 12, pp. 57–62.

[161] Viidik A., A Rheological Model for Uncalcified Parallel-Fibred Collagenous Tissue, J. Biomechanics, 1968, 1, pp. 3–11.

[162] Decraemer W. F., Maes M. A., Vanhuyse V. J., Vanpeperstraete P., A Nonlinear Viscoelastic Constitutive Equation for Soft Biological Tissues Based upon a Structural Model, J. Biomechanics, 1980, 13, pp. 559–564.

[163] Barbenel J. C., Evans J. H., Finlay J. B., Stress-Strain Time Relations for Soft Connective Tissues, In: Kenedi, Editor, Perspectives in Biomedical Engineering, New York, McMillan, 1973, pp. 165–172.

[164] Sanjeevi R., A Viscoelastic Model for the Mechanical Properties of Biological Materials, J. Biomechanics, 1982, 15(2), pp. 107–109.

[165] Sanjeevi R., Somanathan N., Ramaswamy D., A Viscoelastic Model for Collagen Fibers, J. Biomechanics, 1982, 15(3), pp. 181–183.

[166] Terzaghi K., Theoretical Soil Mechanics, New York, John Wiley and Sons, 1943.

[167] Truesdell C., Toupin R., The Classical Field Theories, In Handbuck der Physik, Berlin, Springer- Verlag, 1960, pp. 226–793.

[168] Mow V. C., Kuei S. C., Lai W. M., Armstrong C. G., Biphasic Creep and Stress Relaxation of Articular Cartilage: Theory and Experiments, ASME J. Biomech. Eng., 1980, 102, pp. 73–84.

[169] Simon B. R., Wu J. S., Carlton M. W., Evans J. H., Kazarian L. E., Structural Models for Human Spinal Motion Segments Based on a Poroelastic View of the Intervertebral Disc, ASME J. Biomech. Eng., 1985, 107(4), pp. 327–335.

[170] Chimich D., Shrive N., Frank C., Marchuk L., and Bray R., Water Content Alters Viscoelastic Behavior of the Normal Adolescent Rabbit Medial Collateral Ligament, J. Biomechanics, 1992, 25, pp. 831–837.

[171] Haut R. C., Powlison A. C., The Effects of Test Environment and Cyclic Stretching on the Failure Properties of Human Patellar Tendons, J. Orthop. Res., 1990, 8(4), pp. 532–540.

[172] Atkinson T. S., Haut R. C., Altiero N. J., A Poroelastic Model that Predicts Some Phenomological Responses of Ligaments and Tendons, ASME J. Biomech. Eng., 1997, 119, pp. 400–405.

[173] Bensoussan A., Lions J. L., Papanicolaou G., Asymptotic Analysis for Periodic Structures, Amsterdam, North-Holland, 1978.

[174] Sanchez-Palencia E., Non-Homogeneous Media and Vibration Theory, Berlin, Springer, 1980.

[175] Guedes J. M., Nonlinear Computational Models for Composite Materials Using Homogenization, Ph.D. Dissertation, University of Michigan, 1990.

[176] Suquet P. M., Elements of Homogenization Theory for Inelastic Solid Mechanics, In: Sanchez- Palencia E., Zaoui A., Editors, Homogenization Techniques for Composite Media, Berlin, Springer, 1985.

[177] Brand R. A., What Do Tissues and Cells Know of Mechanics? Ann Med., 1997, 29(4), pp. 267–269.

[178] Ebbeling C. B., Clarkson P. A., Exercise-induced Muscle Damage and Adaptation, Sports Medicine, 1989, pp. 207-234.

[179] Fitts R. H., McDonald K. S., Schluter J. M., The Determination of Skeletal Muscle Force and Power: Their Adaptability with Changes in Activity Pattern, Journal of Biomechanics, 1991, 24, pp. 111-122.

[180] Lieber R. L., Friden J., Muscle Damage is not a Function of Muscle Force but Active Muscle Strain, Journal of Applied Physiology, 1993, 74, pp. 520-526.

[181] Lieber R. L., Mechanical Factors Underlying Muscle Damage, In L. Blankevoort and J. G. M. Kooloos, Editors, Proceedings of the Second World Congress of Biomechanics, July 10-15, 1994, Amsterdam, The Netherlands.

[182] Van der Meulen J. H., Exercise-Induced Muscle Damage: Morphological, Biochemical and Functional Aspects, PhD Thesis, Rijksuniversiteit Limburg, Netherlands, 1991.

[183] Hill A. V., The Heat of Shortening and the Dynamic Constants in Muscle, Proceedings of the Royal Society London, 1938, 126, pp.136-165.

[184] Huxley A. F., Muscle Structure and Theories of Contraction, Progress in Biophysics and Biophysical Chemistry, 1957, 7, pp. 257-318.

[185] Goldman Y.E, Brenner B., Molecular Mechanism of Muscle Contraction, Annual Review of Physiology, 1987, 49, pp. 629-636.

[186] Van Kaam F. A. M., de Beer E. L., Stienen G. J. M., Blange T., The Influence of Velocity of Length Change on Tension Development in Skeletal Muscle: Model Calculations and Experimental Results, Journal of Biomechanics, 1984, 17, pp. 501-511.

[187] Finer J. T., Simmons, R. M., Spudich J. A., Single Myosin Molecule Mechanics: Piconewton Forces and Nanometer Steps, Nature, 1994, 268, pp. 13-119.

[188] Funatsu T., Harada Y., Tokunaga M., Satio K., Yanagida T., Imagining of Single Fluorescent Molecules and Individual Atp Turnovers by Single Myosin Molecules in Aqueous Solution. Nature, 1995, 374, pp. 555-559.

[189] Lomoschitz F., Blackmore C., Mirza S., Mann F., Cervical Spine Injuries in Patients 65 Years Old and Older: Epidemiologic Analysis Regarding the Effects of Age and Injury Mechanism on Distribution, Type, and Stability of Injuries. AJR Am. J Roentgenol, 2002,178 (3), pp. 42-47.

[190] Cholewicki J., McGill S. M., Relationship between Muscle Force and Stiffness in the whole Mammalian Muscle: A Simulation Study, Journal of Biomechanical Engieering, 1995, 117, pp. 339-342.

[191] Ettema G. J. C., Huijing P. A., Skeletal Muscle Stiffness in Static and Dynamic Contractions, Journal of Biomechanics, 1994, 27, pp. 1361-1368.

[192] Myers B. S., Van Ee A., C., Nightingale R. W., Camacho D. L., Chancey V. C., Knaub K. E., Sun E. A., Tensile properties of the human muscular and ligamentous cervical spine, Stapp Car Crash Journal, 2000, 44, pp. 85-102.

[193] Myers B.S., Van Ee C. A., Camacho D.L.A., Woolley C.T., Best T.M., On the Structural and Material Properties of Mammalian Skeletal Muscle and its relevance to human cervical impact dynamics, Stapp Car Crash, 1995, 39.

[194] Hatze H., Myocybernetic Control Models of Skeletal Muscle: Characteristics and Applications, University of South Africa, Muckleneuk, Pretoria, 1981.

[195] Winters J. M., Woo S. L. Y., Multiple Muscle System: Biomechanics and Movement organization. Springer-Verlag, New York, 1990.

[196] Woittiez R. D., A Quantitative Study of Muscle Architecture and Muscle Function. PhD. Thesis, Vrije Universiteit te Amesterdam, ISBN 90-6256-224-8, 1984.

[197] Zuurbier C. J., Architecture and Function of Unipennate Muscle in Isometric and Dynamic Contractions, PhD Thesis, Vrije Universiteit Amsterdam, 1992.

[198] Gareis H., Solomonow M., Baratta R., Best R., D'Ambrosia R., The Isometric Length-Force Models of Nine Different Skeletal Muscles, Journal of Biomechanics, 1992, 25, pp. 903-916.

[199] Kaufman K. R., An K. N., Chao E. Y., Incorporation of Muscle Architecture into the Muscle Length-Tension Relationship, Journal of Biomechanics, 1989, 22, pp. 943-948.

[200] Otten E., Shape Change, Force Production and Pressure Distribution in Skeletal Muscle: A Finite Element Approach, Presentation at Workshop of Biomechanical Division of the Netherlands, Feb. 17th, 1995.

[201] Van der Linden B., Fem Model, Presentation at Workshop Biomechanical Division of Netherlands, 1996.

[202] Van der Linden B., Mechanical Modeling of Skeletal Muscle Functioning, PhD Thesis, University Twente, 1998.

[203] Anton M., Mechanical Models of Skeletal Muscle, PhD Thesis, University of Calgary, 1991.

[204] Panjabi M., Duranceau J., Goel V., Cervical Human Vertebrae Quantitative Three-dimensional Anatomy of the Middle and Lower Regions, Spine, 1992, 17, pp. 299–306.

[205] Panjabi M., Oxland T., Takata K., Goel V., Duranceau J., Krag M., Articular Facets of the Human Spine, Quantitative Three-Dimensional Anatomy, Spine, 1993, 18(10), pp.1298-1310.

[206] Xu R., Burgar A., Ebraheim N., Yeasting R., The Quantitative Anatomy of the Laminas of the Spine, Spine, 1999, 24(2), pp.107-113.

[207] Doherty B., Heggeness M., The Quantitative Anatomy of the Atlas, Spine, 1994, 19(22), 2497-2500.

[208] Doherty B., Heggeness M., The Quantitative Anatomy of the Second Cervical Vertebra, Spine, 1995, 20(5), 513-517.

[209] Dong Y., Hong M., Jianyi L., Lin M., Quantitative Anatomy of the Lateral Mass of the Atlas, Spine, 2003, 28, pp. 860–863.

[210] Naderi S., Guvencer M., Korman E., An Anatomical Study of the C-2 Pedicle, Journal of Neurosurgery, 2004, 3, pp. 306–310.

[211] Schaffler M., Alson M., Heller J., Garfin S., Morphology of the Dens, A Quantitative Study, Spine, 1992, 17(7), 738-743.

[212] Nissan M., Gilad I., A Study of Vertebra and Disc Geometric Relations of the Human Cervical and Lumbar Spine, Spine, 1986, 11(2), pp. 154-157.

[213] Francis C. Dimensions of the cervical vertebrae, Anatomical Record, 1995, 122, pp. 603–609.

[214] Liu Y. K., Krieger K. W., Njus G., Quantitative Geometry of Young Human Male Cervical Vertebrae, NTIS Report No. AFAMRL-TR, 1982, pp. 80-138.

[215] Tan S. H., Teo E. C., Chua H. C., Quantitative three-dimensional anatomy of cervical ,thoracic and lumbar vertebrae of Chinese Singaporeans, European Spine Journal, 2004, 13, pp.137–146.

[216] Panjabi M., Takata K., Goel V., Federico D., Oxland T., Duranceau J., Krag M., Thoracic Human Vertebrae, Quantitative Three-Dimensional Anatomy, Spine, 1991, 16(8), pp. 888-901.

[217] Panjabi M., Chen N., Shin E., Wang J., The Cortical Shell Architecture of Human Cervical Vertebral Bodies, Spine, 2001, 26 (22), pp. 2478–2484.

[218] Carlos Lopez, Biomechanics of the Cervical Spine: Parametric Finit Element Modeling and Analysis of Plated Fusion, University of Illinois at Chicago, Master's Thesis, 2002

[219] Belytschko T., Kulak R. F., and Schultz A. B., Finite Element Stress Analysis of an Intervertebral Disc, J. Biomech., 1974, 7, pp. 277–285.

[220] Yoganandan N., Kumaresan S, Pintar F., Biomechanics of the Cervical Spine Part 2: Cervical Spine Soft Tissue Responses and Biomechanical Modeling, Clinical Biomechanics, 2001, 16, pp. 1-27.

[221] Ng H.W., Teo E.C. and Zhang Q.H., Prediction of Inter-Segment Stability and Osteophyte Formation on the Multi-Segment C2–C7 after Unilateral and Bilateral Facetectomy, 2004, 218 (3), pp. 183-191.

[222] ANSYS 7.0, Educational Version., ANSYS Inc.

[223] Dvorack J, Schneider E, Saldinger P, Rahn B., Biomechanics of the Craniocervical Region: The Alar and Transverse Ligaments, J. Orthopaedic Research, 1988, pp. 452-461.

[224] Panjabi M., Crisco J., Vasavada A. Oda T., Cholewicki J., Nibu K., Shin E., Mechanical Properties of the Human Cervical Spine as Shown by Three-Dimensional Load-Displacement Curves, Spine, 2001, 26 (24), pp. 2692-2700.

[225] Shea M., Edwards W. T., White A. A., Hayes W. C., Variations of Stiffness and Strength along the Human Cervical Spine, J. Biomechanics, 1991, 24, pp. 95-107.

APPENDIX 1
The Origins and Insertions of Muscles in Cervical Spine Region.

Table 21: The origins and insertions of Sternocleidomastoid, Splenius capits, Semispinalis capitis and Semispinalis cervicis [55].

	Flexor Muscle	Origin	Insertion	PCSA (cm^2)
24	Sternocleidomastoid	T1	Skull	4.92
25	Splenius capitis	C7	Skull	1.545
26	Splenius capitis	T2	Skull	1.545
27	Splenius cervicis	T3	C3	0.833
28	Splenius cervicis	T3	C2	0.833
29	Splenius cervicis	T3	C1	0.833
30	Semispinalis capitis	C4	Skull	0.9
31	Semispinalis capitis	C5	Skull	0.9
32	Semispinalis capitis	C6	Skull	0.9
33	Semispinalis capitis	C7	Skull	0.9
34	Semispinalis capitis	T3	Skull	0.9
35	Semispinalis cervicis	T1	C2	0.1275
36	Semispinalis cervicis	T2	C3	0.255
37	Semispinalis cervicis	T3	C4	0.3825
38	Semispinalis cervicis	T4	C5	0.8
39	Semispinalis cervicis	T5	C6	1
40	Semispinalis cervicis	T6	C7	1.1

Table 22: The origins and insertions of Longissimus capitis and Longissimus cervicis [55].

	Flexor Muscle	Origin	Insertion	PCSA (cm^2)
41	Longissimus capitis	C3	Skull	0.1633
42	Longissimus capitis	C4	Skull	0.1633
43	Longissimus capitis	C5	Skull	0.1633
44	Longissimus capitis	C6	Skull	0.1633
45	Longissimus capitis	C7	Skull	0.1633
46	Longissimus capitis	T2	Skull	0.1633
47	Longissimus cervicis	T2	C2	0.2483
48	Longissimus cervicis	T2	C3	0.2483
49	Longissimus cervicis	T2	C4	0.2483
50	Longissimus cervicis	T2	C5	0.2483
51	Longissimus cervicis	T2	C6	0.2483
52	Longissimus cervicis	T2	C7	0.2483

Table 23: The origins and insertions of Levator scapulae and Multifidus cervicis [55].

	Flexor Muscle	Origin	Insertion	PCSA (cm^2)
53	Levator scapulae	Scapula	C1	0.78
54	Levator scapulae	Scapula	C2	0.78
55	Levator scapulae	Scapula	C3	0.78
56	Levator scapulae	Scapula	C4	0.78
57	Multifidus cervicis	C5	C2	0.15
58	Multifidus cervicis	C6	C2	0.15
59	Multifidus cervicis	C6	C3	0.15
60	Multifidus cervicis	C7	C3	0.15
61	Multifidus cervicis	C7	C4	0.15
62	Multifidus cervicis	T1	C4	0.15
63	Multifidus cervicis	T1	C5	0.2
64	Multifidus cervicis	T2	C5	0.2
65	Multifidus cervicis	T2	C6	0.4
66	Multifidus cervicis	T3	C6	0.4
67	Multifidus cervicis	T3	C7	1.1
68	Multifidus cervicis	T4	C7	1.3

Table 24: The origins and insertions of Longus colli, Longus capitis, Scalenus anterior, medius, scalenus and Lumped hypoids [55].

	Flexor Muscle	Origin	Insertion	PCSA (cm^2)
1	Longus colli	T1	C6	0.3914
2	Longus colli	T1	C5	0.3914
3	Longus colli	T1	C4	0.3914
4	Longus colli	T1	C3	0.3914
5	Longus colli	T1	C2	0.3914
6	Longus colli	T1	C1	0.3914
7	Longus colli	T1	Skull	0.3914
8	Longus capitis	C3	Skull	0.3425
9	Longus capitis	C4	Skull	0.3425
10	Longus capitis	C5	Skull	0.3425
11	Longus capitis	C6	Skull	0.3425
12	Scalenus anterior	T1	C4	1.88
13	Scalenus medius	T1	C3	1.36
14	Scalenus posterior	T1	C5	1.05
15	Lumped hyoids	T1	Skull	2.35

Table 25: The origins and insertions of Trapezius [55].

	Flexor Muscle	Origin	Insertion	PCSA (cm^2)
16	Trapezius	T1	Skull	0.4713
17	Trapezius	T1	C1	0.4713
18	Trapezius	T1	C2	0.4713
19	Trapezius	T1	C3	0.4713
20	Trapezius	T1	C4	0.4713
21	Trapezius	T1	C5	0.4713
22	Trapezius	T1	C6	0.4713
23	Trapezius	T1	C7	0.4713

APPENDIX 2

Calculation for Relative Location of Vertebrae

To compute the angle between vertebrae the reported values from Nissan et al. [212] were used. Since the lower endplate depth from the upper vertebra was averaged with the upper endplate depth from the lower vertebra the angle between adjacent vertebrae (Alpha) can be calculated as Equation I (Figure 69).

$$Alpha = 2.[\arcsin(\frac{g-h}{2a_m})] \qquad \text{(Eq. I)}$$

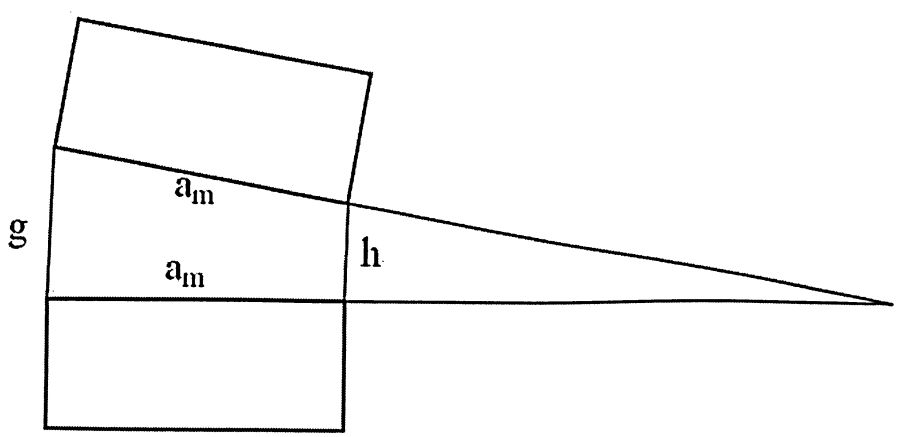

Figure 69: Vertebral calculation of position in space.